

## Department of Precision and Microsystems Engineering

### Synthesis and Control of a 3 Degrees of Freedom Inherently Dynamically Balanced Manipulator for an Unmanned Aerial Vehicle

Mitchell Bey Beacom

Report no : 2021.005  
Coach : Dr. V. van der Wijk  
Professor : Prof.dr.ir. J.L. Herder  
Specialisation : MSD  
Type of report : Masters Thesis  
Date : 29 January 2021

# Abstract

In aerial manipulation, Unmanned Aerial Vehicles (UAVs) are equipped with manipulators to perform a variety of tasks such as contact inspections of critical infrastructure at heights. A fundamental issue is that the shaking forces and moments of the manipulator cause the UAV to tip-over and become unstable. Control based methods have been applied in which the UAV provided a compensation force or moment at the propellers. However, the dynamic model required was too complex to compute on-board in real time and simplifications led to poor performance. This thesis resolves the issue of shaking forces and moments by creating a new manipulator using inherent dynamic balancing principles. The advantage of these principles is that the manipulator architecture achieves both functions of supporting and positioning the end effector as well as balancing. This helps to reduce the weight of the manipulator. The result of the synthesis work is a manipulator which is reactionless, lightweight, has 3 degrees of freedom, and is compatible with a UAV. First a manipulator is designed using inherently force balanced architectures. Next, the active moment balancing is developed by using a redundant architecture: for all end effector paths there exists a manipulator motion in the plane such that no reaction moment is generated. To achieve this a novel control scheme is developed which resolves the kinematic redundancy by minimizing the angular momentum for a 3 degrees of freedom force balance architecture in a 2 degrees of freedom workspace. Finally, a simulation is performed to prove the dynamic balancing and control method. It shows the manipulator is reactionless. However, the control scheme's tracking still needs improvement. This work is useful to enable UAVs with manipulators to perform a variety of tasks such as contact inspections of surfaces at height.

# Contents

<b>1</b>	<b>Introduction</b>	<b>2</b>
<b>2</b>	<b>Literature Review</b>	<b>4</b>
2.1	Introduction	4
2.2	Overview: Application Fields of Floating Base Manipulation	4
2.2.1	Aerial Manipulation	4
2.2.2	Underwater Manipulation	5
2.2.3	Space Robots	5
2.2.4	Ground Robots	5
2.2.5	Cable Robots	5
2.3	Methods for Ensuring Stable Manipulation	5
2.3.1	Category: Avoidance Based Methods	5
2.3.2	Category: Passive Based Methods	8
2.3.3	Category: Active Based Methods	10
2.4	Discussion of Literature Review	17
2.5	Conclusion	18
<b>3</b>	<b>Design of a Lightweight 3 Degrees of Freedom Manipulator with Inherent Dynamic Balancing</b>	<b>19</b>
3.1	Introduction	19
3.2	Application	19
3.3	Design Requirements	19
3.4	Synthesis Methods for a Reactionless Manipulator	21
3.4.1	Force Balancing: Inherent Dynamic Balancing	21
3.4.2	Moment Balancing: Passive and Active Methods	23
3.5	Conceptual Designs of 3 DoF Reactionless Manipulators	25
3.5.1	1 DoF Combinations - Passive	25
3.5.2	Parallel Combination of Mirrored 2 DoF Inherently Balanced Architectures - Passive	26
3.5.3	3 DoF Inherently Force Balanced Manipulator with 3 Counter Rotating Masses - Active	26
3.5.4	2 DoF Inherently Force Balanced Architecture with 2 Counter Rotating Masses - Active	26
3.5.5	3 DoF Actively Reduced Balanced Architecture and 1 Counter Rotating Mass - Active	26
3.6	Concept Selection	27
3.7	Detailed Design	27
3.8	Discussion	28
3.9	Conclusion	28
<b>4</b>	<b>Control for Active Moment Balancing of a 2 Degrees of Freedom Inherently Balanced Manipulator for an Unmanned Aerial Vehicle (Paper)</b>	<b>29</b>
4.1	Abstract	29
4.2	Introduction	29
4.3	Application	30
4.4	Manipulator Design	31
4.5	Approach for Active Balancing	33
4.5.1	Minimizing Angular Momentum	34
4.5.2	Torque Adjusting	34

4.6	Simulation of the Manipulator . . . . .	35
4.6.1	End Effector Path Requirements . . . . .	35
4.6.2	Simulation Explanation . . . . .	35
4.7	Results . . . . .	36
4.7.1	C-Curve Results and Discussion . . . . .	36
4.7.2	Step Results and Discussion . . . . .	37
4.8	Discussion . . . . .	45
4.9	Conclusion . . . . .	45
<b>5</b>	<b>Discussion</b>	<b>47</b>
<b>6</b>	<b>Conclusion</b>	<b>49</b>
<b>A</b>	<b>Appendix: Examples of Methods for Stable Manipulation Summary Table</b>	<b>50</b>
<b>B</b>	<b>Appendix: Benefits and Limitations of Methods for Stable Manipulation Summary Table</b>	<b>51</b>
<b>C</b>	<b>Appendix: Grand 4R and Grand 5R Force Balanced Architecture Derivatives</b>	<b>52</b>
C.1	Grand 4R Architectures . . . . .	52
C.2	Grand 5R Architectures . . . . .	54
<b>D</b>	<b>Appendix: Simulation of Kinematic Reduction</b>	<b>55</b>
<b>E</b>	<b>Appendix: Finite Element of Beam Selection for Detailed Design</b>	<b>56</b>
<b>F</b>	<b>Appendix: Simulation of Active Moment Balancing</b>	<b>58</b>
<b>G</b>	<b>Appendix: Additional Simulation Results</b>	<b>68</b>
G.1	Linear Momentum . . . . .	68
G.2	Feedforward Averaging with Feedback Results . . . . .	68
G.3	H2 Controller Results . . . . .	71
	<b>Bibliography</b>	<b>73</b>

# 1 | Introduction

Mobile robots have been developed to explore and monitor every domain; from space to sky to sea. However, mobile robots have far more potential if they can reach out and make contact with their surroundings. By combining them with manipulators, a host of other tasks become possible in hard to reach areas. This is referred to as mobile manipulation. [1]

Mobile manipulation has been applied primarily for aerial vehicles, space robots, ground rovers, underwater vehicles, and cable robots. In each field the mobile robot provides course positioning as well as auxiliary support such as power and communication. The manipulator then performs a fine positioning or a dexterous manipulation task. These tasks can vary from assembling a space station, to patching an offshore platform, to checking the structural integrity of a bridge. [1]

A fundamental issue with mobile manipulation is that the manipulator has been attached to an unsupported base. When the manipulator is not supported, this research area is referred to as floating base manipulation. The issue is that manipulator motion causes reaction forces and moments that are imparted on the base: these are referred to as the shaking forces and moments. The challenge is then how to maintain stability and positioning precision with these shaking forces and moments.

Aerial manipulation is when an aerial vehicle is used as the mobile robot. While helicopters were originally used dating back to 2014, [2] and there have been some developments with fixed wing aerial vehicles, Unmanned Aerial Vehicles (UAVs), in particular multicopters, are the most popular currently. [3] Of all of the mobile manipulation fields, aerial manipulation is most limited by instability from the shaking forces and moments. In this domain, instability causes the UAV to tip over which can result in a catastrophic failure. In comparison to other mobile manipulation fields, the relative size of the manipulator in comparison to the mobile base is much larger. This means the shaking forces and moments have a larger impact on the stability. Additionally, the UAV field comes with other challenges. The UAV payload is strictly limited by the lift capacity of the UAV, so the manipulator must be lightweight.

UAVs equipped with manipulators have the potential to perform tasks with significant societal impact. In agriculture, a UAV with a manipulator could pick fruit, collect soil samples, monitor for pests, or prune trees. This would increase crop yield and reduce food prices. For bridges, wind turbines, and oil and gas refinery tanks, a UAV with a manipulator can reach out and make contact with the surface to check its structural integrity. One method that can be used is ultrasonic thickness inspection. With this technology, the cost to inspect critical infrastructure could be reduced and dangerous manual inspection at heights can be avoided. To achieve this, the issue of stability from the shaking forces and moments of the manipulator must be resolved.

There have been a variety of attempts in literature to solve these issues, however, they have not been successful. [4] First control based methods were applied in which the UAV propellers created compensation forces and moments to cancel the shaking forces and moments; initially in feedback, then in feedforward. [5] [4] The limitation was that the dynamic model was too complex to process in real time and simplifications led to errors which impacted the performance. Next, path planning was applied to both the globally redundant system and to redundant manipulators [6] [2] [7]. By using a redundancy multiple paths are possible and one can be selected such that one of the shaking forces or moments could be eliminated. These trajectories had to be computed offline which meant they required the predictability of a lab environment. Additionally there were still unresolved shaking forces and moments. Finally, dynamic balancing was applied, including using an actively controlled counter rotating mass to cancel a reaction moment and dual arms to resolve some of the reaction forces and moments by symmetry [8]. By adding an additional mass or arm the weight increases substantially, and still only some of the shaking forces and moments were resolved.

A variety of active mechanisms were applied to the attached manipulators to partially resolve shaking forces

or moments. An actively controlled sliding battery pack was attached to a UAV. [9] Similarly, the entire manipulator was attached to a slider. [10] Finally a 1 degree of freedom (DoF) pantograph was moment balanced with an active countermass [11]. These methods are either limited to only resolving one shaking force or moment or to only resulting in a 1 DoF manipulator. However, they have potential to balance shaking forces or moments that cannot be resolved by the manipulator design.

In parallel the development of passively balanced manipulators were being developed. The first method was to attach a counterweight to the other end of a rotating rod. [12] [13] This achieved 1 DoF force balancing. The limitation of adding counterweights was that it significantly added weight. For UAVs the weight is limited by the lift capability. A heavier payload reduces the flight time because a greater lift force is required from the motors. For the DJI m600 for example, a 6kg payload halves the flight time in comparison to no added payload. [14] Next inherently balanced architectures were applied to mobile robots based on a balanced four bar and a simple pantograph for force balancing. [15] [16] By repeating a 1 DoF balanced unit the weight and complexity grew substantially. In [17] the method of inherent dynamic balancing was used to create a 1 DoF manipulator that is force and moment balanced to attach to a UAV. There is the potential to go to a higher number of DoFs based on this method while reducing the weight. There is still a need for a lightweight, reactionless, 3 degrees of freedom manipulator that can be attached to a UAV.

The aim of this thesis is to apply inherent dynamic balancing principles to the synthesize and control of a reactionless, lightweight, 3 degrees of freedom (x,y,z) manipulator for a UAV. This will be accomplished first by designing a manipulator in Chapter 3 using inherent dynamic balancing. To achieve this design, a method for active moment balancing is required. This is developed in Chapter 4, the academic paper, in which a novel control scheme is developed for a redundant 3 degree of freedom inherently force balanced architecture in a 2 degree of freedom workspace. The control scheme ensures no reaction moment is generated by resolving the kinematic redundancy such that the angular momentum is minimized. Finally the results of this research and the future work for the area are assessed in Chapter 5. This thesis will focus on the field of aerial manipulation, however, this development can also further the other fields of mobile manipulation and floating base manipulation.

# 2 | Literature Review

## 2.1 Introduction

The aim of this chapter is to address the question: how can stable manipulation be best performed on a floating base? In this chapter the state of the art in the area of floating base manipulation will be reviewed and assessed.

First the research area of floating base manipulation must be dissected into application areas. While aerial manipulation, in which UAVs are commonly used, is the focal point of this literature review, the other application fields face similar challenges. The other application areas are underwater manipulation, space robots, ground robots, and cable robots. An overview is provided of each, along with the common tasks and mobile robots that are used.

Each of these application fields have a similar issue. The motion of the manipulator causes shaking forces and shaking moments to act on the base. For a mobile robot, this causes instability. In reviewing the literature of each field, it was found that similar methods are used across different application fields. For some application fields the methods work better than for others. Therefore, the methods that are used to ensure stable manipulation were compiled regardless of their application area.

The different methods found in literature were divided into three categories: avoidance, passive, and active. For each method examples are provided to highlight if there are methods which have not been applied to certain applications. Each method is then analyzed for its benefits and limitations. Finally the most promising method for further research is found in order to synthesize and control a manipulator for a UAV.

## 2.2 Overview: Application Fields of Floating Base Manipulation

This section details the primary fields in which mobile manipulation is performed. A brief description of the commonly used robots are provided along with the advantages and challenges of the field. Additionally, some of the tasks which must be performed are outlined.

### 2.2.1 Aerial Manipulation

In this field Unmanned Aerial Vehicles (UAVs) are equipped with robotic manipulators to perform a variety of tasks such as assembly, contact inspection, remote sensing, search and rescue, and many others. [3] [4] The benefits of adding a manipulator are that most UAVs are underactuated with only 4 DoF, so an added manipulator with 2 or more DoF can match the 6 DoF workspace. [4] It also allows robotic interaction in hard to reach areas. [3] The challenges in the field are primarily the unsupported base and the non-linear coupling dynamics, along with the payload weight constraints and that the propulsion varies in close proximity to the ground or walls. [4] Historically the the UAV platform was helicopters, however, currently quadrotors are widely used for their simplicity, hovering capability, low cost, and available control schemes. [4] Aerial manipulation can be performed by robotic manipulators, grippers, a rigid tool connected to the UAV, or a tether. [4] This paper will focus primarily on those with robotic manipulators as this area is considered to be the most promising. [4]

## 2.2.2 Underwater Manipulation

In the subsea field Autonomous Underwater Vehicles (AUVs) are augmented with typically one or two anthropomorphic arms. [18] These AUVs are used for pipe inspection, salvaging, cleaning, drilling, and many other tasks. [18] These tasks typically involve high loads, so the manipulators are heavy and in a serial configuration with hydraulic or electric actuation. [18] A major challenge of the field besides dynamic coupling are the added mass of the fluid during manipulator motion and the environmental challenges of a pressurized and corrosive environment. [18]

## 2.2.3 Space Robots

In the space domain satellites are equipped with lightweight manipulators for capturing space debris and performing maintenance tasks. [1] [19] The most famous examples include the Canadarm and Canadarm 2. [1] The dynamic coupling of the manipulator can cause the satellite to lose contact with the command post on earth if it alters the alignment of the communication equipment, and can also cause the arm to miss its target. [1] As there are limited external disturbances in space addressing the dynamic coupling is a significant research focus.

## 2.2.4 Ground Robots

In this domain manipulators are mounted to rovers. They are used primarily for exploration on earth and other planets as well as for operations covering large areas such as agriculture and mapping. [1] Wheeled robots are the most popular for their low energy consumption, speed, and stability. [1] This field differs from the others as the rover can impart forces on the ground. Primarily the issue is then with tipover stability.

## 2.2.5 Cable Robots

Cable robots involve a platform suspended by multiple actuated wires. They have low moving inertia and a very large workspace. [20] By adding a manipulator to the platform the workspace of the manipulator can be greatly enlarged. The primary challenges of the field are that the cable can only provide a tensile force, and so the force closure must always be maintained to ensure stability. [20] Mobile manipulation in this field is relatively unexplored, likely due to the already existing stability issues.

## 2.3 Methods for Ensuring Stable Manipulation

This section details the various methods used across mobile manipulation fields to limit the negative impacts of manipulator motion on the base. These methods are divided into three primary categories: avoidance, passive, and active. For each method examples will be provided and then the advantages and limitations will be discussed. For a summary of the examples found for each method in each field refer to Appendix A. For a summary of the benefits and limitations of each method refer to Appendix B.

### 2.3.1 Category: Avoidance Based Methods

This category is characterized by the fact that the dynamic coupling is not directly resolved by the method. Instead, the impact of the dynamic coupling is avoided or reduced. These methods do not directly solve the issue of stability but are widely used, especially in industry. The first is to minimize the relative moving mass of the manipulator with respect to the base, the second is to grab on to a fixed base.

## Reduce Moving Mass

This method relies on the principle that the larger the moving mass of the manipulator, the larger the driving forces required, and in turn the large the reaction forces. If the moving mass of the manipulator is much smaller with respect to the mass of the base, the relative disturbance will be smaller. This is similar to how industrial robots are attached to large, rigid bases.

### Examples

In the space and subsea fields weight reduction is already crucial, and the benefit of the reduced dynamic coupling effects have been studied in detail. [1] In the space domain, weight reduction is critical because of rocket payload limitations. The manipulators used in space such as the Canadarm are designed to be as lightweight as possible; in fact they cannot support their own weight under gravity. [1] In the field of AUVs there is a common industry standard on the relative weight: from 1.5% -5.4%. [18] In addition, [21] has developed a lighter manipulator and used the hydrostatic restoring forces to stabilize the vehicle. If the centre of gravity of the vehicle is below the centre of buoyancy, this creates a pendulum effect that is commonly used to passively maintain the orientation of AUVs. [1] By minimizing the weight of the manipulator, the hydrostatic force is enough to maintain stability.

In the cable and ground robot fields the required relative weights to maintain stability is not as formally addressed. In [22] a cable robot with suspended fingers are used for fine stage manipulation. The coupling dynamics are not formally addressed but the relatively weight of the fingers is small. In the ground robotics field the relative weight is typically addressed using a variety of tipover stability criteria. The most basic is that the centre of gravity of the system must lie within the region created by the ground contact area. [23]

For UAVs there also isn't a standing benchmark on the acceptable relative weights, however [4] identifies this as an important research area. The commercially available Prodrone PD6B-AW-ARM shown in Figure 2.1 appears to use a larger 6 rotor base. [24] However, there are novel manipulators that have been developed to reduce the moving mass. Both achieve this by placing the motors at the base rather than in a serial configuration. In [25] a 6 DOF parallel manipulator is attached to a UAV, while in [26] a serial manipulator with differential joints and timing belts are used. These are shown in Figure 2.2 and Figure 2.3 respectively.



Figure 2.1: Prodrone PD6B-AW-ARM. Source: [24]

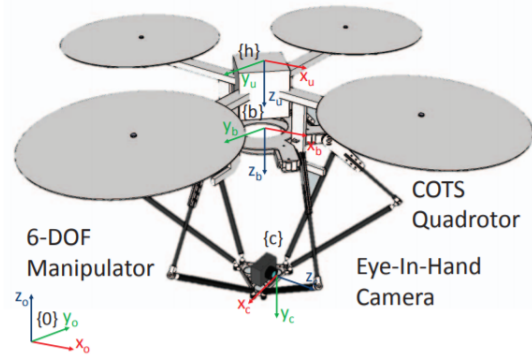


Figure 2.2: Aerial Parallel Manipulator. Source: [25]

### Discussion

Reducing the moving mass of the manipulator is a prominent method to try to avoid the impacts of dynamic coupling. For fields such as subsea where there are hydrostatic restoring forces to stabilize and the vehicles are already quite large in comparison to the manipulator this may be an effective solution. Across all fields this is



Fig. 2. PULSAR robot arm (motors in blue, servos in green)

**Figure 2.3:** Aerial Differential Manipulator. Source: [26]

a good design principle in general, however, as the requirements for positioning accuracy and weight reduction become stricter this is not an effective solution.

### **Attach to a Fixed Base**

To avoid the issue of manipulator reaction forces and moments on a moving base an additional gripper or manipulator can be mounted to the base to transfer the reaction force to the ground.

#### *Examples*

This method is used in the subsea and aerial domains. In certain maintenance and inspection tasks such as in the oil and gas industry as well as for certain operations in the sea floor, a secondary arm on an AUV is used to grab on to a stationary object. [18] For aerial manipulation, perching has been proposed where the UAV uses a manipulator to momentarily attach itself to a fixed base similar to a bird. [4] Some novel configurations have also been proposed such as [27] where an upper gripper is used to attach to a rod as shown in Figure 2.4.



**Figure 2.4:** Seperate Rod Grasping. Source: [27]

#### *Discussion*

This method is very limited to a few tasks where a fixed base is accessible. For those specific tasks it eliminates the reaction problem. However, for most tasks a fixed base is not accessible, and the grasping or perching operation to steady the vehicle may suffer from the same dynamic coupling issues.

### 2.3.2 Category: Passive Based Methods

Passive methods resolve the dynamic coupling impacts through a more fundamental and inherent approach. These methods eliminate the dynamic impacts on the base through a specific choice of the mechanical design of the manipulator. There are two types of passive methods: counterweights and inherently balanced architectures.

#### Counterweights

To eliminate the reaction forces from a rotating mass this method uses a counter rotating mass to balance the forces applied to the base by the manipulator. Typically the manipulator is attached to a pivot point and at the other end of the same link the counter mass is attached.

#### Examples

Counterweights have been attached to manipulators in the aerial and space domains only. In the Aeroarms project, a significant research effort on using UAVs for maintenance and inspection, a rotating link is connected to the UAV. [12] To reduce the reaction force on the UAV base the batteries are attached to the other end of the link and rotate with the end effector, as shown in Figure 2.5. [12] In the design of a reactionless pointing mechanism for satellite antennas the actuators were placed at the other end of the pivot to balance the forces, as shown in Figure 2.6. [13] The reaction moments were cancelled by using an additional passive joint so that the moment cannot be transferred to the base. [13]



Figure 2.5: Inspection UAV with rotating batteries for force balance. Source: [12]

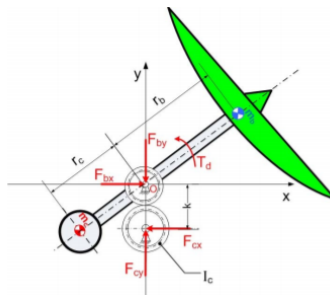


Figure 2.6: Balanced antenna pointing mechanism. Source: [13]

#### Discussion

This method is a very simple way of force balancing a 1 DoF link and can be quite effective if the mass and length parameters are well defined. The drawback is that a counterweight adds weight and energy consumption which for mobile robotics is strictly limiting. Using functional weight such as the batteries and actuator is better than just a counterweight, but still by moving this mass the energy consumption increases. This method

also does not scale well to higher DoFs as counterweights must be added for each. Additionally, the moment balancing is not fully resolved by this method.

### Inherently Balanced Architectures

In this method novel mechanical architectures are composed for the manipulator. For all motion paths of these mechanisms no reaction force is applied to the base. This is achieved by selecting the geometrical, mass, and inertial parameters in such a way that the reaction forces are balanced.

#### Examples

The two methods for creating an inherently balanced manipulator for mobile robotics are by using a combination of pantographs or balanced four bars. These structures are inherently force balanced, so combinations of them yield balanced mechanisms. A pantograph based manipulator for a demining rover was developed for stability but also for reducing the energy consumption. [16] As shown in Figure 2.7, the end effector and counterweight are balanced using a pantograph architecture. [16] Similarly, a pantograph based mechanism was proposed for a space robot. [28] The moment balancing is achieved by having a passive joint at the base. [28] Also for a space, reactionless spatial 3 and 6 DoF manipulators were constructed from a combination of inherently balanced four bar linkages as shown in Figure 2.8. [15]



Figure 2.7: Pantograph based manipulator for demining. Source: [16]

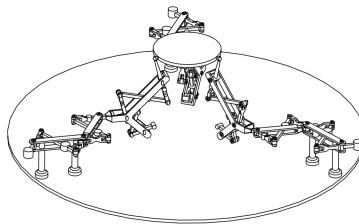


Figure 2.8: Balanced four bar based 6 DoF Manipulator for space. Source: [15]

#### Discussion

This field is promising in that there are no limitations placed on the path of the manipulator, no added counterweights, and it is possible to achieve complete force and moment balancing. Since it can be difficult to generate these novel architectures very few have been applied to mobile manipulation. In the case of the balanced four bar based approach, the complexity builds substantially with the number of degrees of freedom. This method is relatively unexplored but offers great potential. The limitation is that a novel manipulator must be developed and applied.

### 2.3.3 Category: Active Based Methods

Active methods typically involve solutions that rely on control to maintain the base stability. These methods involve either preemptive planning or real time response. The first method involves changing the actuation. The second two methods, local and global redundancy, capitalize on the redundancy of the system to generate reactionless paths. The next methods, feedback and feed forward base control use the vehicle actuators to counter the reaction forces. Finally, additional arms can be used to counter the reactions along with a variety of novel mechanisms.

#### Gyroscopic Actuation

In gyroscopic actuation the force generated by unbalancing a spinning mass is used to drive the actuator. This actuation does not impose a reaction on the base as only a force to move the manipulator is generated. In the same vein, a spinning mass has a resistance to change. By adding a constant spinning mass to the system, higher order disturbances can be rejected.

##### *Examples*

Gyroscopic actuation has only been proposed in the space domain. Control moment gyroscopes (CMGs) which use a constant speed rotor with a gimbal that changes the direction of the rotors angular momentum have been used to actuate a prototype space manipulator, as shown in Figure 2.9. [29] For a cable driven aerial camera system, a patent was filed to add spinning mass gyroscopes which resist high rate disturbances. [30]

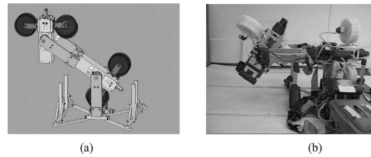


**Figure 2.9:** Gyroscopic actuation of a space manipulator. Source: [29]

##### *Discussion*

Gyroscopic actuation has yet to be applied outside the space domain. Likely for high load applications the gyroscopic force is too small or would require extremely large spinning masses. Using spinning masses to reduce higher order disturbances could be useful for external forces, but for large coupling forces this is not an adequate solution.

#### Globally Redundant Path Planning

For most vehicle manipulator systems adding the number of degrees of freedom of the vehicle and the manipulator sum to more than the workspace. This is because the vehicle typically has enough actuators to position and orient the vehicle. In addition, a manipulator is added with multiple degrees of freedom. Since the primary goal of a vehicle manipulator system is to position the end effector, there are multiple configurations and paths in which the system reaches the desired end position. Therefore, a path can be selected that achieves a variety of secondary objectives. For this study the most relevant is maintaining the base position and orientation.

##### *Examples*

This method is commonly used for free floating spacecraft. [1] These spacecraft do not have base actuators and it is crucial to maintain the orientation of the communication equipment. [1] Therefore, the manipulator path is chosen such that once the path is completed the end effector position is achieved and a critical orientation of one of the faces is maintained for communication with earth. [1]

This method has then been applied to both UAVs and AUVs. In [6] a path for the UAV and the manipulator are optimized using quadratic programming first to reach the target end effector position, and second to minimize a variety of cost functions including the centre of gravity displacement and transmitted forces between the UAV and manipulator. Similarly, in [31] the path of a 6 DOF manipulator on a AUV is selected to minimize the AUV motion.

#### *Discussion*

This method is effective in the space field because each movement is meticulously planned and there are few external disturbances in space. However, with the other fields there are a host of disturbances which can cause the path to no longer reach the desired end position, in which case a correction will cause a reaction. The computation required for each path is significant, especially for a UAV with limited on-board processing. Finally, the functionality of the system is significantly reduced if it can only follow a set of prescribed paths.

### **Locally Redundant Path Planning**

This method is similar to the globally redundant case, however, in local redundancy the manipulator and vehicle are separated and the manipulator dynamics are addressed. A redundant manipulator which has more than 6 DOF is applied. The additional DOF of the manipulator are used to generate paths that are reactionless at the connection to the vehicle.

#### *Examples*

Redundant manipulators have been either academically proposed or applied to space, aerial, and cable robots. In the space domain this method has been explored in depth. The method is referred to as null space control as the additional unwanted velocity contribution is projected into the null space. [1] As in the global method, the primary goal is to obtain the end effector position and the secondary is to maintain the spacecraft attitude for communication. [1]

In the early stages of aerial manipulation a 7 DoF KUKA industrial manipulator was attached underneath a helicopter as shown in Figure 2.10. [2] The manipulator redundancy was then used to maintain a constant centre of gravity (CoG) position. It was identified that the CoG position was more important than the inertial forces as the arm was moved slowly. [2] A hyper-redundant manipulator was proposed for aerial manipulation as shown in Figure 2.11. [7] Hyper-redundancy is when the manipulator has far more degrees of freedom than required. These additional degrees of freedom were used to minimize the reaction transferred to the base, however, the proposal was not tested on an actual UAV. [7]



**Figure 2.10:** Redundant manipulator attached to helicopter. Source: [2]

In the cable field redundant manipulators have been proposed to improve stability, particularly to avoid tip-over. In [32] a planar robot is considered in which a 4 DoF manipulator is suspended from two actuated wires. The redundant degree of freedom is used to maintain the horizontal position of the CoG. [32] In the spatial case, a 6 wire platform with a 7 DoF manipulator is used to decrease the reaction force and maximize the minimum wire tension to avoid overturn. [33] This is shown in Figure 2.12.

#### *Discussion*



**Figure 2.11:** Hyper-redundant manipulator for UAVs. Source: [7]

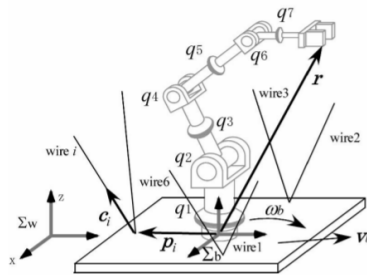


**Figure 2.12:** Redundant manipulator suspended by cables. Source: [33]

The benefit of this method is that the manipulator can have no impact on the base and the two can be decoupled. The drawbacks of planning, as discussed in global redundancy, also apply to this method. Additionally, the extra degrees of freedom add complexity, weight, and power consumption. For mobile manipulation, the added weight is a significant drawback. For AUVs in particular, redundant manipulators have not been applied. This is likely because there are already high loads and nonlinear impacts of the hydraulic manipulators; adding joints is not practical.

### Feedback Base Control

In this method the base vehicle uses position, velocity, or acceleration sensors to monitor the movement of the base during the manipulator actuation. Once the state of the vehicle is altered the on-board actuators counter the reaction forces to return the base to the desired state. This is referred to as station keeping. [18]

#### Examples

This method is the current industry standard in Remotely Operated Vehicles (ROVs) in the subsea field. [18] Two pilots remotely control the robot, one to maintain the base position, another to perform the manipulation task. Feedback base control is also used in cable robots where force sensors are attached to the cable to use an automated closed loop position control. [34]

In the early development of aerial manipulation there were control schemes which used a quadrotor to perform reactive station keeping during manipulator motion. [5] Since a quadrotor is underactuated with 4 DOF it cannot exert a reaction force in any direction. Therefore, some novel UAVs have been proposed with 6 rotors that are tilted, as shown in Figure 2.13, so that they can exert a force in any direction. [35]



**Figure 2.13:** Hexrotor with tilted propellers for force exertion. Source: [35]

### *Discussion*

This method is one of the most simple to apply and in many cases was the first step towards mobile manipulation. However, there is no guarantee that the system remains stable as the vehicle actuators can become saturated and as a result uncontrollable. It also results in imprecise positioning as the vehicle senses and responds to disturbances with a limited bandwidth.

### **Feed Forward Base Control**

Similar to the previous method the manipulator moves and the base actuators provide a reaction force to maintain the position and stability of the vehicle. However, in this method a dynamic model of the manipulator-vehicle interaction is created. The calculated compensation of the base is then performed preemptively.

### *Examples*

This method is used in all fields besides ground robots. In the space domain free flying spacecraft (those with base actuators) use a combination of reaction wheels and thrusters to maintain their orientation with respect to earth. [1] A kinematic and dynamic model of the spacecraft and manipulator are generated. For small perturbations reaction wheels which use gyroscopic actuation are used to steady the base, for larger perturbations the thrusters are used. [1]

For both UAVs and AUVs a nonlinear, coupled dynamic model is created. Then a wide variety of advanced techniques are used to control the simultaneous system including impedance, backstepping, LQR, and more. [4] [18] A significant majority of the research is on linearizing or simplifying the model so that the onboard processor can quickly and accurately control the vehicle.

In the cable robot field a model of the expected disturbance forces at the base as a result of end effector disturbances is then treated as a trajectory error at the cable actuator. [36] This is likely how in Figure 2.14 a cable robot can suspend a heavy manipulator.

### *Discussion*

This method has been researched in depth by applying a wide variety of advanced control techniques to various fields. The benefit is that off-the-shelf components can be readily applied and stability can be maintained. However, there is still a significant power consumption in cancelling the reaction by using the base actuators. Additionally, the models are highly complex and require more computational power than is typically available on, for instance, a UAV. [4] This method constantly has a trade off between computation time and accuracy.

### **Dual or Multi Arm Control**

Instead of using the base actuators another method is to actively control another arm or multiple arms. The basic principle is that in order to cancel the reaction forces another arm can perform a similar but mirrored motion.



**Figure 2.14:** Cogiro Cable Robot with industrial manipulator. Source: [37]

### Examples

In the first case an additional arm or arms are used purely for stabilization. This method has been used in space, UAV, cable, and underwater robots. In [38] the reaction forces from the motion of a 6 DoF arm on a space satellite is cancelled by a separate 3 DoF arm, as shown in Figure 2.15. The trajectory of the reaction arm is planned such that the centroid position is maintained. [38] On a UAV two arms are moved simultaneously and mirrored about the horizontal centre to cancel the forces in the horizontal and vertical direction. [39] In the cable field two arms are moved mirrored in the vertical centre as shown in Figure 2.16 . [40] It has been proposed in the underwater field to use multiple small arms as paddles to stabilize the base. [18]

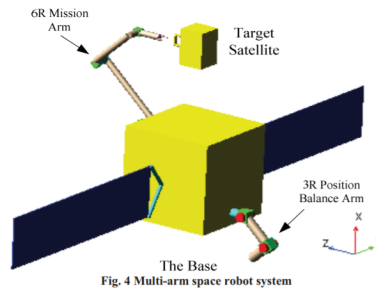


**Figure 2.15:** Second Arm for stabilizing satellite. Source: [38]

In the second case, the additional arm is used for the manipulation task. Using a dual arm aerial manipulator, valve opening was performed with the help of the symmetric arm configuration and the pure rotational yaw motion. [8] The aerial manipulation process is shown in Figure 2.17. In the space domain the secondary arm can be used for a coordinated capture and manipulation. For the initial motion towards the object, a virtual base was assigned to one end effector and the rest of the manipulator links and base were treated as a hyper redundant manipulator. [19] The modelling is shown in Figure 2.18.

### Discussion

In the case where the additional arm is used purely for stabilization this may be more effective than using the base actuators if the power consumption is lower. However, by adding another arm purely for stabilization the added weight and complexity is not efficient. If, however, a second arm is required for the manipulation then a coordinated approach can be quite effective. The limitation is that if the arms need to move independently then a reaction will be generated. Additionally, most papers only propose two arms but to completely balance

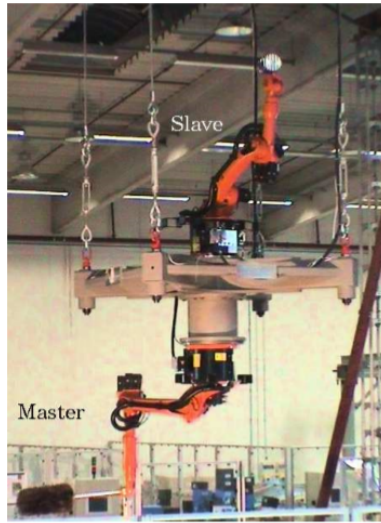


**Figure 2.16:** Master and slave arm suspend by cables. Source: [40]



**Figure 2.17:** Dual arm aerial manipulation for valve turning. Source: [8]

the system four arms would be needed, which further increases the weight and complexity.

### Reactive Mechanism Control

This method involves adding a separate mechanism or creating a novel architecture with some form of active control to cancel or eliminate the reaction force or moment on the base. It includes using a moving mass, additional actuators, or an additional degree of freedom.

#### *Examples*

The most common way of having a reactive mechanism is to use a separate, actively controlled countermass. To limit the added weight the battery of a UAV has been placed on a slider to actively balance the motion of a manipulator. [9] Similarly, a pantograph based manipulator was developed which had on one side an end effector and on another an actively controlled countermass. [11] These are shown in Figure 2.19 and Figure 2.20 respectively. In subsea it has been proposed to maintain the attitude of the vehicle with an actively controlled rotating counterweight. [41] For a 6 wire cable robot with a manipulator, four active counterweights on sliders were added to the base for stabilization, as shown in Figure 2.21. [42]

There are also a variety of other separate mechanisms that have been proposed. Instead of having a sliding counterweight, the entire manipulator was placed on a controlled slider to maintain the attitude of a UAV, as

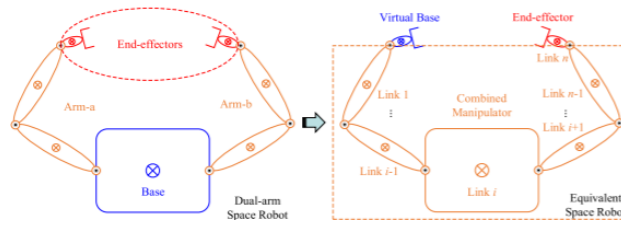


Figure 2.18: Coordinated capture model using hyper redundancy. Source: [19]

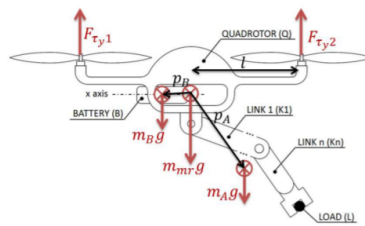


Figure 2.19: UAV with sliding battery as countermass. Source: [9]

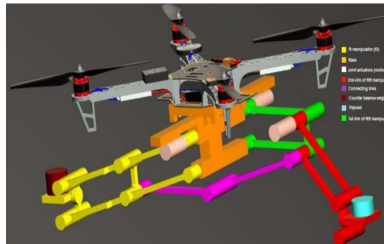


Figure 2.20: UAV with active pantograph balancing. Source: [11]

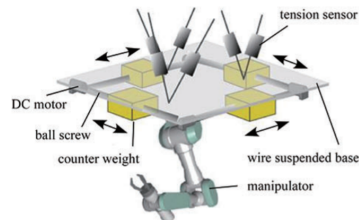
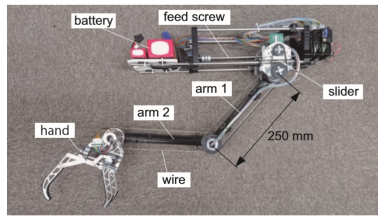


Figure 2.21: Cable robot with four sliding counterweights. Source: [42]



**Figure 2.22:** UAV with manipulator on slider. Source: [10]



**Figure 2.23:** UAV with fans to suppress swinging. Source: [43]

illustrated in Figure 2.22. [10] For an aerial vehicle with a slung load rather than a manipulator, a ducted fan device was attached to the end effector as shown in Figure 2.23. [43] This allows for a force to be applied at the end of the wire to suppress the swinging motion. [43]. Finally, a patent was filed for a payload management system on a UAV in which the internal packages were redistributed to maintain the CoG position. [44]

### *Discussion*

The solutions proposed can be quite effective in suppressing one of the reaction forces or moments using a countermass or an incorporated DoF. Having a separately controlled mechanism also allows for compensating environmental interaction and payload forces. However, typically only one force or moment is suppressed and the others must be countered via the base. For most of the methods this is the moment that impacts the attitude of the vehicle to avoid tip-over. For the methods that counter all of the reaction forces and moments the added weight and the modelling complexity is quite significant.

## **2.4 Discussion of Literature Review**

From the previous analysis it is apparent that the methods developed for one field can be applied to the others. For instance, the field of cable robots can be expanded greatly by applying most of the methods that have already been developed in other areas. For the control based methods in particular the space field is quite mature and can help expand the others. For active stabilization mechanisms, inspiration can be drawn from the aerial manipulation field.

Besides applying an already developed method to a new field there is an opportunity to expand on some methods which have not been explored in detail. In particular the passive methods are relatively unexplored in mobile manipulation. There are only a few examples and they are either very simple, for example just one counterweight, or they are only theoretical proposed and impractical, such as the balanced four bar based manipulator.

In terms of the three categories (avoidance, passive, and active), the passive methods have the most potential for mobile manipulation. The avoidance methods don't fully address the dynamic coupling impacts which are crucial to stability. The active methods require additional energy consumption, preemptively planning trajectories, limiting the allowable paths, or a level of computational power which is often not available on-board. The limitation of the passive category is that at the moment the solutions are either incomplete or purely theoretical.

In the passive category the most promising and challenging method is the inherently balanced architectures. By adding counterweights the mass and energy consumption grows. With inherently balanced configurations there are additional links, however, they are used for the manipulation task rather than just for balancing. Inherently balanced architectures in mobile manipulation is still in its infancy. However, its resolution of the shaking force and moments as well as its limited added weight makes it a very promising method. In addition, the active mechanisms are also promising in resolving an additional shaking force or moment. However, they don't scale well to resolving all of the shaking forces and moments. Therefore, if an inherently balanced architecture cannot fully resolve the shaking forces and moments, an active mechanism could be applied.

These methods could have the most significant impact in the UAV field. Currently aerial manipulation is limited by the complex models and processing time required for the current control methods. They greatly exceed the computational power of the available UAVs so they have to be planned in advance. While many of the other fields have resolved the dynamic coupling impacts enough to achieve most tasks, aerial manipulation is still behind in commercial application. A successful resolution could bring this field to fruition.

## 2.5 Conclusion

From the outcome of the literature survey it is apparent that applying inherently balanced architectures to aerial manipulation is the most promising area of research. With inherently balanced configurations there are additional links, however, they are used for the manipulation task rather than just for balancing. Due to its resolution of the shaking force and moments as well as its limited added weight, this makes it a very promising method. In cases where inherent balancing cannot fully resolve some of the reaction forces or moments, adding an active approach can also be promising. This is because the active mechanisms were shown to effectively eliminate an unresolved shaking force or moment for many different manipulator configurations with minimal adjustments. Aerial manipulation is one of the most challenging fields for floating base manipulation; the solutions which are effective in this field can be translated to the others. The inherently balanced architecture method is the most suitable for its guaranteed stability, low energy consumption, and functional added weight.

# 3 | Design of a Lightweight 3 Degrees of Freedom Manipulator with Inherent Dynamic Balancing

## 3.1 Introduction

In the previous chapter it was identified that applying inherent dynamic balancing principles to the field of aerial manipulation has significant potential. The aim of this chapter is to synthesize an inherently dynamically balanced manipulator for a UAV. First the intended application is described and design requirements are set. Next the possible synthesis methods are described including using inherent dynamic balancing to resolve the reaction forces and a combination of passive and active methods to resolve the moment balancing. By applying these methods a variety of concepts are created. Finally one concept is selected and a detail design is described. The design from this then used as a basis in the next chapter to develop a novel control scheme.

## 3.2 Application

In the literature UAVs augmented with manipulators have been proposed as a solution for a wide variety of tasks, typically involving: reaching out and making contact, performing a pick and place operation, or a dexterous manipulation. [4] However, the capabilities of aerial manipulation are still very limited. The tasks that have actually been performed in the literature are very simple. Additionally, UAV operators in industry were contacted. Most currently only perform visual inspections with the UAVs and one company used a rigid rod attached to the UAV to try to make light contact with a surface.

Reaching out and performing a light contact was then selected as the task. UAV operators were contacted to determine the potential applications for this technology and the requirements. One option was close proximity sensing of orchards and vineyards in agriculture. The UAV flies through the orchard while the manipulator reaches through the canopy to check for infestations. Another option was to perform ultrasonic thickness inspection of wind turbines and oil storage tanks. The UAV approaches the surface, and the manipulator reaches out with an ultrasonic probe to make contact with the surface and measure the thickness. This would then be used to determine the structural integrity of the turbine blade or oil tank. Both of these application had similar design requirements. They are described in the next section.

## 3.3 Design Requirements

The UAV is tasked with providing the course positioning and performing station keeping. The manipulator performs a fine positioning tasks to scan a surface and make light contact. In order for the UAV operators to adopt this new technology there were a variety of requirements. The manipulator could not impart reaction forces or moments on the UAV. The UAV operators would not fly closer than 2m to an object for safety so the manipulator had to have a reach of 2m. The manipulator had to be configurable with their fleet of heavy lift UAVs in terms of payload and sizing. One heavy lift UAV, the DJI s1000, was selected. [45] These design requirements were formalized and are described below. Functions are what the design must do to meet its goal, objectives are what the design should optimize, and constraints must be met in order for the design to be viable. Figure 4.1 shows the task requirements and Figure 4.2 illustrates the UAV sizing limitations.

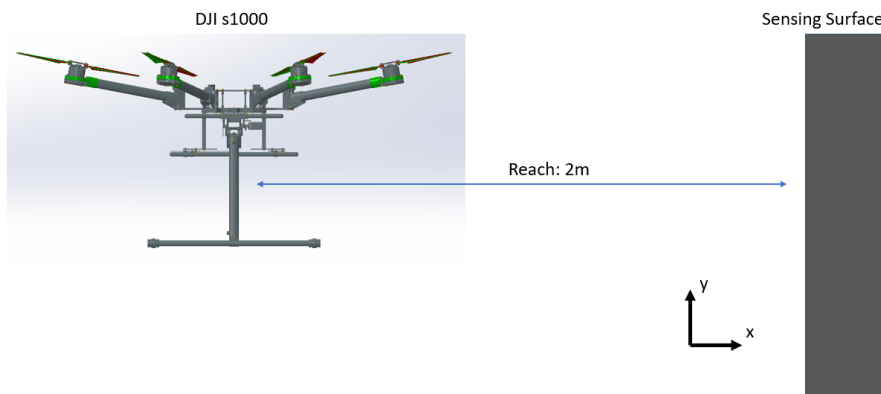


**Figure 3.1:** Orientation and position of the UAV when performing the task: 2m away from a vertical wall. Axis directions are defined.

**Functions:**

- Perform fine positioning in 3 DoF ( $x, y, z$ )
- Reach Beyond the UAV base ( $x$ )

**Objectives:**

- Minimize weight of the manipulator
- Maximize the reach for the sensor

**Constraints:**

- Reactionless
- Weight of Manipulator:  $< 6.8\text{kg}$  [45]
- Support Payload:  $> 300\text{g}$
- Reach:  $> 2\text{m}$  ( $x$ )
- Can't interfere with UAV or landing gear

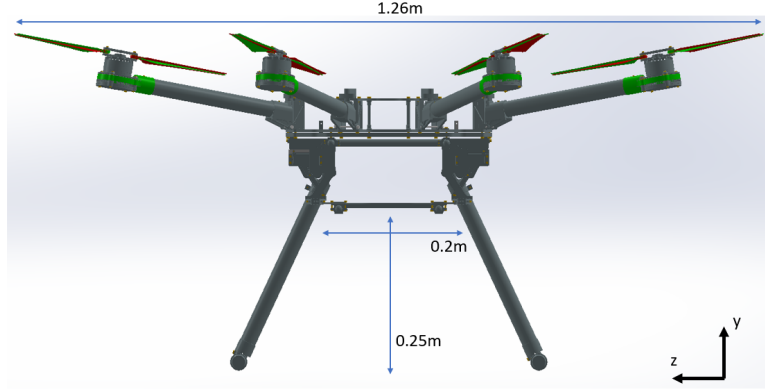


**Figure 3.2:** Dimensions of the reference UAV for compatibility: DJI s1000. [45]

### 3.4 Synthesis Methods for a Reactionless Manipulator

To create a reactionless manipulator both the shaking forces and shaking moments had to be resolved in the design. The first section details the method applied for resolving the shaking forces which is inherent dynamic balancing. The second section details the methods to resolve the shaking moments which include both passive and active options.

#### 3.4.1 Force Balancing: Inherent Dynamic Balancing

There are many force balanced architectures that have been identified in the literature. In [46] van der Wijk used the method of principal vector linkages to identify force balanced architectures up to 4 DoF. These are typically in-plane, however they can be extended to spatial arrangements. [46] Van der Wijk used the method of linear momentum to define the force balance conditions. [46] The 3 DoF standard pantograph architecture is shown as an example in Figure 3.3. In this Figure the solid lines are linkages and the circles are joints. The link masses are modelled with a lumped centre of mass  $m$  at a vector position defined by  $p$ . The vectors  $a$  are the lengths that are critical to the force balance conditions which will be described later.  $S$  is the invariant common centre of mass (CoM) of the entire architecture. In this paper the centre of mass of each link will remain in line with the respective link. By fixing point  $S$  to the base of the UAV, no shaking forces are applied since the position of the centre of mass remains constant.

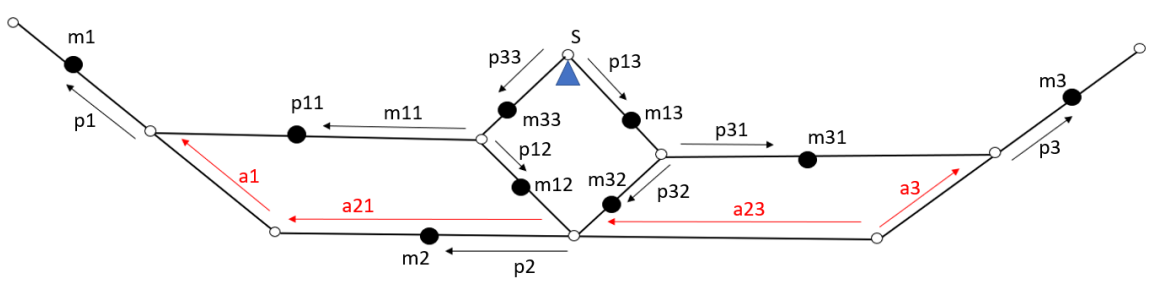


**Figure 3.3:** Standard 3 DoF Pantograph Principal Vector Linkage Architecture [46].  $S$  is the common CoM and the base joint. Lumped masses are  $m$ , the positions of the link CoM are  $p$ , and the critical lengths for balancing are  $a$ .

In [47] and [48] van der Wijk identified the Grand 4R and Grand 5R which contain the complete, pantograph

based, inherently force balanced architectures in 2 DoF and 3 DoF respectively. Van der Wijk, however, only identified closed architectures. Novel open architectures have the potential to achieve a higher reach for a given weight. In this paper the inner and outer links were removed from the highly redundant architecture while maintaining the same kinematic degrees of freedom. An arrangement was first highlighted from the Grand 4R. It had to pass through the common CoM and incorporate linkages on either side for balance. Next the kinematic degrees of freedom were checked using the formula below where  $n$  is the number of linkages and  $j$  is the number of joints.

$$DoF = 3(n - 1) - 2j$$

To increase the number of DoFs linkages were removed. To decrease the number of DoFs linkages were extended to another joint as long as the Grand 4R architecture allowed it. The linkages can also be extended beyond the joint to add an additional reach for manipulator or a counterweight for a certain DoF.

An example for a novel 2 DoF mechanism derived from the Grand 4R is shown in Figure 3.4 which is termed the Double Four. In this figure the Grand 4R architecture is shown with the over-layed black lines indicating the new arrangement. In the case of the Double Four,  $n = 7$  and  $j = 8$  which confirms it has 2 DoF. Figure 3.5 illustrates the Double Four architecture.

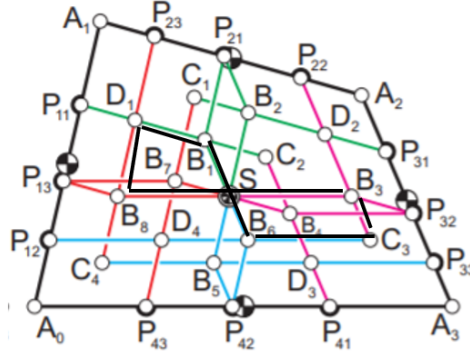


**Figure 3.4:** Derivation of an Open Architecture from the Grand 4R. The redundant, force balanced Grand 4R is composed of the colourful links. The new derivation is over-layed in black.  $S$  is the invariant common CoM of the entire architecture.

Finally the force balance conditions were derived using van der Wijk's method of linear momentum. [46] This yielded the force balance conditions listed below in which  $m_2^a = m_2(1 - p_2/L_2)$  and  $m_2^b = m_2(p_2/L_2)$ .

$$\begin{aligned} m_2^a a_1 - p_1 m_1 &= 0 \\ (m_1 + m_2^a + m_5) a_2 - m_4 p_4 - L_4 m_5 - m_6 p_6 &= 0 \\ (m_2^b + m_6) a_3 + m_3 p_3 - p_5 m_5 - L_3 m_6 &= 0 \end{aligned}$$

Additional 2 DoF force balanced architectures that were derived from the Grand 4R, and 3 DoF architectures from the Grand 5R are listed in Appendix C. Simple 2 DoF architectures were found from the Grand 4R, however, on expanding to the Grand 5R the novel architectures became far more complex than the standard ones. Therefore, for manipulators greater than 2 DoF the traditional arrangements from [46] are preferable for their simplicity.

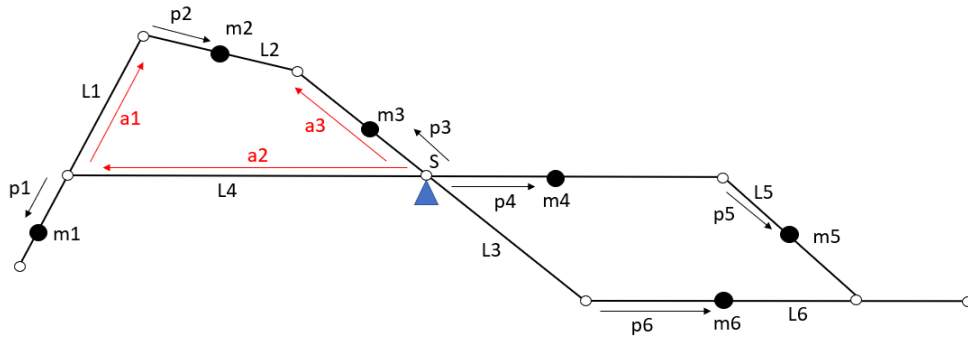


**Figure 3.5:** Newly Derived Double Four 2 DoF Force Balanced Architecture. S is the common CoM and the base joint. Lumped masses are  $m$ , the positions of the link CoM are  $p$ , and the critical lengths for balancing are  $a$ .

### 3.4.2 Moment Balancing: Passive and Active Methods

Given an architecture that is already force balanced, the reaction moment must then be resolved to construct a completely reactionless manipulator. There is no effective theoretical method in the literature to resolve the moment balance inherently. Therefore, synthesis methods were generated to resolve the shaking moment both passively and actively. The passive options were to mirror the architecture or to kinematically reduce the DoFs. The active options were to add a counter rotating mass, or actively reducing the DoFs. Each of these methods are described below.

#### Duplicate Mirrored Architecture

The simplest method to ensure moment balancing is to add an identical but mirrored architecture. For each rotation there is an equal, opposite rotation. Using the Double Four from the previous chapter, a 2 DoF reactionless manipulator was constructed using two separated connections to the base as in Figure 3.6 or at one point as in Figure 3.7. In both cases they were joined by extending link 6 and adding a joint at the connection. The previous force balance conditions still applied. This method would significantly add weight when constructed as a manipulator. However, for heavy lift applications or those requiring high stiffness, the redundant connections to the base could be useful.

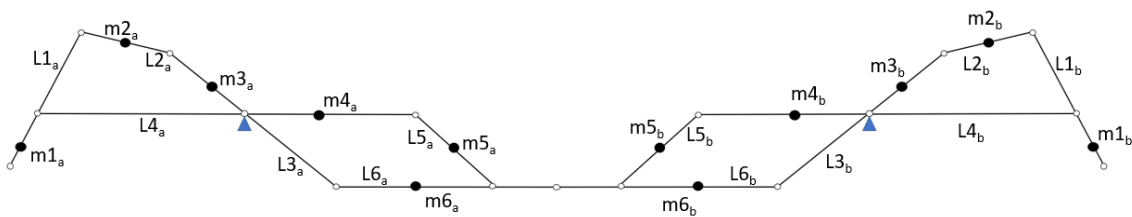


**Figure 3.6:** Duplicate Mirrored Moment Balancing of the Double Four with Separate Base Connections. The base connections are shown in blue.

#### Kinematic Degree of Freedom Reduction

In [17] van der Wijk reduced a 2 DoF pantograph to a 1 DoF moment balanced mechanism by applying an internal motor to find the reactionless path and constraining the mechanism to this path by a slider. To

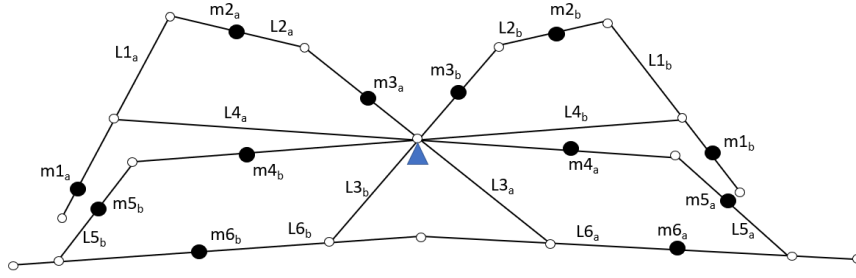


**Figure 3.7:** Duplicate Mirrored Moment Balancing of the Double Four with Conjoined Base Connections.

determine whether this method could be extended to higher dimensions, this paper investigates reducing a 3 DoF force balanced architecture to a force and moment balanced 2 DoF architecture. Artobolevski's alternative form to the 3 DoF architecture was used; as identified in [46] and shown in Figure 3.8.

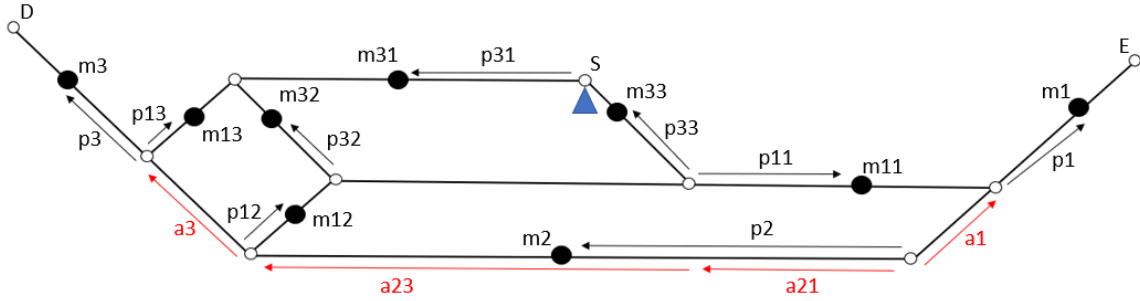


**Figure 3.8:** 3 DoF Force Balanced Architecture: Artobolevski's Alternative [46]. S is the common CoM and the base joint. Lumped masses are  $m$ , the positions of the link CoM are  $p$ , and the critical lengths for balancing are  $a$ .

To determine the reactionless paths of a point attached to a link, the 3 DoFs were actuated in connection to the base with torques  $T_1$  acting on link 31,  $T_2$  acting on link 33, and  $T_3$  acting on link 13. For a range of torques  $T_1$  and  $T_2$ ,  $T_3$  was actuated to ensure moment balance according to the formula:  $T_1 + T_2 + T_3 = 0$ . The path generated by point D in Figure 3.8 was plotted as shown in Figure 3.9. For more information on the simulation refer to Appendix D.

The path for both  $x$  and  $y$  relative to the base was shown to change for different applied torques. By limiting the point to a slider path a reaction force will be generated since it will be forced off the reactionless path. Another option is to find a consistent relative distance in both  $x$  and  $y$  of two points to create a new link. However, the position of these will also change for varying torques. To address this, one option is to optimize the relative masses, lengths, and inertias as well as the point location on the links to minimize this reaction force. This is referred to as partial balancing. This method would have to be determined for each instance and would only work for a small range. The goal of this paper, however, is to instead find a global, inherent solution.

### Active Counter Rotating Mass

Since the passive methods do not effectively resolve the reaction moment, an active solution was implemented. In literature it is common to attach a separate, actively controlled counter rotating mass to cancel the reaction moment. The counter rotating mass can be connected to the base at any location, so the weight of the counter rotating mass can be used to balance the weight of a manipulator. However, this method adds signif-

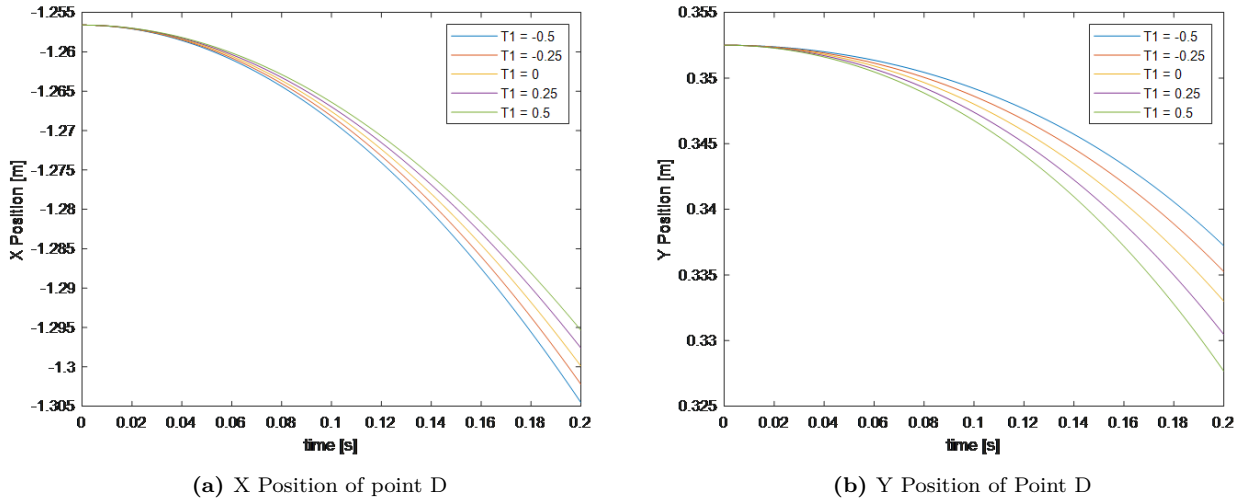


**Figure 3.9:** Path of Point D from Moment Balanced Artobolevski's Alternative for Varying Torque 1 Inputs. This shows a consistent slider path cannot be found.

icant weight as a large counter rotating mass must be attached to achieve a similar reaction moment to the manipulator.

### Active Degree of Freedom Reduction

Instead of adding a counter rotating mass, another active method is to constrain the manipulator to a reactionless path using an additional actuator. This achieves the same goal as kinematic reduction. If all three actuators are connected to the base, as described in the kinematic reduction section, then the third actuator torque is calculated as before. However, if only two actuators are connected at the base, for instance to actuate link 31 and link 11 from Figure 3.8 then the sum of these two torques must be zero. The third actuator applies the torque internally, in which case the torque only generates motion of the manipulator. A control method is required for a 3 DoF manipulator such that for a given X,Y (2DoF) end effector position the 3 actuators will arrive at that point with a moment balanced motion.

## 3.5 Conceptual Designs of 3 DoF Reactionless Manipulators

Conceptual designs were generated using the force and moment balancing theory developed in the previous sections. It was shown in Section 3.4.1 that there are a wide variety of force balanced architectures. These can also be adapted out of plane to create spatial architectures. However, the moment balancing theory and synthesis techniques limit the possibilities for synthesis. The different arrangements are described below, the first few using passive moment balancing techniques and the last few using active techniques.

### 3.5.1 1 DoF Combinations - Passive

In literature there are already examples of combining 1 DoF balanced units in serial and parallel arrangements. [49] [15] In using a force and moment balanced four bar the complexity grew substantially. [15]. One conceptual design is to use the reduced pantograph that is force and moment balanced as described in [17]. This was

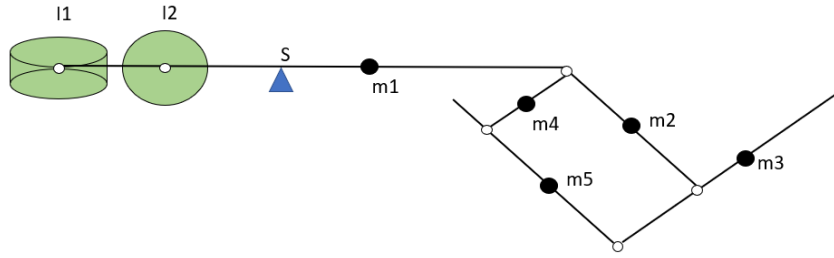


**Figure 3.10:** 2 DoF Inherently Force Balanced Architecture Actuated Out of Plane with 2 Active Counter Rotating Masses. The green disks are counter rotating masses, S is the base joint,  $m$  is the respective link mass.

arranged in both a serial and parallel configuration. Since these arrangements are already inherently force and moment balanced they create a passive solution.

### 3.5.2 Parallel Combination of Mirrored 2 DoF Inherently Balanced Architectures - Passive

By taking the mirrored Double Four of Figure 3.7 and adding spherical joints, the 2 DoF architecture was used to create a 3 DoF manipulator. This arrangement is also moment balanced by symmetry out of plane. This creates a passive arrangement.

### 3.5.3 3 DoF Inherently Force Balanced Manipulator with 3 Counter Rotating Masses - Active

By incorporating active moment balancing, another option was investigated by using a 3 DoF force balanced architecture such as the classic principal vector linkage of Figure 3.3. This arrangement was made spatial by adding spherical joints. Then 3 separate active counter rotating masses were attached to the base of the UAV to compensate for the shaking moments in each plane. This active solution requires a significant addition of weight and complexity.

### 3.5.4 2 DoF Inherently Force Balanced Architecture with 2 Counter Rotating Masses - Active

Another method developed was to use a 2 DoF inherently force balanced architecture, such as a standard pantograph. These 2 DoF were actuated in plane while the entire architecture was also actuated out of plane to achieve 3 DoF. Finally both the moment in plane and out of plane was countered by 2 separate, actively controlled counter rotating masses. The pantograph was placed at the end of a rigid beam and the reaction wheels were placed at the other. In order to ensure force balance the weight of the counter masses was balanced by the weight of of manipulator to ensure the centre of gravity remained at the base of the UAV. This option is illustrated in Figure 3.10 where the green disks indicate the counter rotating masses.

### 3.5.5 3 DoF Actively Reduced Balanced Architecture and 1 Counter Rotating Mass - Active

A 3 DoF force balanced architecture which is actively reduced to a 2 DoF force and moment balanced architecture was implemented. One option was to use the standard 3 DoF arrangement shown in Figure 3.3 . Another option

was to use an asymmetric alternative form which is known as Artobolevski's alternative. This is illustrated in Figure 3.8. By using this alternative form a longer reach was achieved by the manipulator.

This architecture was combined with a 1 DoF balanced unit. One option was to first attach the 2 DoF unit to the base of the UAV at point  $S$  and then add an out of plane 1 DoF unit at point  $E$ . Some options for the 1 DoF unit were equal opposite sliding masses or a counter rotary counter mass. The 2 DoF unit would have to support the weight of the 1 DoF unit. This would make the links larger which would add significant weight. A better option was to rotate the 2 DoF unit out of plane at point  $S$ . To counter the moment an active counter rotating mass was used. Alternatively, the rotation of the UAV could be used as the moment in this plane does not impact the tip-over stability of the UAV. This concept is illustrated in Figure 3.11.

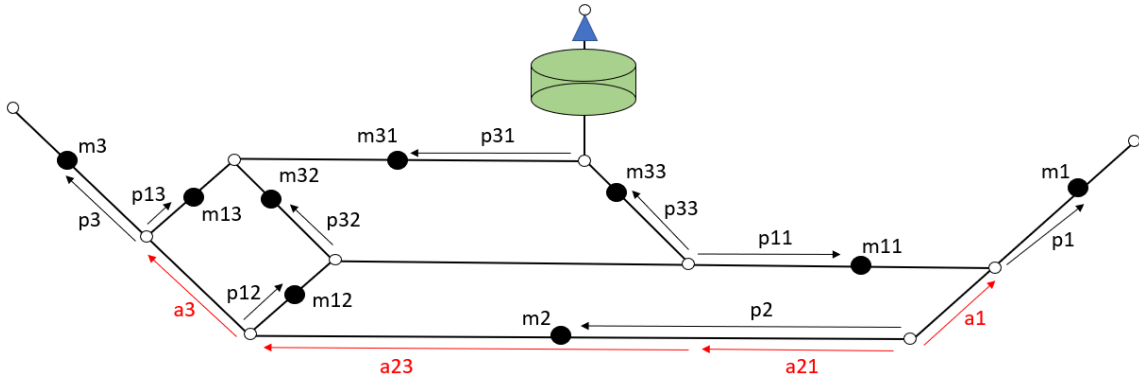


**Figure 3.11:** 3 DoF Spatial Manipulator: Actively balanced Artobolevski's alternative with out-of-plane rotation.  $S$  is the common CoM and the base joint and the green disks are counter rotating masses. Lumped masses are  $m$ , the positions of the link CoM are  $p$ , and the critical lengths for balancing are  $a$ .

### 3.6 Concept Selection

The serial 1 DoF rotation with a 3 DoF actively reduced architecture from Figure 3.11 was used to achieve this task. The configuration allows for a long reach in the  $x$  direction. The weight can be reduced by using fewer linkages than the other alternatives. It also does not impede the foldable landing gear when deployed. Artobolevski's configuration was used over the standard 3 DoF architecture because the asymmetry can be used to extend the length of one side of the manipulator while maintaining the force balance conditions.

### 3.7 Detailed Design

The final design is shown in Figure 4.3. The manipulator was designed to be constructed from square aluminum 15mm by 15mm beams with a 1mm wall thickness. A basic finite element analysis was used to confirm the structural integrity of these beams; this is described in detail in Appendix E. The beams were designed to be joined using steel plates with an axle and bushings. The end effector was placed at the end of link 1 with a 300g payload for the sensor. The motors to actuate link 31 and link 33 were placed at the base. The third motor was placed on link 3 to actuate the joint connecting link 13 and link 3. It was placed in this location as a counterweight to increase the reach of the manipulator.

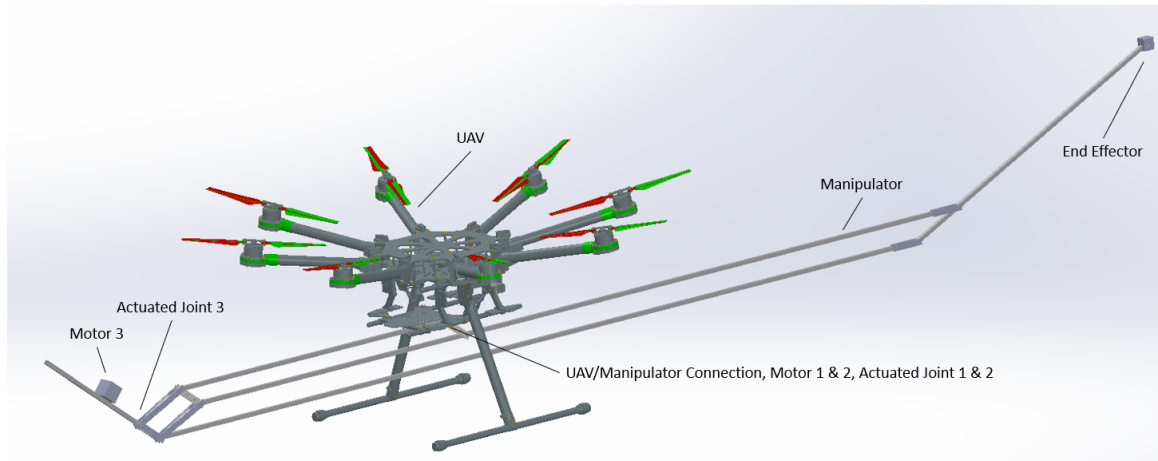


**Figure 3.12:** Design of a 3 DoF Reactionless Manipulator Attached to a UAV. The base attachment, end effector, and motor positions are indicated.

### 3.8 Discussion

A novel manipulator was designed using inherent dynamic balancing which was lightweight, reactionless and 3 DoF. Therefore, the aim of this Chapter was achieved. The design meets the requirements set in industry for close proximity sensing. Its below the weight budget of the UAV with remaining budget for additional components. It reaches 2m and is compatible with the UAV.

The inherently force balanced architectures effectively resolved the issue of shaking forces. New architectures were derived, however, the original offer the best options for a UAV. The best architecture was found for this application, and in searching, options for other applications were also found.

The area that must be improved is the synthesis for moment balancing. In theory the best option is a passive kinematic one, however, there is no indication that one exists. A partial solution could be useful in cases of small displacements or when the paths stay relatively consistent. An active approach is more versatile. Using counter rotating masses is not ideal because it adds a significant weight to the manipulator. The best option is to reduce the architectures actively. However, a method to achieve this must still be developed. By increasing this to higher dimensions a higher DoF manipulator can be synthesized with fewer counter rotating masses.

### 3.9 Conclusion

Using inherent dynamic balancing principles, a novel manipulator was synthesized for a UAV which was lightweight, reactionless, and 3 DoF manipulator. It can achieve the task of reaching out and making contact to sense an external surface. It was found that the best design required taking a 3 DoF inherently force balanced architecture and actively reducing it to a 2 DoF force and moment balanced architecture. The control scheme for moment balancing through reduction must still be developed. This is done in the next chapter.

# 4 | Control for Active Moment Balancing of a 2 Degrees of Freedom Inherently Balanced Manipulator for an Unmanned Aerial Vehicle (Paper)

## 4.1 Abstract

In aerial manipulation, Unmanned Aerial Vehicles (UAVs) are equipped with manipulators to perform a variety of tasks, including sensing in hard to reach areas. A significant limitation of equipping UAVs with manipulators is that the shaking forces and shaking moments of the manipulator cause the UAV to become unstable. To resolve this, an inherently dynamically balanced manipulator was designed in the previous chapter which does not impart shaking forces and moments to the UAV. It was found that the lightest and most compatible manipulator design required a novel control methodology for active moment balancing which will be developed in this paper. For a state of the art 2 DoF manipulator in a 2 DoF workspace, there is one motion that moves the manipulator from the end effector initial position to its desired position. For a 3 DoF inherently force balanced manipulator in a 2 DoF workspace, there are infinite motions which achieve the desired end effector position. The challenge is to create a control methodology such that the manipulator achieves the end effector position with no reaction moment generated. This is achieved by selecting the manipulator motion such that the angular momentum is minimized and then adjusting the input torques. These methods are applied to a rigid body feedforward control scheme for a 3 degrees of freedom force balanced architecture in a 2 degrees of freedom workspace. A simulation is performed to validate the method, and it is found that the method achieves moment balancing. The tracking of the desired end effector path is better for small displacements and further work can yield better performance for larger displacements.

## 4.2 Introduction

In mobile manipulation a manipulator is attached to a mobile robot to expand its workspace. [1] Within this field, aerial manipulation is when an Unmanned Aerial Vehicle (UAV) is used: typically a quadcopter or octocopter. [3] Aerial manipulation can be used to perform a variety of tasks including: reaching out and making contact for an inspection, performing a pick and place to move a payload, or performing a dexterous manipulation for a repair. [4] This paper focuses on reaching out from the UAV and performing a light contact with an external surface to perform close proximity sensing. This can be used, among others, to check for infestations in crops for agriculture or to check the structural integrity of critical infrastructure. [4]

The problem with attaching a manipulation to a UAV is that the reaction forces and moments of the manipulator, referred to as the shaking forces and moments, cause the UAV to become unstable. This is because the shaking forces and moments cause the UAV to tip and become uncontrollable. First control based methods were applied in which the UAV provided a compensation force or moment at the propellers. [5] [4] However, the dynamic model required was too complex to compute onboard in real time. A better method is to resolve the shaking forces and moments at the manipulator so that they are not transferred to the UAV. This involves designing the

manipulator such that it is dynamically balanced. First passive methods were explored using counterweights to force balance [12] [13], which significantly increased the weight. Next inherently balanced architectures were developed, however, they only incorporated lower degree of freedom (DoF) balanced units which does not scale well to higher DoFs. [15] [16] [17]. Additionally, a variety of active mechanisms were applied to the attached manipulators to partially resolve shaking forces or moments [9] [10] [11]. These methods were either limited to only resolving one shaking force or moment or to only resulting in a one DoF manipulator. Finally, counter rotating masses have been applied for dynamic balancing, however, they add a significant amount of weight. A preferable option would be to construct a higher DoF dynamically balanced manipulator. In this way the architecture not only provides the structure of the manipulator but also ensures balancing.

A 3 DoF reactionless manipulator using inherent force balancing was developed to be attached to a UAV. The manipulator incorporated a 3 DoF inherently force balanced architecture for a 2 DoF planar workspace for active moment balancing. This is because for any end effector path there exists a manipulator motion in the 2 DoF workspace such that the manipulator does not impart a reaction moment. The challenge is in creating a control methodology to achieve this form of active moment balancing. For a state of the art 2 DoF manipulator in a 2 DoF workspace, the motion to achieve the desired end effector position is given. However, for the novel manipulator, a control methodology must be created which resolves the kinematic redundancy and selects the manipulator motion that eliminates the shaking moment.

The goal of this paper is to develop a control based approach for active moment balancing of a 3 DoF force balance architecture in a 2 DoF workspace.. This will be achieved by first outlining the application and manipulator design in Section 4.3 and Section 4.4 respectively. Next a control based method will be proposed in Section 4.5. To evaluate these methods they will be applied to a multibody dynamic model in a simulation in Section 4.6. An end effector path will be prescribed and the resulting tracking error and reaction forces and moments will be shown in Section 4.7. Finally, the effectiveness of the approach will be evaluated in Section 4.8.

### 4.3 Application

UAV operators were contacted to determine potential applications. While the literature has proposed complex tasks for aerial manipulation, most operators still only use UAVs for filming and visual inspections. This is because the state of the art is still not able to handle complex interaction tasks with many external forces and moments. Therefore, the task selected was the simplest in terms of external forces and moments: to reach out and perform a light contact from the hovering UAV. This can be used for sensing in a variety of industries such as: infestations in agriculture, or ultrasonic thickness testing for wind turbines.

There is a need by UAV operators to have the manipulator be configurable with their current heavy lift UAVs, such as the DJI s1000 [45]. Therefore, the manipulator had to weigh less than 6.8 kg and not interfere with the UAV in terms of sizing. [45] They wanted the UAV to remain 2m away from the sensing surface to ensure the propellers would not make contact from a wind gust. Therefore, the manipulator had to have a long reach for the given weight. The UAV had to be 3 DoF for fine positioning in  $x, y, z$  while the UAV performed course positioning. The manipulator had to hold a 300g sensor as the end effector. Figure 4.1 shows the required orientation of the UAV and defines the axes. Figure 4.2 illustrates the UAV dimensions for reference; the UAV must be configurable with these dimensions.

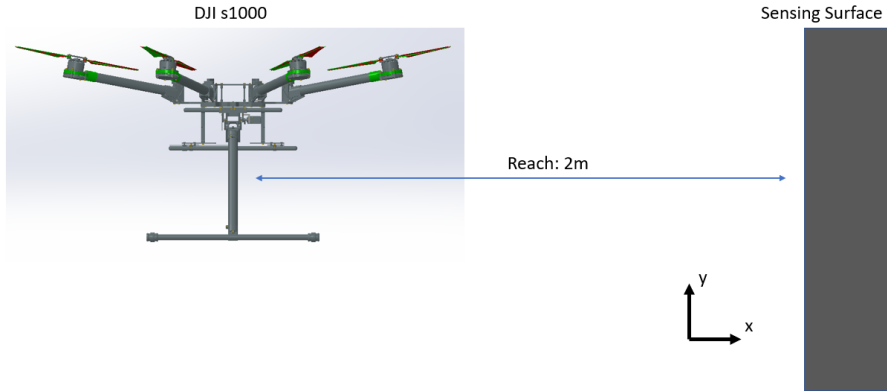


**Figure 4.1:** Orientation and position of the UAV when performing the task: 2m away from a vertical wall. Axis directions are defined.

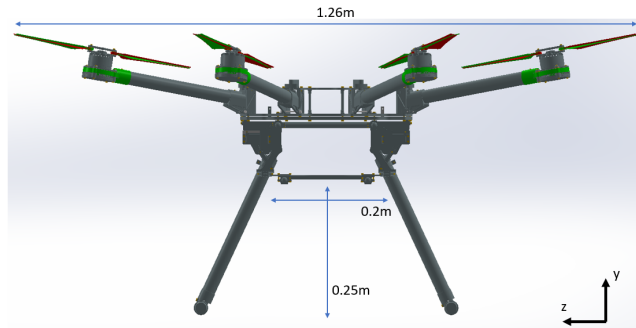


**Figure 4.2:** Dimensions of the reference UAV for compatibility: DJI s1000. [45]

## 4.4 Manipulator Design

A manipulator was designed for the application described in the previous section. The design is shown in Figure 4.3. The manipulator was created based on Artobolevski’s configuration which is a 3 DoF force balanced architecture. [46] This architecture was used to achieve the  $x, y$  plane positioning of the end effector. For the  $z$  positioning a rotational DoF was applied at the base with an active rotary counter mass. The focus of this paper is on the 3 DoF force balanced architecture in-plane.

The sensor end effector was placed at the rightmost point, as indicated in Figure 4.3. The manipulator is connected to the UAV at one point which is shown in the figure. The manipulator is actuated by three motors. The first two motors are connected to the base and actuate the two beams that are also connected to the base. The third motor is connected to the rightmost beam and actuates the joint labelled ”Actuated Joint 3” in Figure 4.3.

A kinematic and dynamic model was developed for the manipulator which is illustrated in Figure 4.4. The beams are represented as links with a lumped masses ( $m$ ) and inertias ( $I$ ) at the link centre of mass. In the figure the solid lines are linkages and the circles are joints. The position of the link centre of mass (CoM) and centre of distribution of the link inertia are defined by  $p$ . In this paper the centre of mass of each link remains in line with the respective link. The vectors  $a$  are link lengths which are used for the force balance equations which are derived later in this section. Point  $S$  is the invariant common CoM of the entire architecture. By

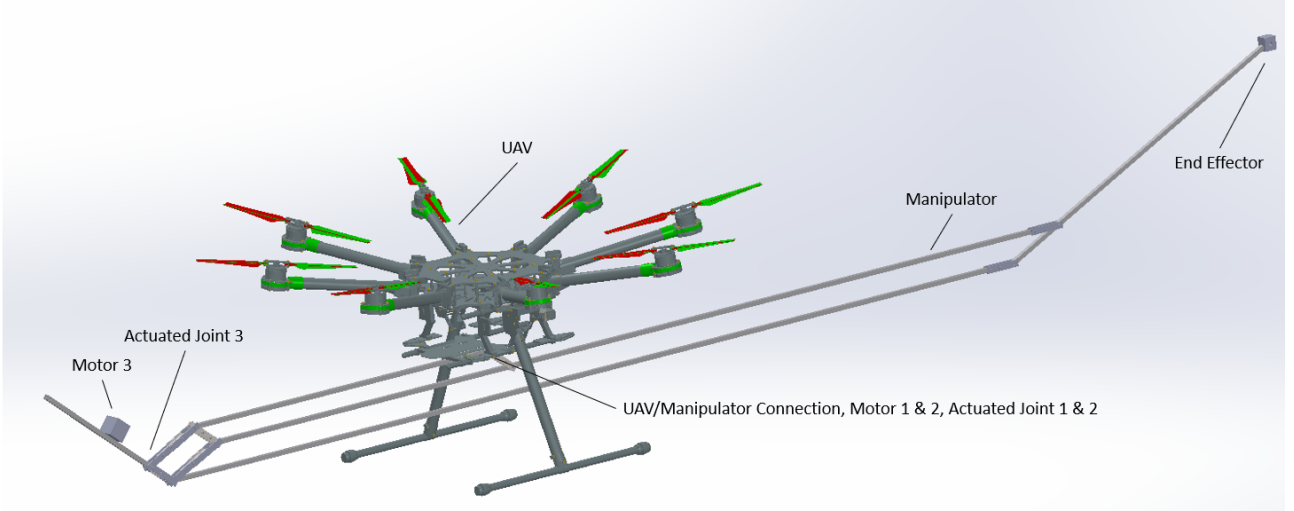


**Figure 4.3:** Design of a 3 DoF reactionless manipulator attached to a UAV. Base connection, end effector position, motor positions and actuated joints and all indicated.

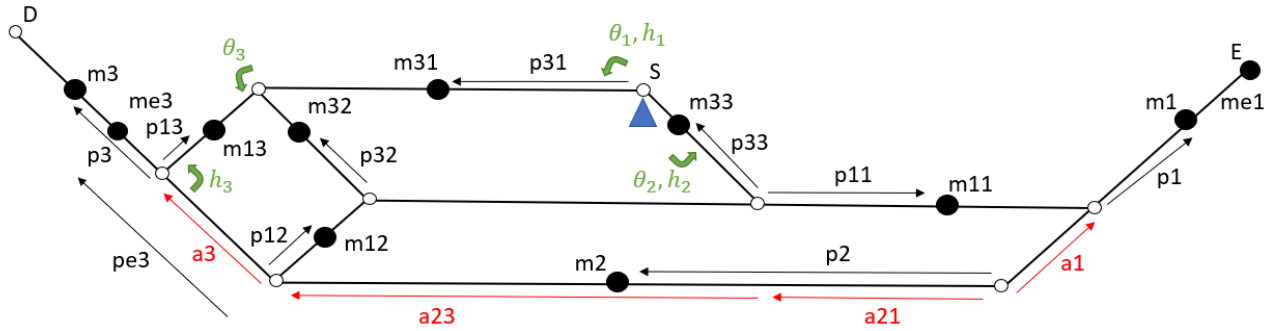


**Figure 4.4:** Manipulator kinematic & dynamic model with links, joints, lumped masses and locations of the link centre of masses.

fixing point  $S$  to the base of the UAV, no shaking forces are applied since the centre of mass of the architecture remains constant at the base of the UAV.

The three independent DoFs in Figure are indicated as:  $\theta_1, \theta_2, \theta_3$ . The angular position of these DoFs were measured using hinges, indicated by:  $h_1, h_2, h_3$ . The angular position of the first and second DoF were the same as their respective hinges, while the third DoF was measured at the joint between link 3 and link 13. Therefore DoF 3 was determined by a combination of  $h_2, h_3$ . The relation between hinges and angles are listed below. The motor torques were applied at the same points as the hinges.

$$\begin{aligned}\theta_1 &= h_1 \\ \theta_2 &= h_2 \\ \theta_3 &= h_3 + h_2\end{aligned}$$

The sensor end effector was placed at the rightmost point and the third motor was mounted on the leftmost

link as illustrated in Figure 4.3. In the model shown in Figure 4.4 the sensor and motor are modelled by lumped masses  $m_{e1}$  and  $m_{e3}$  respectively. The sensor is placed at point E at the end of the link and the third motor position is defined by  $p_{e3}$  as shown in Figure 4.4. Both are small components in comparison to the large manipulator, therefore, the inertia about their respective centre of masses is not considered. The motor placement was offset to help obtain greater reach while still maintaining the force balance conditions. The force balance conditions are listed below, where  $m_{tot} = 2.479\text{kg}$  is the total moving mass of the manipulator. The force balance conditions were derived using the conservation of linear momentum [46] and are listed below. In the table below the manipulator parameters are listed. The resulting lengths which are critical to the force balancing are:  $a_1 = 0.158\text{m}$ ,  $a_{21} = 1.414\text{m}$ ,  $a_3 = 0.071\text{m}$ .

$$a_1(m_{tot} - m_{11} - m_{33} - m_{32} - m_{31}) = m_1 p_1 + m_{e1} l_1 + m_{12} p_{12} + m_{13} p_{13}$$

$$a_3(m_{tot} - m_{31} - m_{13}) = m_3 p_3 + m_{e3} p_{e3} + m_{32} p_{32} + m_{33} p_{33}$$

$$a_{21}(m_{32} + m_{12} + m_{13} + m_3 + m_{e3} + m_1 + m_{e1} + m_2) = m_{31} p_{31} - m_{11} p_{11} + m_2 p_2 + l_2(m_{32} + m_{12} + m_{13} + m_3 + m_{e3})$$

Link Masses (g)	Mass Positions (m)	Link Inertias (kg m <sup>2</sup> )
$m_1 = 415$	$p_1 = 0.209$	$I_1 = 0.00865$
$m_2 = 406$	$p_2 = 1.044$	$I_2 = 0.223$
$m_3 = 119$	$p_3 = 0.016$	$I_3 = 0.00176$
$m_{11} = 415$	$p_{11} = 0.439$	$I_{11} = 0.225$
$m_{12} = 119$	$p_{12} = 0.070$	$I_{12} = 1.97 \times 10^{-4}$
$m_{13} = 119$	$p_{13} = 0.070$	$I_{12} = 1.97 \times 10^{-4}$
$m_{31} = 142$	$p_{31} = 0.403$	$I_{31} = 0.00993$
$m_{32} = 59$	$p_{32} = 0.037$	$I_{32} = 3.37 \times 10^{-5}$
$m_{33} = 59$	$p_{33} = 0.037$	$I_{32} = 3.37 \times 10^{-5}$
$m_{e1} = 300$	-	-
$m_{e3} = 600$	$p_{e3} = 0.250$	-

## 4.5 Approach for Active Balancing

In this section the active balancing approach is proposed by controlling the three motors of a 3 DoF force balanced architecture such that a desired end effector position is achieved with moment balanced motion. The control scheme is shown in Figure 4.5 which is based on a standard rigid body feedforward scheme. The novel aspects are highlighted in red. The scheme is described below.

An  $X_e, Y_e$  position for the end effector is specified as an input. Using the inverse kinematic model a set of different angles which achieve this position are determined. Using the minimizing angular momentum approach described below, the three angles with the lowest angular momentum are chosen. Next, fourth order point to point trajectories are generated to achieve the change in the angles based on the current and desired angular position. By integrating these trajectories the required acceleration is found. By multiplying by the inertia the feedforward torques ( $T$ ) are determined. By integrating further the position profiles are also derived. Given the difference in the reference angular position compared to the actual angular position a feedback torque is applied. Both of these torques are adjusted to ensure balancing. This is described more below. These torques are then fed into the model of the simulator. From the output angular positions the end effector position and resulting linear ( $L$ ) and angular momentum ( $H$ ) are determined. The two novel methods added to the rigid body feedforward scheme are described below: minimizing the angular momentum and torque adjusting.

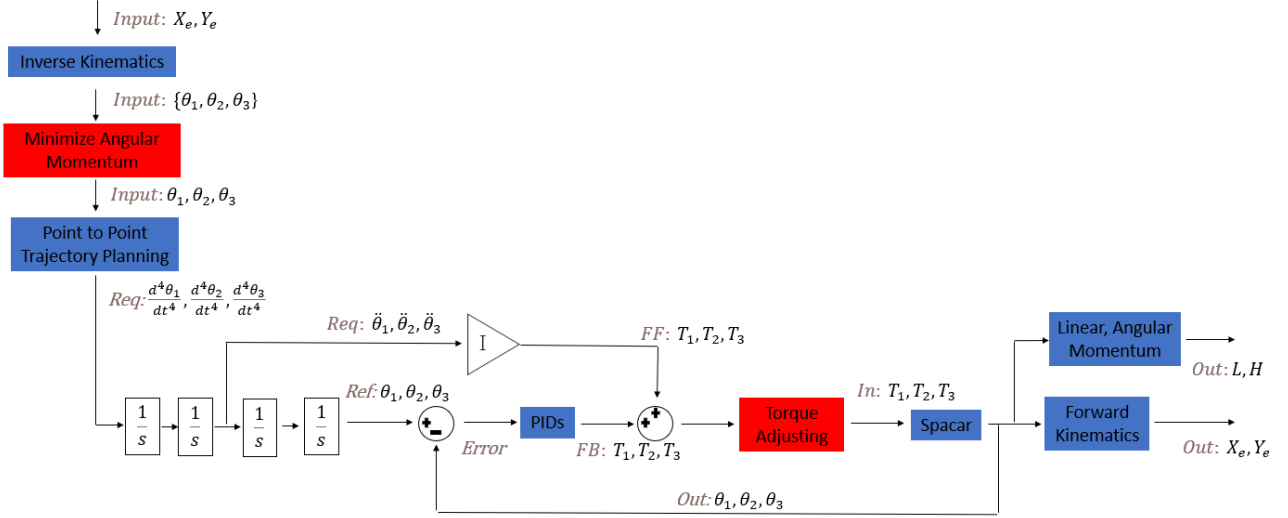


**Figure 4.5:** Control scheme for a 3 DoF redundant manipulator in a 2 DoF workspace with moment balanced motion. The scheme is based on rigid body feedforward control with novel aspects in red.  $X_e, Y_e$  is the cartesian end effector position,  $\theta_s$  are the manipulator DoFs,  $T_s$  are the applied torques,  $L$  is the linear momentum, and  $H$  is the angular momentum.

#### 4.5.1 Minimizing Angular Momentum

The first method developed was to minimize the angular momentum. For a desired end effector position there were multiple angles which resolved the inverse kinematics since the manipulator was redundant. Therefore the challenge was to select the next set of angles such that no reaction moment was generated. In theory, if the angular momentum is zero for the motion from one end effector position to another then the reaction moment is also zero. [46] First the angular momentum was derived for the manipulator. This is shown below where  $H$  is the angular momentum,  $I$  is the inertia of each link and  $r$  is the position of the point mass from the centre of mass of the manipulator. The  $z$  subscript indicates the  $z$  component of the cross product.

$$H = (I_{31} + I_{11} + I_2)\dot{\theta}_1 + (I_{33} + I_{32} + I_3)\dot{\theta}_2 + (I_{13} + I_{12} + I_1)\dot{\theta}_3 + \sum_{i=1}^n m_i (\bar{r}_i \times \dot{\bar{r}}_i)_z$$

First it was attempted to solve for the angular velocities such that the angular momentum is zero. However, the positions and velocities of the point masses are based on nonlinear sine and cosine equations which cannot easily be separated. Therefore, an optimization was performed which is described in the next paragraph.

To determine the angles which result in the lowest reaction moment, a range of sets of angles were computed which resolved the inverse kinematics. Given the timestep as well as the current and desired end effector position, the angular velocities and point mass velocities were linearly approximated. The angular momentum was then computed and the angles with a resulting minimum angular momentum were selected. These are then inputted into the trajectory generators.

#### 4.5.2 Torque Adjusting

Minimizing the angular momentum provides a prediction for moment balanced motion to the next desired end effector position. However, in linearly approximating the angular velocities and point mass velocities errors

arise that can result in the angular momentum not remaining zero and a reaction moment generated. To ensure the reaction moment is zero the input torques to the system must be adjusted. Torque 1 ( $T_1$ ) and torque 2 ( $T_2$ ) are responsible for the reaction moment of the manipulator, while torque 3 ( $T_3$ ) has no impact.

The torque adjusting method developed was to calculate the average magnitude ( $T_{av}$ ) of torque 1 and torque 2, and then set them equal and opposite one another. The formula is shown below where the average is a plus since the torques have opposite signs. This can be performed for the feedforward torques, the feedback torques, or both. However, this method does not resolve the kinematic redundancy in converting from a 2 DoF  $X, Y$  position to a 3 DoF angular position so this method must be used in combination with minimizing the angular momentum.

$$\begin{aligned} T_{av} &= \frac{T_1 + T_2}{2} \\ T_1 &= +T_{av} \\ T_2 &= -T_{av} \\ T_3 &= T_3 \end{aligned}$$

## 4.6 Simulation of the Manipulator

This section outlines the simulation that was performed to validate the proposed control scheme for active moment balancing of a 3 DoF force balanced manipulator in a 2 DoF workspace. First the end effector path requirements are outlined which were set to mimic the close proximity sensing task. Next the simulation is explained in detail.

### 4.6.1 End Effector Path Requirements

For the simulation, an endpoint motion was chosen representing a close proximity sensing application. To achieve this, the UAV must perform station keeping while the manipulator performs a fine positioning task. The aim is for the manipulator to position the sensor so that it can cover a surface. Therefore a C-curve was taken to simulate the manipulator approaching a surface and then moving down to perform the next measurement. Figure 4.6 illustrates the required path with the black arrows. The manipulator is shown in blue in the middle of the path. The red dash indicates the original manipulator configuration. To create the C-curve three steps were performed: -0.1m in X, -0.1m in Y, 0.1m in X. Each step was performed in 0.5s in series. The initial conditions were:  $\theta_1 = 180^\circ, \theta_2 = 290^\circ, \theta_3 = 225^\circ$ .

### 4.6.2 Simulation Explanation

The global control scheme was applied, as shown in Figure 4.5. More information is provided in Appendix F. The manipulator was first modelled in Spacar, a multibody dynamic simulator. The inputs were the three applied torques. The outputs were the angular positions and velocities of the three hinges as well as the lumped mass positions and velocities. The model was then linearized. This makes the plant of the control scheme. Additionally, Spacar was used to find the linearized reduced mass matrix.

Offline, the required C-curve was discretized into three steps. For each required step the inverse kinematics was determined and the angular momentum minimized. This was then fed into a fourth order point to point trajectory planner.

In real time using simulink, the remainder of the control scheme was applied. Three separate PID controllers for each DoF were used for feedback control. Using the angular and lumped mass position and velocities the

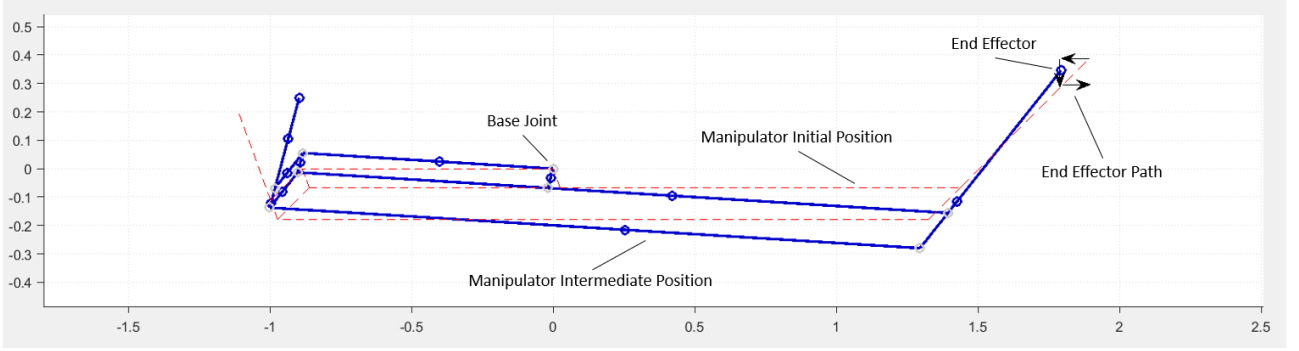


**Figure 4.6:** Manipulator performing the required end effector path. The initial and an intermediate manipulator position is illustrated as well as the end effector required C-curve.

linear and angular momentum was determined. The time derivative of the angular momentum was taken to determine the reaction moment applied to the base. Additionally, the position of the end effector was plotted and the position error was also determined to quantify the tracking error. The formulas are listed below where  $L$  is the linear momentum and  $M$  is the reaction moment applied to the base.

$$\bar{L} = \sum_{i=1}^n m_i \bar{r}_i$$

$$H = (I_{31} + I_{11} + I_2)\dot{\theta}_1 + (I_{33} + I_{32} + I_3)\dot{\theta}_2 + (I_{13} + I_{12} + I_1)\dot{\theta}_3 + \sum_{i=1}^n m_i (\bar{r}_i \times \dot{\bar{r}}_i)_z$$

$$M = \frac{dH}{dt}$$

## 4.7 Results

Three control aspects were analyzed. The first control aspect was minimizing the angular momentum. When this was applied it is referred to as “Hmin” in the graph legends. To compare this to a baseline,  $h_2$  was controlled to stay at a constant angular position and only  $h_1$  and  $h_3$  were used to achieve the end effector position. This is referred to as the “2D” case. The next control aspect was using either just feedforward control, referred to as “FF” or using feedforward and feedback control, referred to as “FF+FB”. The final control aspect was the adjusting of the input torques. This is referred to as “Tadj”. First a c-curve was implemented. To investigate some of the errors, a step was performed with each control aspect. For all results the linear momentum was zero, indicating no shaking forces. For each result, the shaking moment, x position error, y position error, and x-y position were plotted.

### 4.7.1 C-Curve Results and Discussion

In this section the C-curve is prescribed. The actively balanced case with feedforward and feedback control is compared to the 2D baseline with feedforward and feedback. Three steps were performed: -0.1m in X, -0.1m in Y, 0.1m in X. Each step was performed in 0.5s in series, with the first step starting at 0.5s. The initial conditions were:  $\theta_1 = 180^\circ, \theta_2 = 290^\circ, \theta_3 = 225^\circ$ .

## C-Curve Results

The reaction moment, position error in X, position error in Y, and X-Y position are plotted in Figure 4.7, Figure 4.8, Figure 4.9, and Figure 4.10 respectively.

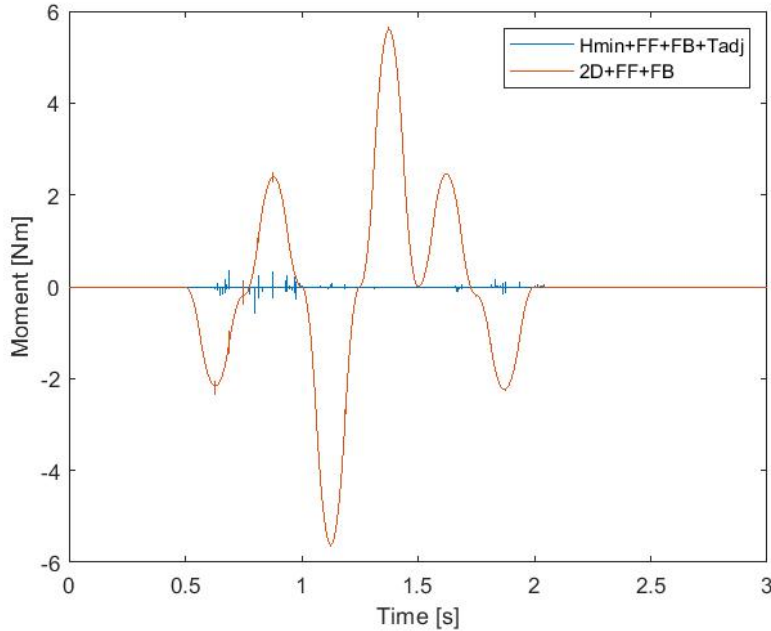


**Figure 4.7:** Reaction Moment From a C-curve of 0.1m Steps over 0.5s. The novel control scheme eliminates the reaction moment.

## C-Curve Discussion

The C-curve reaction moment results of Figure 4.7 show that the actively balanced manipulator had no reaction moment. In comparison, the 2D case imparted a moment of nearly 6Nm. This indicates that the moment balancing is effective. However, from Figure 4.10 it is apparent that the actively balanced case does not follow the desired trajectory. To determine the cause of the positioning error, each control method was investigated for a smaller step.

### 4.7.2 Step Results and Discussion

The manipulator was tasked with performing an end effector step of -0.02m in the X direction for a time increment of 0.5s. This was also started at 0.5s. The initial conditions were again:  $\theta_1 = 180^\circ$ ,  $\theta_2 = 290^\circ$ ,  $\theta_3 = 225^\circ$ . The tracking performance and reaction moment was compared for these two cases while adding different control techniques.

## Feedforward Results

First only feedforward control was implemented for both cases. The reaction moment, X position tracking error, Y position tracking error, and X-Y position are shown in Figure 4.11, Figure 4.12, Figure 4.13, and Figure 4.14 respectively.

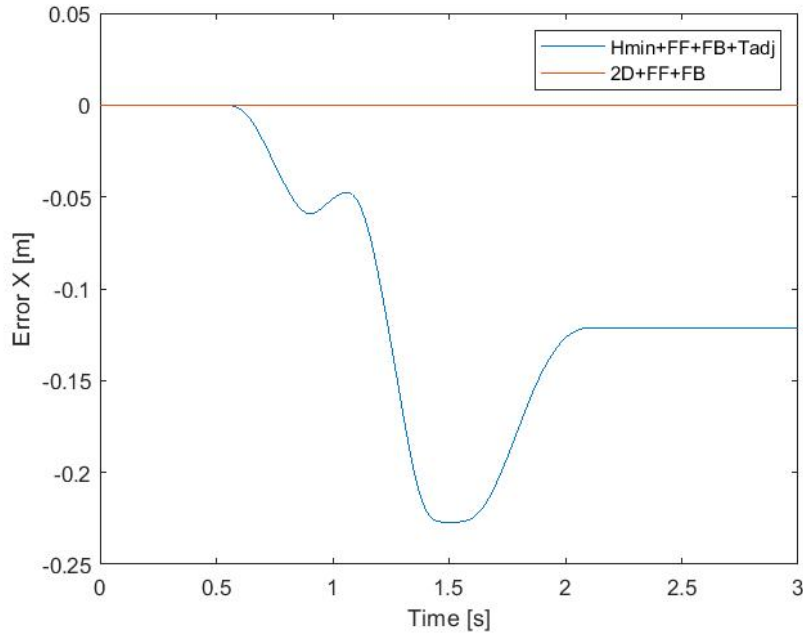


**Figure 4.8:** Position Error in X From a C-curve of 0.1m Steps over 0.5s. The novel control scheme has a higher tracking error in X than the baseline.

### Feedforward Discussion

From Figure 4.11 it is shown that the minimized angular momentum case has a significant improvement in the reaction moment for feedforward control. By also including torque adjusting the reaction moment is eliminated for both cases. In terms of positioning error the minimized angular momentum case has a slightly higher error than the 2D case when only feedforward is applied. When applying the torque adjusting, the position error increase for both cases, however, there is a lower position error for the minimized angular momentum case. This is a good result because it indicates that minimizing the angular momentum improves the performance both for just feedforward control and with torque adjusting in comparison to the 2D case. Including the torque adjusting to the feedforward control has a trade off for both cases as it eliminates the reaction moment but degrades the tracking performance.

### Feedforward & Feedback Control Results

Next feedback control was added. First only feedforward and feedback was applied to the two cases. Next, the input torques from both the feedforward and feedback signals were torque adjusted. The resulting reaction moment, X position error, Y position error, and X-Y position are shown in Figure 4.15, Figure 4.16, Figure 4.17, and Figure 4.18 respectively. The feedback control applied was three separate PD controllers for each DoF. Additionally, an H2 controller was applied. The results were comparable to the PD control with a marginally better tracking performance but higher reaction moments. Additionally, adjusting of only the feedforward torques and not the feedback torques was implemented, however, it gave a similar result as just feedforward and feedback. Both of these results can be found in Appendix G.

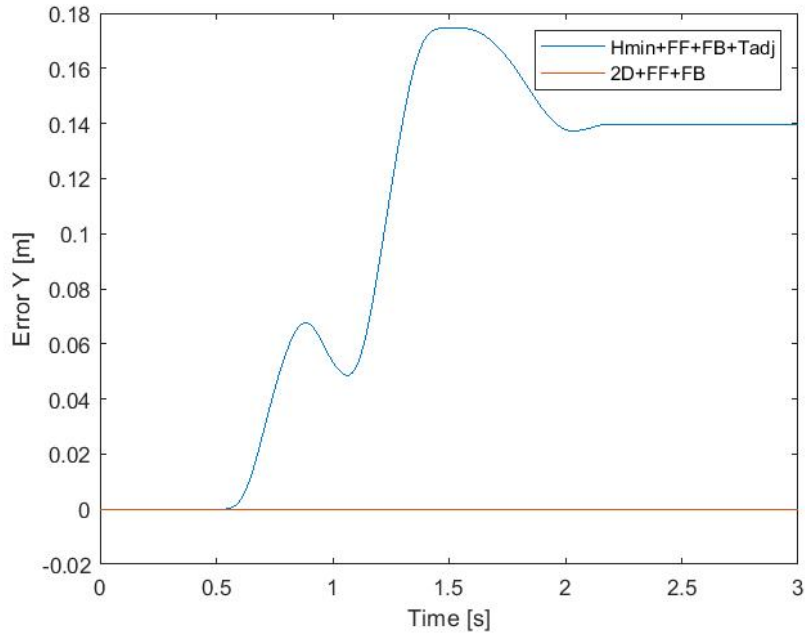


**Figure 4.9:** Position Error in Y From a C-curve of 0.1m Steps over 0.5s. The novel control scheme has a higher tracking error in Y than the baseline.

### Feedforward & Feedback Control Discussion

From Figure 4.15 again minimizing the angular momentum with feedforward and feedback control has a lower reaction moment than for the 2D case. Once the torques are adjusted, for both cases the reaction moment is eliminated. From Figure 4.16 and Figure 4.17 it is shown that introducing torque adjusting increases the position error for both cases. However, for the minimized angular momentum case the resulting position error was less. In comparison to only the feedforward case there was also a reduction in the position error. Therefore, the best option is active balancing with feedforward and feedback control with torque adjusting.

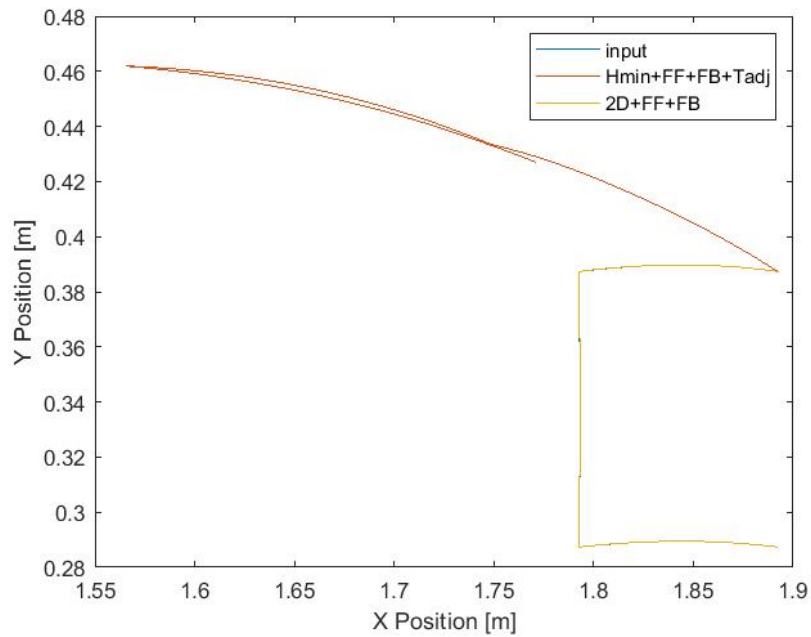


**Figure 4.10:** XY Position From a C-curve of 0.1m Steps over 0.5s. The baseline follows the input more closely than the novel control scheme.

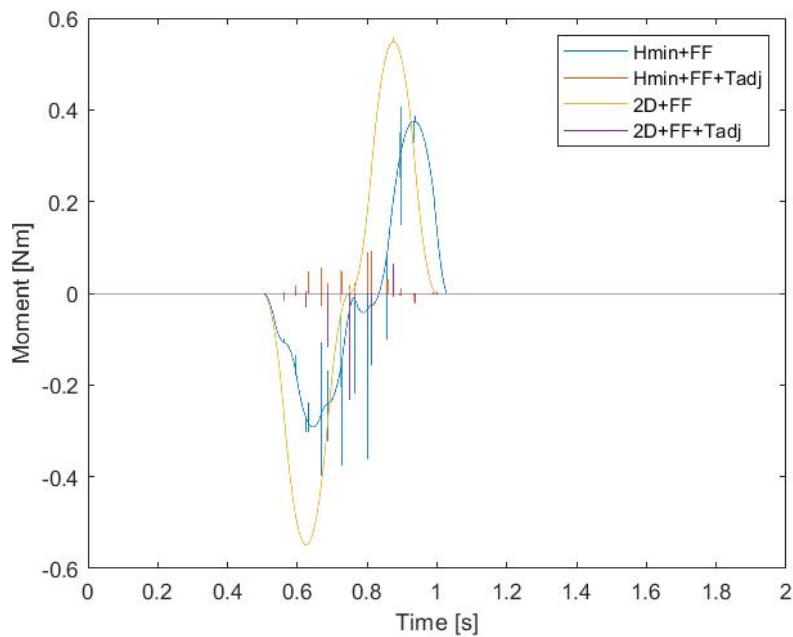


**Figure 4.11:** Reaction Moment From a -0.02m Step in X over 0.5s using Feedforward Control. Minimizing the angular momentum reduces the reaction moment. Adjusting the torques eliminates the reaction moment.

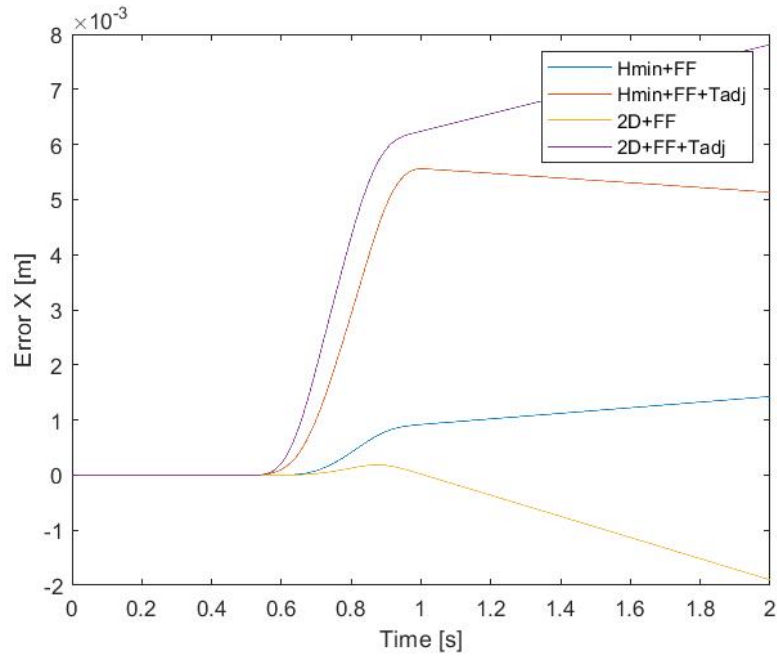


**Figure 4.12:** Position Error in X From a  $-0.02\text{m}$  Step in X over  $0.5\text{s}$  using Feedforward Control. Adding torque adjusting increases the tracking error in X, more so for the baseline than for the minimized angular momentum case.

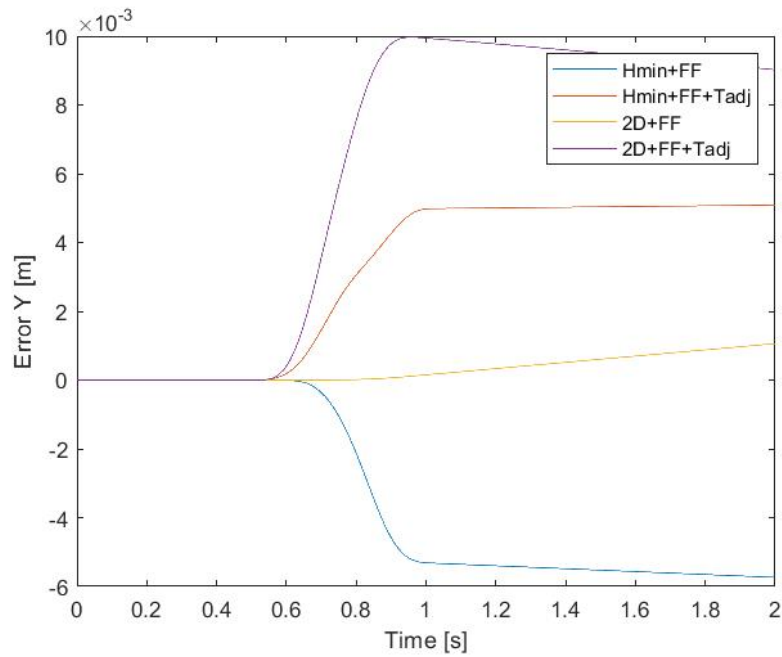


**Figure 4.13:** Position Error in Y From a  $-0.02\text{m}$  Step in X over  $0.5\text{s}$  using Feedforward Control. Adding torque adjusting increases the tracking error in Y, more so for the baseline than for the minimized angular momentum case.

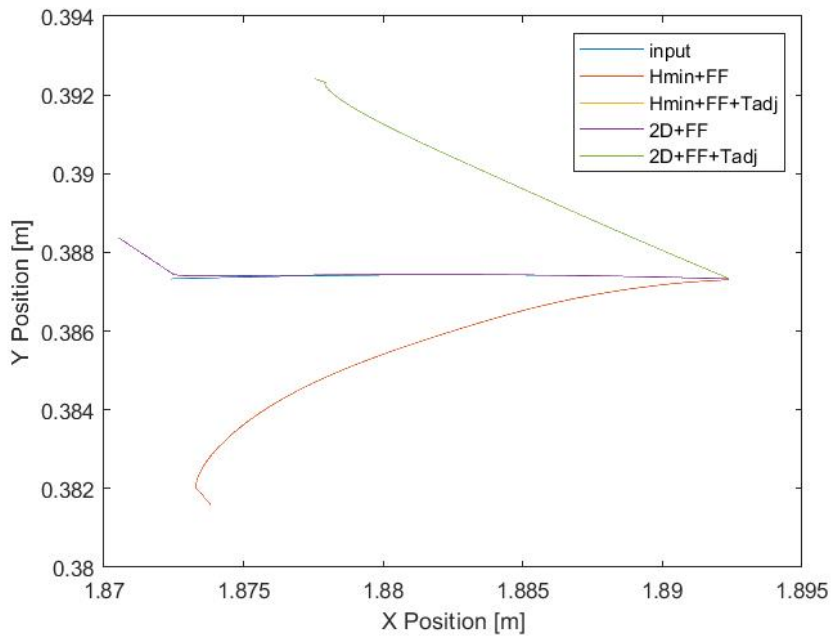


**Figure 4.14:** X-Y Position From a  $-0.02\text{m}$  Step in X over  $0.5\text{s}$  using Feedforward Control. Adding torque adjusting increases the tracking error, more so for the baseline than for the minimized angular momentum case.

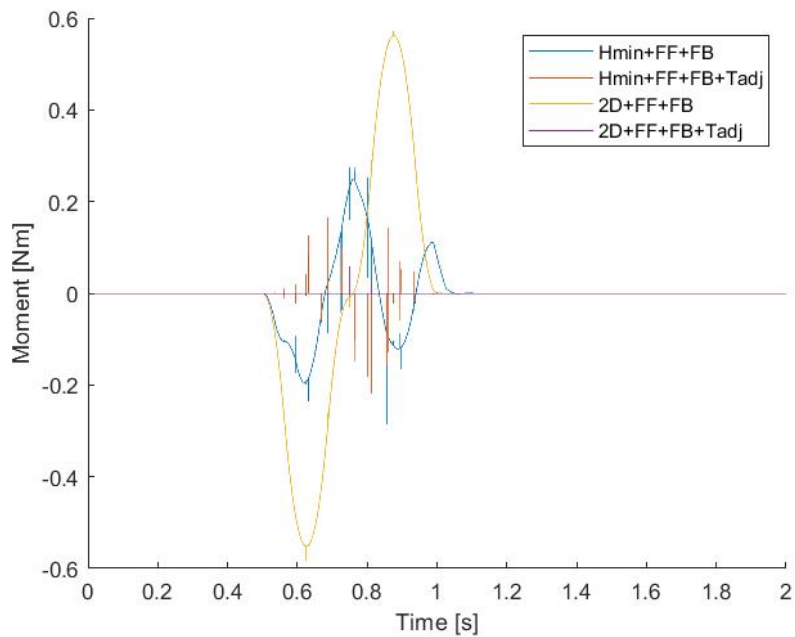


**Figure 4.15:** Reaction Moment From a  $-0.02\text{m}$  Step in X over  $0.5\text{s}$  using Feedforward and Feedback Control. Minimizing the angular momentum reduces the reaction moment. Adjusting the torques eliminates the reaction moment.

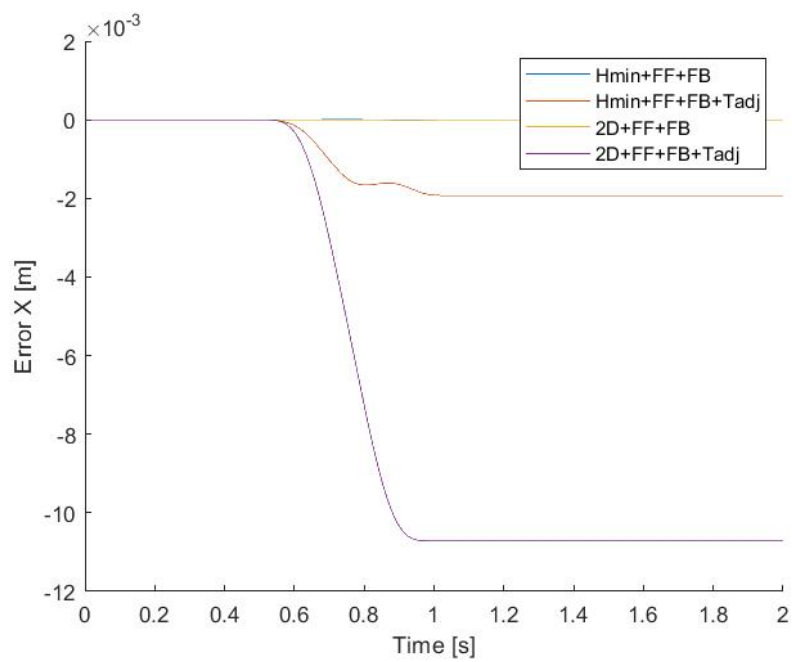


**Figure 4.16:** Position Error in X From a -0.02m Step in X over 0.5s using Feedforward and Feedback Control. Adding torque adjusting increases the tracking error in X, more so for the baseline than for the minimized angular momentum case.

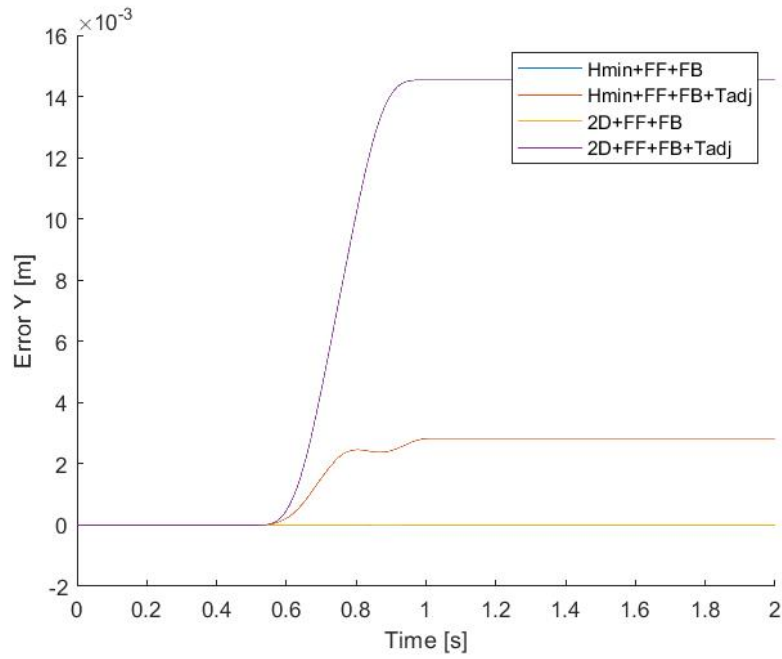


**Figure 4.17:** Position Error in Y From a -0.02m Step in X over 0.5s using Feedforward and Feedback Control. Adding torque adjusting increases the tracking error in Y, more so for the baseline than for the minimized angular momentum case.

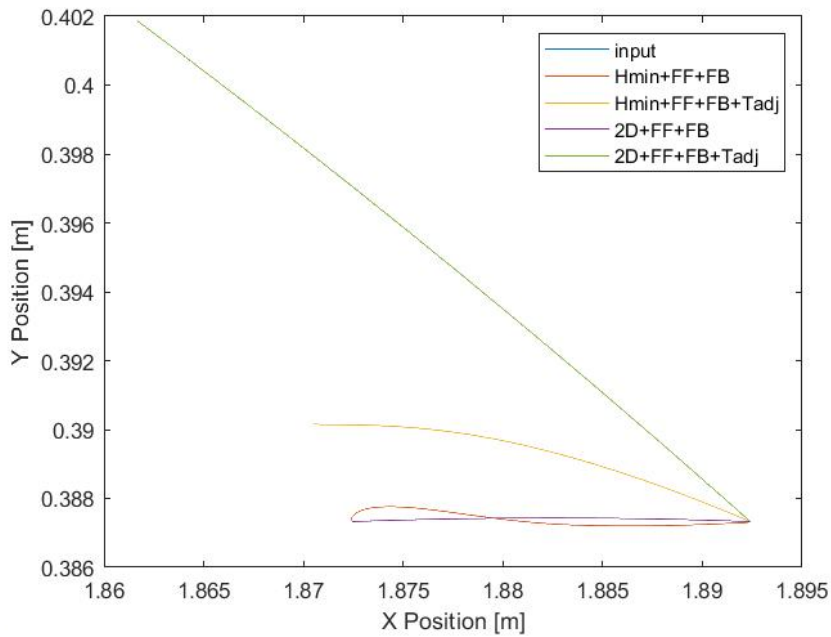


**Figure 4.18:** X-Y Position From a -0.02m Step in X over 0.5s using Feedforward and Feedback Control. Adding torque adjusting increases the tracking error, more so for the baseline than for the minimized angular momentum case.

## 4.8 Discussion

This paper achieved its goal in developing a novel control scheme for a redundant 3 DoF force balanced architecture in a 2 DoF workspace with moment balanced motion. It was developed for a reactionless, lightweight manipulator that can be attached to an Unmanned Aerial Vehicle. The control scheme was successful in eliminating the shaking moment applied to the base of the UAV. However, the control scheme had a significant tracking error. This tracking error was greater for the larger displacements of the C-curve in comparison to the smaller displacements of the step.

The issues in tracking error arose because a variety of approximations were used. Selecting the next three angles with a minimum angular momentum was performed offline before running the simulation. Therefore, any position errors from the first step added to the error in the next step. Additionally, the next angles were applied to a point to point trajectory tracker which didn't consider moment balancing. To compensate for this, torque adjusting was performed. This torque adjusting was the most significant source of tracking error. In the feedforward control the reduced mass matrix was used to determine the feedforward torque from the input accelerations. This reduced mass matrix was approximated by the linearized model based on the starting position, however it changes based on the position of the manipulator. Finally, the feedback control was implemented to improve the tracking performance but it degraded the balancing performance.

To improve this method reactionless trajectories instead of points must be determined. Yoshida identifies a reactionless trajectory generation strategy based on the coupling momentum between the the base and the manipulator. [50] [51] To keep the momentum constant the joint velocities  $\vec{\phi}$  can be found using the following formula where  $\mathbf{I}$  is the identity matrix,  $\mathbf{H}_{\mathbf{bm}}$  is the coupling matrix,  $\mathbf{H}_{\mathbf{bm}}^+$  is the pseudo dot inverse of  $\mathbf{H}_{\mathbf{bm}}$ , and  $\vec{\xi}$  is an arbitrary vector. [50] [51]

$$\vec{\phi} = (\mathbf{I} - \mathbf{H}_{\mathbf{bm}}^+ \mathbf{H}_{\mathbf{bm}}) \vec{\xi}$$

The angular momentum that has been derived is similar to the coupling momentum described by Yoshida. By using this formulation for the joint velocities it is possible that reactionless trajectories could be developed instead of a point to point approximation.

The final aspect that must be improved is the rigid body feedforward control. Instead of using an approximation for the reduced mass matrix based on a linearization at the initial configuration, a real time approximation must be performed. By deriving the Lagrange equations and inputting the current angular position, a live inertia estimation can be computed. This would greatly improve the accuracy of the feedforward control. In this case there would be no need for the feedback control which doesn't necessarily take into account moment balancing. However, if a feedback control scheme was still required, then a moment balanced feedback method would also have to be developed.

## 4.9 Conclusion

A control approach for active moment balancing was developed. This approach involved controlling 3 motors of a 3 DoF inherently force balanced architecture in a 2 DoF workspace. By using the kinematic redundancy, the motion was optimized such that the angular momentum was minimized. Then the input torques were further adjusted. This was developed to enable a new dynamically balanced, 3 DoF lightweight manipulator design for a UAV. The manipulator was simulated and it showed no reaction moment would be applied to the base of the UAV. This is a substantial improvement to the aerial manipulation field. This enables higher number of degrees of freedom for dynamically balanced manipulators without having to rely on heavy counter rotating masses. More research is required to reduce the tracking errors; particularly in finding reactionless trajectories

and improving the feedforward model. By resolving the reaction moment at the manipulator instead of at the UAV, the field of aerial manipulation can more readily be applied in industry. This has the potential to allow commercial UAVs to perform close proximity sensing in a variety of industries including agriculture or renewable energy.

## 5 | Discussion

The research performed is a significant improvement to the aerial manipulation field. For the methods involving passively balanced manipulators, the state of the art was a UAV with a 1 DoF rigid rotating rod and batteries attached to force balance, [12] as well as a 1 DoF pantograph based manipulator. [17] By applying higher DoF pantograph based inherently force balanced architectures in this thesis, the manipulators constructed had more DoFs than the state of the art. This allows the manipulator to perform fine positioning in  $x, y, z$ , whereas the previous manipulators could not. This thesis has investigated using architectures that have not been proposed for aerial manipulation, and mobile manipulation in general. Additionally, novel force balanced architectures were synthesized which could also further this field.

For the moment balancing of force balanced architectures an active method was proposed. This involved creating a control scheme to select the motion of a 3 DoF manipulator in a 2 DoF workspace such that no reaction moment was generated. The state of the art for an active mechanism approach is a 2 DoF serial manipulator with a sliding countermass. [10] This only resolves one shaking moment and not the shaking forces. Another state of the art is a UAV with an 2 DoF pantograph with an active countermass. [11] Although this is force and moment balanced, the manipulator is effectively 1 DoF. Therefore, the research expands significantly on the number of DoFs for the manipulator. Additionally, in comparison to using multiple counter rotating masses, the use of the manipulator architecture for balancing is a design approach that can lead to mass reduction. This is because the architecture itself achieves dynamic balancing and can therefore be optimized for the lowest weight.

In comparison to the higher DoF control based approaches where the UAV propellers provide a compensation force and moment, [5] [4] the method proposed in this thesis is a significant improvement. The manipulator designed can be attached to commercial UAVs with less adjustment and added complexity to the UAV control structure. This is because the shaking forces and moments are compensated at the manipulator. From the perspective of the UAV, the manipulator is equivalent to a rigid body. This means it could more readily be applied to UAV fleets of industry operators. Additionally, this approach doesn't require precomputing trajectories which means it can perform better outside a laboratory setting.

To realize these improvements in aerial manipulation there is still additional work which must be performed. One aspect that must still be improved upon is the integration of the manipulator with the UAV. Inherent dynamic balancing resolves the issues of the shaking forces and shaking moments. However, by attaching the manipulator there are still other aspects that must be considered. These include the manipulator inertia, wind forces, and control hierarchy. Each of these aspects are explained below.

When the manipulator is in different positions the inertia from the perspective of the UAV changes. If the inertia changes rapidly then the stabilization of the UAV could be impacted. There are onboard inertia estimators on some UAVs. However, the allowable change in the inertia still must be determined. Then the rate of change of the inertia of the manipulator must be limited in either the mechanical design or using the controller.

Another aspect that must be considered is the force of the wind that will act on the manipulator and in turn the UAV. Most UAVs already have limitations on the maximum wind speed. This wind speed requirement could be reduced based on the expected drag of the manipulator and the stability requirements of the UAV.

A complete control system for the UAV and manipulator must still be developed. There are a variety of control hierarchies that have been implemented in the aerial manipulation papers. [4] One option is to have two completely separate control structures: one for the manipulator and one for the UAV. This has the added benefit that the manipulator is completely modular so it can be attached to commercial UAVs. It is also much more simple to implement. This would require the UAV to arrive at the desired location and perform station keeping while the manipulator performs its task. Another option is to have a fully integrated control system

between both. In this case it is possible for the manipulator and UAV to work more concurrently to perform a task.

In some of the papers that use active methods to ensure stable manipulation, the active mechanisms are used to also counter the external force and moments that are applied. These arise from the tasks, such as an abrupt contact force from touching a surface or a weight force from picking up an object. There are already papers on the modeling of these interaction forces so these can readily be applied to the work performed in this thesis. For this concept the active DoF reduction of the manipulator could be used for not just the moment balancing of the manipulator, but also to counter the externally applied moment. This is especially useful because the active DoF acts in a plane which will cause the UAV to tip. For a large impact, the active DoF could be driven to counter the moment. This would prevent the UAV actuators from becoming saturated. This would require a further investigation into the contact forces and control of the manipulator.

In general, the approach of using higher DoF inherently force balanced architectures and actively reducing them to be moment balanced is a significant improvement to the area of mobile manipulation. For cable robots, the resolution of the shaking forces and moments would be very helpful. This is because the base can only be supported by tensile forces from the cables. For the space domain this method would be very useful as the weight requirements are even stricter than for UAVs. However, for space robots reducing energy consumption is very important so allowing rotations which don't impact the alignment of the communication equipment with earth could be allowed.

For underwater manipulation and ground robots the method developed is less useful. For underwater manipulation the added mass must also be considered for dynamic balancing. The added mass arises from the motion of the fluid during manipulator motion. [18] Therefore, to dynamically balance the manipulator the amount of fluid displacement must be uniform in each direction. The symmetric concepts such as the one shown in Figure 3.6 would then be better suited for this task. Another aspect that must be considered for underwater manipulation is that the loads are typically much higher; hydraulic actuators are often used. [18] An additional actuator would be a significant added weight, so the active DoF reduction would not be a good choice.

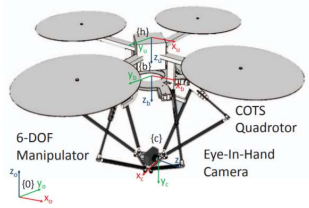
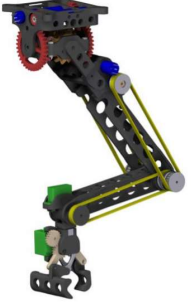
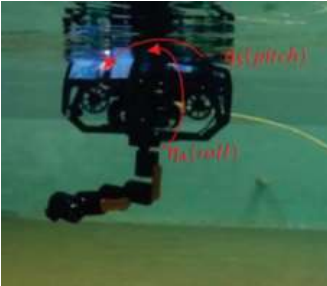
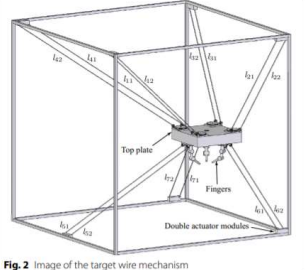
For ground robots some of the shaking forces and moments can be transferred to the ground. Therefore, a fully reactionless manipulator is not required. Instead inherent dynamic balancing can be used to resolve some of the forces or moments that have the greatest impact on tip-over. Based on the dynamics of the vehicle, additional constraints on the other shaking forces and moments can be imposed.

## 6 | Conclusion

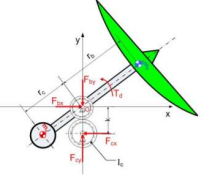
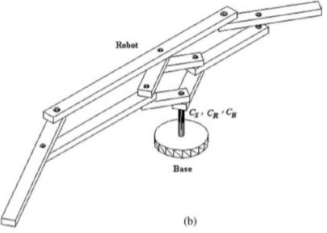
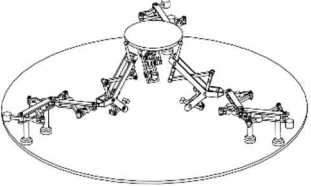
A novel manipulator was designed and controlled to be attached to a UAV. This manipulator is inherently dynamically balanced: it does not impart shaking forces or shaking moments to the UAV. In the design of the manipulator, novel and higher DoF inherently force balanced architectures were applied. By achieving 3 degrees of freedom the manipulator can provide fine positioning in  $x, y, z$  and reach out to perform an inspection of a surface while the UAV provides course positioning. By achieving 2m reach of the manipulator, the UAV can remain a safe distance from the contact surface. This is a significant improvement from the state of the art, as those UAV manipulators have lower DoFs, unresolved shaking forces and moments, or complicated control schemes which are not viable outside a laboratory setting. In designing the manipulator it was identified that a lighter and more compatible concept would be created by reducing a redundant inherently force balanced architecture to be moment balanced. This was achieved through a novel control scheme in which 3 motors were controlled for a 3 DoF force balanced architecture such that in a 2 DoF workspace no reaction moment was generated. The kinematic redundancy was resolved by selecting a set of manipulator angles such that the angular momentum was minimized. After the input torques were further adjusted. A simulation was performed to verify the control scheme and it was shown to effectively eliminate the shaking moment. The manipulator that was synthesized and controlled is a significant improvement to the aerial manipulation field. This can enable a variety of tasks including the inspection of critical infrastructure such as bridges and wind turbines. The manipulator can perform contact inspections such as ultrasonic thickness testing. This can be done in a safer and more cost effective manner than having a technician hang from ropes. The novel methods developed in this thesis can also improve other mobile manipulation fields as well as the research area of floating base manipulation. This is because the other fields face the similar issue of shaking forces and moments of the manipulator impacting the stability of the base.

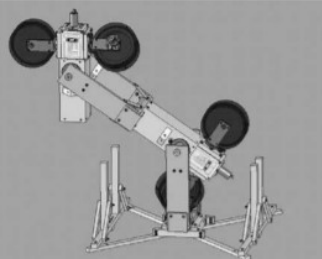
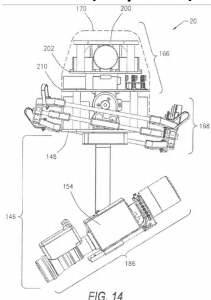
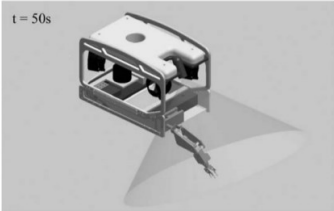
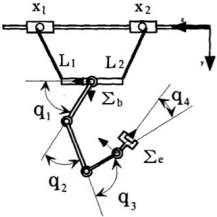
# A | Appendix: Examples of Methods for Stable Manipulation Summary Table

This Appendix summarizes the examples found in literature of stable floating base manipulation. For each method the examples found in the corresponding field are listed. The table is divided by the method categories of avoidance, passive, and active.

Method	Space	Ground Robots	UAVs	ROVs	Cable Robots
<p>Reduce Moving Mass</p>	<p>Vehicle Manipulator Systems: -Manipulators are already as light as possible for rocket payload limitations</p>		<p>Prodrone PD6B-AW-ARM</p>  <p>A Parallel Manipulator for Mobile Manipulating UAVs</p>  <p>Modeling and control of an aerial robocrane using a wire driven system:</p>  <p>Design, Modeling and Control of a 5-DoF Light-Weight Robot Arm for Aerial Manipulation</p>  <p>Fig. 2. PULSAR robot arm (motors in blue, servos in green)</p> <p>-Limit moving mass by having motors at base with differential joint and timing belts</p>	<p>Underwater manipulators a review: -Industry standard in terms of relative weight</p> <p>SeaArm - A Subsea Multi-Degree of Freedom Manipulator for Small Observation Class Remotely Operated Vehicles</p>  <p>-Keep manipulator mass small and rely on hydrostatic restoring forces of the ROV to stabilize</p>	<p>Kinematical and static force analysis on redundant drive wire mechanism with velocity constraint modules to reduce the number of actuators</p>  <p>Fig. 2 Image of the target wire mechanism</p> <p>-Two stages, course by redundant pulleys and fine by light fingers</p>

Attach to a Fixed Base			<p>A Multirotor Platform Employing a Three-Axis Vertical Articulated Robotic Arm for Aerial Manipulation Tasks</p>  <p>-grab on to rod from above</p>	<p>Underwater manipulators a review: Two manipulators, one is to perform manipulation task, another to grab on to platform</p>	
------------------------	--	--	---	--	--

Method	Space	Ground Robots	UAVs	ROVs/AUVs	Cable Robots
Counterweights	<p>Design of a reactionless pointing mechanism for satellite</p>  <p>antennas -Actuators used as counterweight about the joint</p>		<p>The AEROARMS Project: Aerial Robots with Advanced Manipulation Capabilities for Inspection and Maintenance</p>  <p>-Battery to force balance arm</p>		
Inherently Balanced Architectures	<p>Reactionless space and ground robots: novel designs and concept studies</p>  <p>-Structure composed of multiple pantographs</p> <p>Synthesis of Reactionless Spatial 3-DoF and 6-DoF Mechanisms Without Separate CounterRotations</p>  <p>-Composed of balanced four bars</p>	<p>A New Approach to Humanitarian Demining</p>  <p>-Counterweight placed on other side of pantograph -for energy consumption rather than stability</p>			

Method	Space	Ground Robots	UAVs	ROVs	Cable Robots
Gyroscopic Actuation	Reducing Base Reactions With Gyroscopic Actuation of Space-Robotic Systems  -Change direction of spinning mass				Aerial Camera System US Patent (Skycam)  -Spinning mass gyros resist high rate disturbances
Globally Redundant Path Planning	Vehicle Manipulator Systems: Free floating spacecraft are globally redundant Select path so end effector position is achieved and craft orientation unchanged		Trajectory Generation for Unmanned Aerial Manipulators Through Quadratic Programming  -Optimize path for primary end effector tracking and secondary CoG displacement and transmitted forces	Redundancy resolution for underwater mobile manipulators  -Primary task is end effector position, secondary is to minimize ROV motion	
Locally Redundant Path Planning	Vehicle Manipulator Systems: Use null space to add additional control objective to redundant manipulator so it doesn't affect the base		Aerial manipulation robot composed of an autonomous helicopter and a 7 degrees of freedom industrial manipulator  -7Dof manipulator -Redundancy used to maintain CoG position		Development of a Manipulator Suspended by Parallel Wire Structure  -Choose trajectory so CoG horizontal position is constant

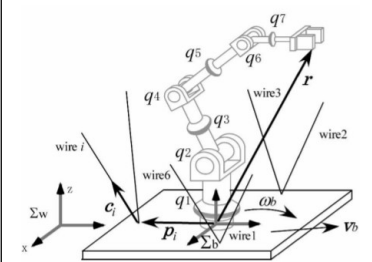
-Inertial forces not important because arm moves slowly

A hyper-redundant manipulator for Mobile Manipulating Unmanned Aerial Vehicles



-Hyper-redundancy used to further limit base reactions

Control of a Redundant Manipulator Mounted on a Base Plate Suspended by Six Wires

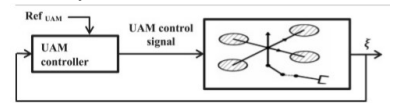


-6 wire platform, 7 Dof manipulator  
-decrease reaction force or maximize the minimum wire tension to avoid overturn

Feedforward Base Control

Vehicle Manipulator Systems:  
-Free flying spacecraft use reaction wheels and thrusters to maintain base orientation wrt earth

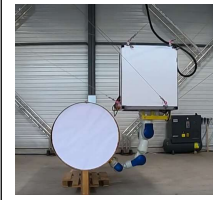
Aerial Manipulation – A literature survey



-Manipulator and UAV simultaneously controlled in a unified system using nonlinear coupled dynamic model  
-Feedback linearization, impedance, backstepping, LQR, etc

Underwater manipulators a review:  
Use accurate dynamic modelling and advanced control techniques

Cable Driven Parallel Robots Robust Internal Force-Based Impedance Control for Cable-Driven Parallel Robots



-account for end effector disturbances as trajectory errors at actuator

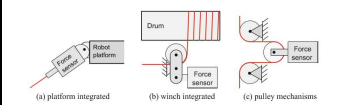
Feedback Base Control

Hexrotor UAV Platform Enabling Dexterous Interaction with Structures- Flight Test



Underwater manipulators a review:  
-One pilot to keep ROV base stable, another to perform manipulation.  
-Use station keeping algorithms for base, control manip as if fixed.

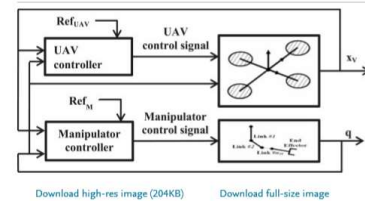
Cable Driven Parallel Robots Book



-Various force sensor position for closed loop control

-tilted rotors, 6 DOF, can exert reaction force in any direction

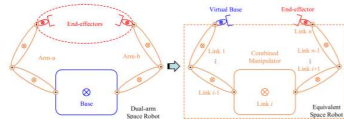
### Modeling and Control of Aerial Manipulation Vehicle with Visual sensor



- Quadrotor with a two link manipulator
- Quadrotor performs reactive station keeping while manipulator moves

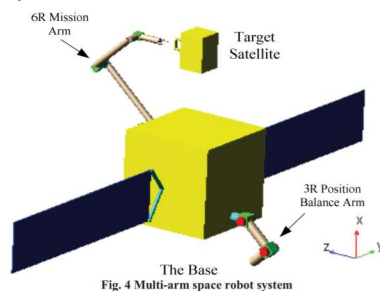
Dual or multi arm

Virtual-base modeling and coordinated control of a dual-arm space robot for target capturing and manipulation



- Assign virtual base to one end effector and treat the rest as a hyper-redundant system

### Base Centroid Virtual Manipulator Modeling and Applications for Multi-arm Space Robots



- Plan trajectory of balance arm to maintain centroid position

### Modeling and Control of MM-UAV: Mobile Manipulating Unmanned Aerial Vehicle



- Forces in x and y cancel due to symmetric motion

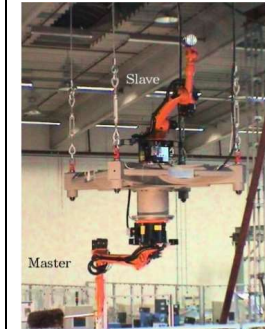
### Towards Valve Turning using a Dual-Arm Aerial Manipulator



- Symmetric arms, yaw rotation motion

Underwater manipulators a review:  
Multiple small arms used as paddles for base motion compensation

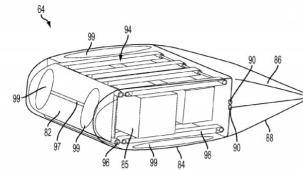
### Reactionless Control for two Manipulators Mounted on a Cable-Suspended Platform:



- Second arm to cancel reaction

Reactive Mechanism

Autonomous Payload Parsing Management System and Structure for an Unmanned Aerial Vehicle



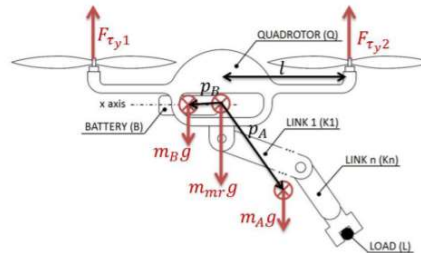
-Redistribute payload parcels within UAV to maintain CoG of the UAV

Long-Reach Aerial Manipulation Employing Wire-Suspended Hand With Swing-Suppression Device:



-Swing suppression with fans

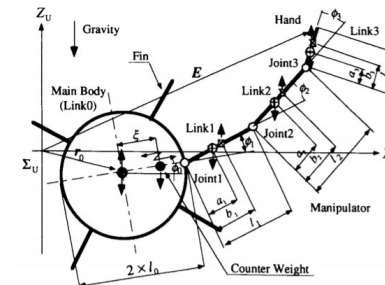
A multilayer control for multirotor UAVs equipped with a servo robot arm



-Battery on slider as an active CW

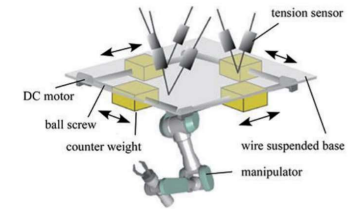
Development of a 4-Joint 3-DOF robotic arm with anti-reaction force mechanism for a multicopter:

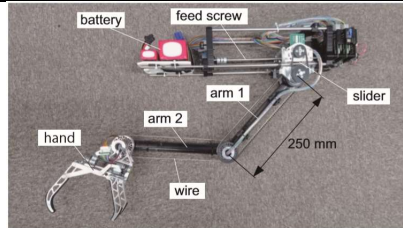
Motion Control of Unconstrained Underwater Robot Considering Gravity and Buoyancy



-Body attitude maintained by actively controlled counterweight

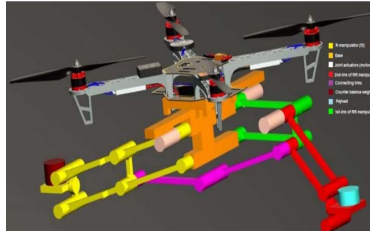
Reaction force control of counter weights for a manipulator suspended by 6 wires





-Sliding Dof to cancel reaction

Stable Under-Actuated Manipulator  
Design For Mobile Manipulating  
Unmanned Aerial Vehicle (MM-UAV)



-Pantograph based manipulator with  
actively controlled countermass

# **B | Appendix: Benefits and Limitations of Methods for Stable Manipulation Summary Table**

This Appendix summarizes the benefits (pros) and limitations (cons) of the methods found in literature for stable floating base manipulation. For each method some specific comments that pertain to certain fields of floating base manipulation are added. The table is divided by the method categories of avoidance, passive, and active.

Avoidance

Method	Pro	Con	Application
Reduce Moving Mass	<ul style="list-style-type: none"> <li>- Established industry standard practice</li> <li>- Good design principle</li> <li>- Simple</li> </ul>	<ul style="list-style-type: none"> <li>- Doesn't fully resolve this issue</li> <li>- Under greater stability or positioning requirements it is no longer effective</li> </ul>	<ul style="list-style-type: none"> <li>- Can be used for all as a design rule</li> </ul>
Attach to a Fixed Base	<ul style="list-style-type: none"> <li>- Can avoid dynamic coupling issue altogether</li> </ul>	<ul style="list-style-type: none"> <li>- Only if a fixed base is available</li> <li>- Movement to grab the base will still be impacted by the dynamic coupling</li> </ul>	<ul style="list-style-type: none"> <li>- Only for a few instances where fixed bases are available such as AUV operations on offshore platforms, some UAV tasks</li> <li>- Not feasible for the other fields</li> </ul>

Passive

Method	Pro	Con	Application
Counterweights	<ul style="list-style-type: none"> <li>- Good for 1 DoF force balance</li> <li>- Simple to apply</li> </ul>	<ul style="list-style-type: none"> <li>- Doesn't scale well to higher DoF</li> <li>- Moment is still unresolved</li> <li>- Adds weight and energy consumption</li> </ul>	<ul style="list-style-type: none"> <li>- Can be used for all</li> </ul>
Inherently Balanced Architectures	<ul style="list-style-type: none"> <li>- Added links are functional: used for the primary task</li> <li>- Force and moment resolved</li> <li>- No planning, or limitations on path</li> </ul>	<ul style="list-style-type: none"> <li>- Complexity can increase with higher DoF especially if one balanced unit is repeated</li> </ul>	<ul style="list-style-type: none"> <li>- Can be used for all</li> </ul>

## Active

Method	Pro	Con	Application
Gyroscopic Actuation	<ul style="list-style-type: none"> <li>- Can keep serial manipulator configuration and just change the actuator</li> </ul>	<ul style="list-style-type: none"> <li>- To get a high force the spinning mass would have to be very large, adding weight and energy consumption</li> </ul>	<ul style="list-style-type: none"> <li>- Only applicable to space domain or for instances where a very low force is required</li> </ul>
Globally Redundant Path Planning	<ul style="list-style-type: none"> <li>- Low energy consumption as no base actuation required</li> <li>- Can use off the shelf components without any modification</li> </ul>	<ul style="list-style-type: none"> <li>- Limited to a few fixed paths</li> <li>- Needs pre-emptive planning</li> <li>- Disturbances can cause path to not achieve desired end position</li> <li>- Base position is still slightly altered, just optimized to minimize the impact</li> </ul>	<ul style="list-style-type: none"> <li>- Effective in the space domain: limited disturbances and planning is common</li> <li>- Can be applied to optimize a trajectory if some base motion is allowable (UAV, AUV)</li> <li>- Not applicable to cable and ground applications</li> </ul>
Locally Redundant Path Planning	<ul style="list-style-type: none"> <li>- Base unaffected by manipulator</li> <li>- Only need a model for the manipulator</li> </ul>	<ul style="list-style-type: none"> <li>- Limited to a few fixed paths</li> <li>- Needs pre-emptive planning</li> <li>- Disturbances can cause path to not achieve desired end position</li> <li>- Additional DoFs add weight, complexity, energy consumption</li> </ul>	<ul style="list-style-type: none"> <li>- Effective on large vehicle systems where base position is very important such as space and cable robots</li> <li>- The additional DoFs are not feasible for AUVs because there are already limitations with the high loads and nonlinear actuation of the hydraulic manipulators</li> </ul>
Feedback Base Control	<ul style="list-style-type: none"> <li>- Simple to apply</li> <li>- No model needed</li> <li>- Off the shelf components</li> </ul>	<ul style="list-style-type: none"> <li>- No guarantee of stability because the base actuators can saturate</li> <li>- Rely on accuracy of vehicle sensors and feedback bandwidth</li> </ul>	<ul style="list-style-type: none"> <li>- Effective for applications where base accuracy is not as important and stability is not difficult to maintain (AUVs)</li> </ul>
Feedforward Base Control	<ul style="list-style-type: none"> <li>- Better guarantee than feedback of stability</li> <li>- Off the shelf components</li> </ul>	<ul style="list-style-type: none"> <li>- Rely on accuracy of the model</li> <li>- Models need to be linearized for onboard computation</li> <li>- Frequently exceed onboard processing</li> </ul>	<ul style="list-style-type: none"> <li>- For simple tasks this is effective but with greater complexity the models become too complicated</li> <li>- Need lots of onboard computational power, so not effective for UAVs</li> </ul>
Dual or multi arm	<ul style="list-style-type: none"> <li>- Relatively simple to add a mirror arm</li> </ul>	<ul style="list-style-type: none"> <li>- Motion is limited</li> <li>- Added weight, complexity, energy consumption from another arm</li> <li>- Mostly 2 arms used but 4 needed for total balancing</li> </ul>	<ul style="list-style-type: none"> <li>- Effective if the task requires symmetric motion from two arms: valve turning (UAV), two arm capture (space), etc</li> <li>- Otherwise other methods are more efficient</li> </ul>
Reactive Mechanism	<ul style="list-style-type: none"> <li>- Can be used to counter other forces than the manipulator such as a collision or picking up a payload</li> </ul>	<ul style="list-style-type: none"> <li>- Typically only counters one force</li> <li>- Total balancing doesn't scale well</li> </ul>	<ul style="list-style-type: none"> <li>- Effective in suppressing one force that is critical to stability, for instance tip over in UAVs</li> <li>- For complete balancing the added complexity isn't feasible for instance in the space domain</li> </ul>

# C | Appendix: Grand 4R and Grand 5R Force Balanced Architecture Derivatives

This appendix lists the force balanced architectures that are derived from van der Wijk's Grand 4R and Grand 5R architectures. [47] [48] As in the thesis the solid lines are links, the white circles are joints, and the solid circles are point masses. S is the invariant common centre of mass of the architecture and also the base connection. The dashed lines indicate some of the options for extending the links. These extensions arise from choosing internal architectures. The Grand 4R architectures are 2 DoF and the Grand 5R architectures are 3 DoF.

## C.1 Grand 4R Architectures

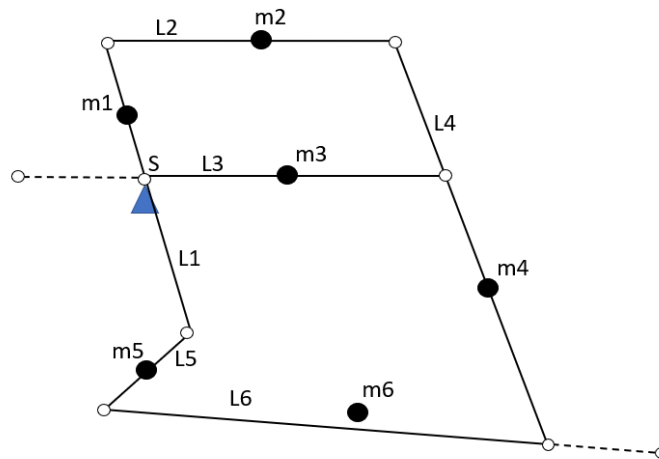
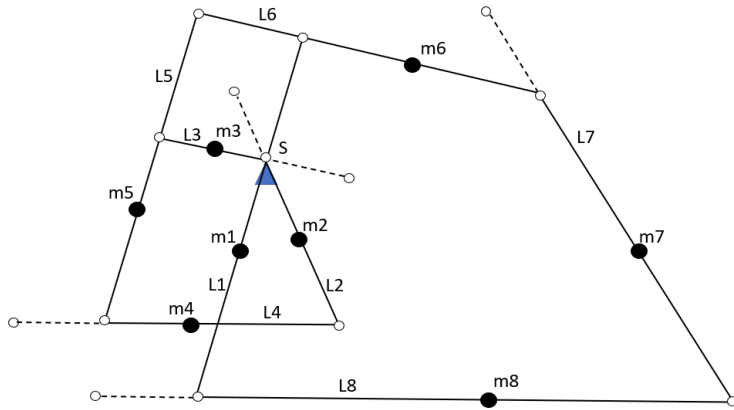
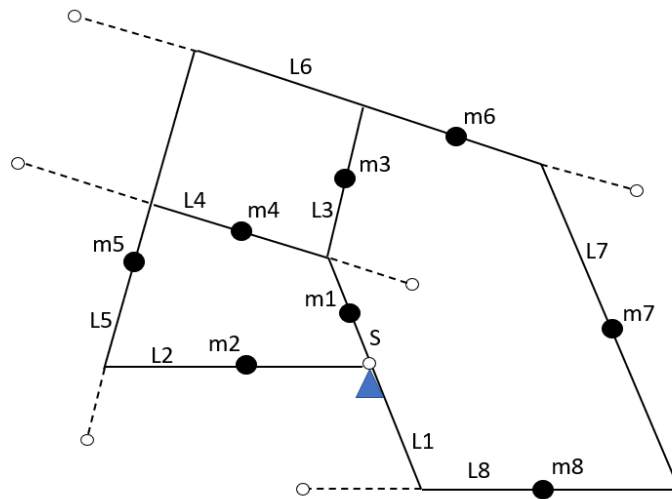


Figure C.1: Grand 4R Derivation 1



**Figure C.2:** Grand 4R Derivation 2



**Figure C.3:** Grand 4R Derivation 3

## C.2 Grand 5R Architectures

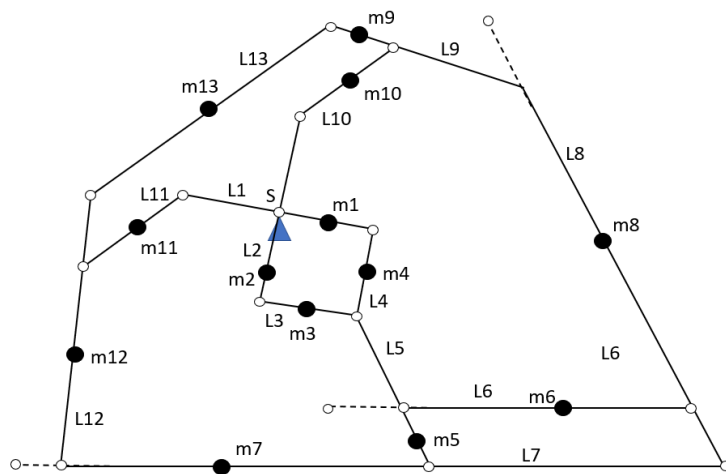


Figure C.4: Grand 5R Derivation 1

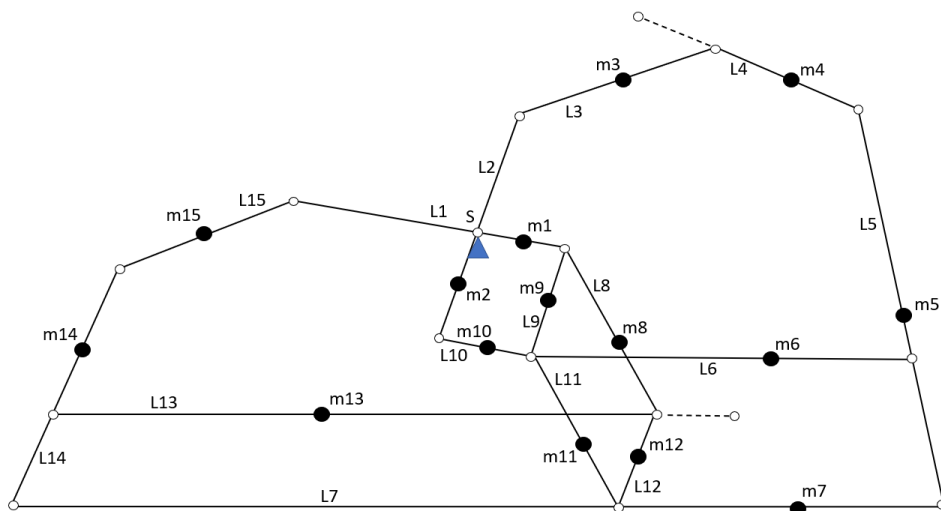


Figure C.5: Grand 5R Derivation 2

# D | Appendix: Simulation of Kinematic Reduction

The manipulator is simulated using SPACAR, Matlab, and Simulink. In a Matlab script the mass, length, and inertia parameters are defined. Then the principle vector lengths are calculated using the force balance conditions for the inherently balanced architecture. For the 3 DoF architecture 3 initial angles are set to fully define the positions of the architecture. Next the position of each joint and point mass is calculated based on the starting position of the link, the angle of the link and the length.

In the matlab script the SPACAR model is then constructed using SPAScripting. A 2D model is initialized. Then the beam elements are created using the locations defined previously. If two links are connected by a joint then they are constrained in translation. For a link with an intermediate joint, a second beam is attached after the joint and is constrained in rotation. Additional beams are constructed which are constrained in both translation and rotation to the links in order to define the location of the point mass along the link. Next the nodal loads (mass and inertia) are defined at the end of the additional beams. The origin, which is point S, is fixed in translation. Hinges, which are pure rotations are connected between the beams. Figure xx illustrates the joint numbers, beam numbers, and hinge numbers.

In Section 3.4.2 the applied torques act between the base and the links. One side of hinge 1 and hinge 2 are fixed in terms of rotation to connect them to the base. Hinge 13 is created which actuates beam 10 and is also fixed in rotation to the base. The rest of the hinges are released. The torque on hinge 1 hinge 2 and hinge 3 are set as inputs and the endpoint position of beam 12 is set as outputs to generate the plots. For the simulation of the final design there is no hinge 13. Hinge 1 and 2 are still connected in rotation to the base. The applied torque of hinge 1,2 and 12 are set as inputs. The positions are also set as outputs along with the reaction moments. The SPACAR model is then constructed as a .dat file.

Simulink is then used to simulate the manipulator. An embedded function sets the input torques. These are fed into a block which integrates the SPACAR .dat file. The outputs are then sent to scopes to view the results.

# E | Appendix: Finite Element of Beam Selection for Detailed Design

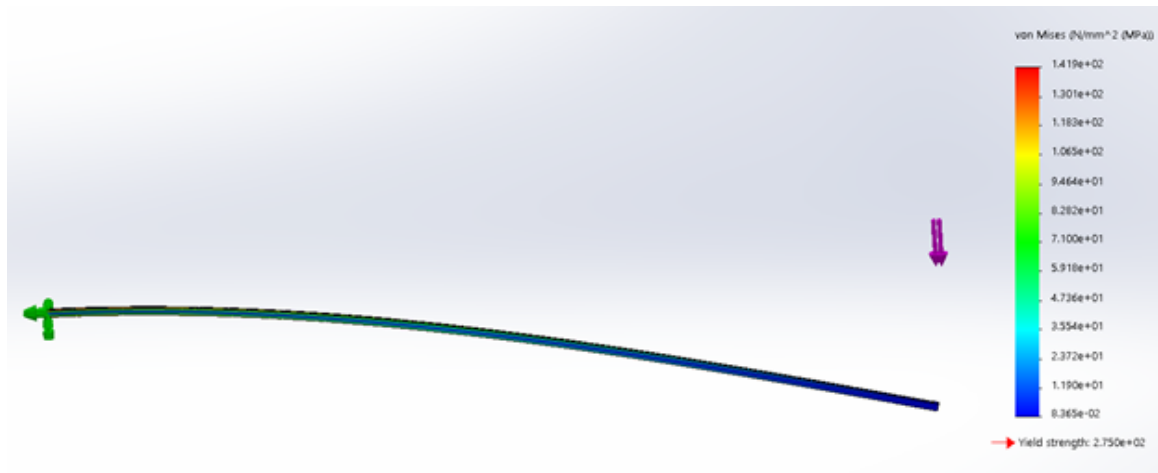
The manipulator is to be constructed from a hollow aluminum beam of 15mm by 15mm with a 1mm wall thickness. To make sure the beam can handle the loads a static fem analysis was performed in solidworks. The largest length and weights are listed below. The characteristic length of 1.3m and 1kg weight were selected as that is larger than the worst case in the manipulator.

Back Beam: Stepper Motor 620g [52]  $l_{31} = 0.95\text{m}$   $l_{13} = 0.12\text{m}$   $L = 1.07$

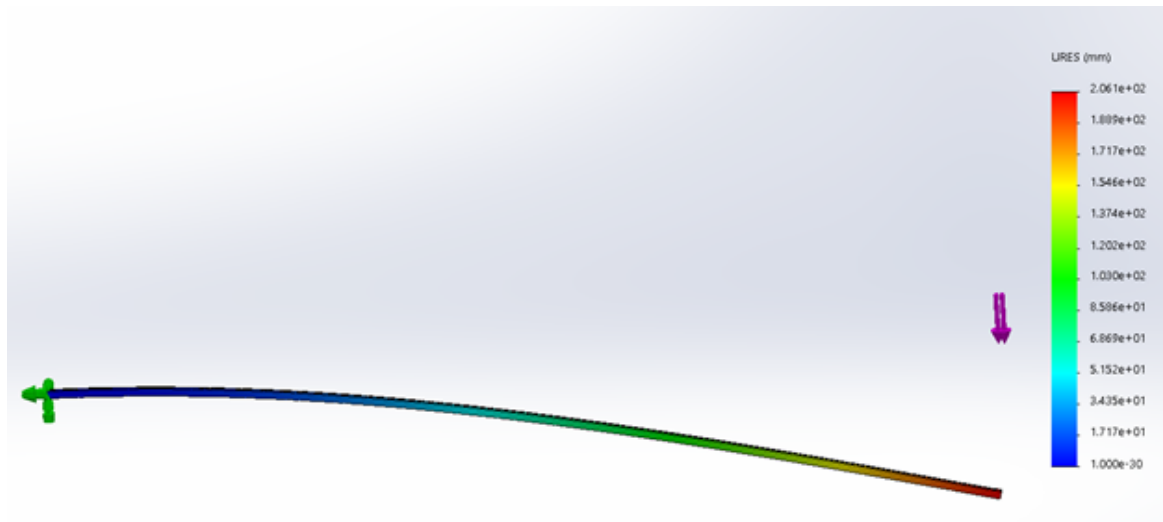
Front Beam: Payload = 300g Rod 1 = 120g

Assumption: characteristic Length of 1.3m, 1kg weight

Von Mises Stress for 1kg applied load, cantilever:



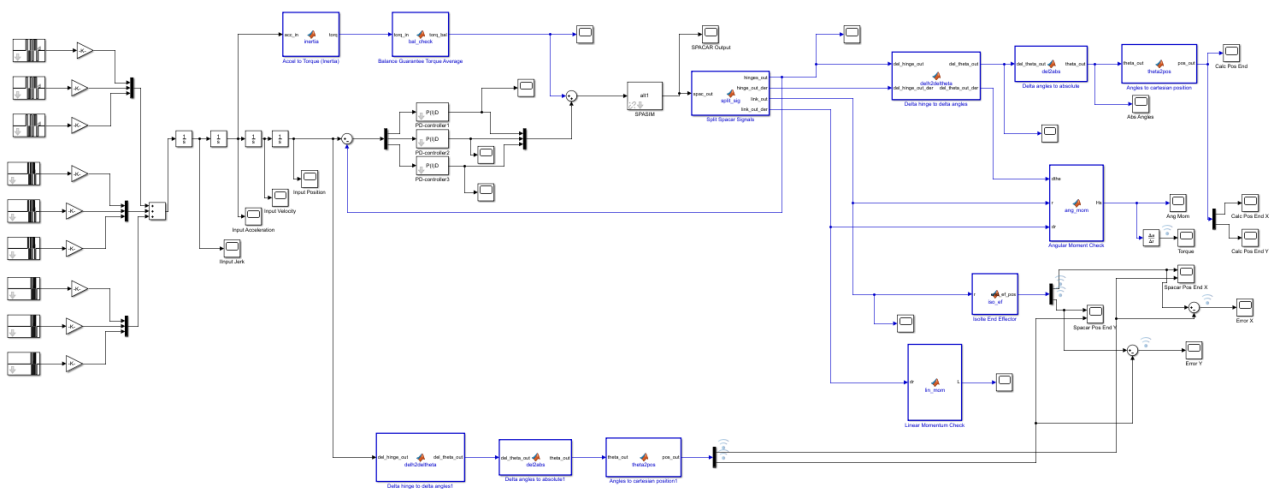
Displacement:



# F | Appendix: Simulation of Active Moment Balancing

This appendix details the active moment balancing simulation. A screen grab is provided of the simulink model. After the offline code is shown which does the inverse kinematics, angular momentum minimization, and calculations to feed into the trajectory generators. After that the Spacar code is shown which is the multibody model/ the plant.

**Simulink:**



**Code Offline**

**Spacar:**

```

%% initialize
step1 = [-0.1; 0];
step2 = [0; -0.1];
step3 = [0.1; 0];

global tol del vmax amax jmax dt

vmax = 100;
amax = 100;
jmax = 100;
dt = 0.5;
tol = 1;
del = linspace(-1,1,200);

%% step 1
pos_in1 = X(10,:) + step1;
theta_in1 = [th1; th2; th3];
[th_input_s1, hing_in_s1, djmax_s1] = inv_kin_balanced(pos_in1, theta_in1);

%% step 2
pos_in2 = pos_in1 + step2;
theta_in2 = th_input_s1;
[th_input_s2, hing_in_s2, djmax_s2] = inv_kin_balanced(pos_in2, theta_in2);

%% step 3
pos_in3 = pos_in2 + step3;
theta_in3 = th_input_s2;
[th_input_s3, hing_in_s3, djmax_s3] = inv_kin_balanced(pos_in3, theta_in3);

```

```

function [theta_input, hing_in, djmax] = inv_kin_balanced(pos_in, theta_req)

global m1 m11 p11 q11 m2 m3 m31 p31 q31 l2 e2 f2 m12 m13 m32 m_e1 m_e3 l33 a21 l1 a1 tol del vmax amax jmax dt ...
       l31 l32 a3 l3 p12 p13 p32 p33 m33 p_me3 p1 p2 p3 a23 l11 l12 l13 l1 l2 l3 l11 l12 l13 l31 l32 l33

%% loop

P2 = pos_in;
r1 = l33;
r2 = (l1-a1);

X_in = zeros(10,3);
XM_in = zeros(10,3);
X_f = zeros(10,3);
XM_f = zeros(10,3);
H_hist = zeros(length(del),1);
H_bnd = zeros(length(del),1);
theta_hist = zeros(3, length(del));
H_min = [];
theta_input = zeros(3,1);
ang_in = zeros(3,1);

ind = 0;

th1_in = theta_req(1);
th2_in = theta_req(2);
th3_in = theta_req(3);

% dist original

X_in(1,:) = [0,0,0];
X_in(2,:) = X_in(1,:) + l31*[cos(th1_in), sin(th1_in),0];
X_in(3,:) = X_in(2,:) + l32*[cos(th2_in), sin(th2_in),0];
X_in(4,:) = X_in(1,:) + l33*[cos(th2_in), sin(th2_in),0];
X_in(5,:) = X_in(4,:) + a21*[cos(th1_in + pi), sin(th1_in + pi),0];
X_in(6,:) = X_in(5,:) + a1*[cos(th3_in), sin(th3_in),0];
X_in(7,:) = X_in(6,:) + l2*[cos(th1_in), sin(th1_in),0];
X_in(8,:) = X_in(7,:) + a3*[cos(th2_in - pi), sin(th2_in - pi),0];
X_in(9,:) = X_in(7,:) + l3*[cos(th2_in - pi), sin(th2_in - pi),0];
X_in(10,:) = X_in(6,:) + l1*[cos(th3_in + pi), sin(th3_in + pi),0];

XM_in(1,:) = X_in(5,:) + p1*[cos(th3_in + pi), sin(th3_in + pi),0];
XM_in(2,:) = X_in(6,:) + p2*[cos(th1_in), sin(th1_in),0];
XM_in(3,:) = X_in(8,:) + p3*[cos(th2_in + pi), sin(th2_in + pi),0];
XM_in(4,:) = X_in(4,:) + p11*[cos(th1_in + pi), sin(th1_in + pi),0];
XM_in(5,:) = X_in(7,:) + p12*[cos(th3_in + pi), sin(th3_in + pi),0];
XM_in(6,:) = X_in(8,:) + p13*[cos(th3_in + pi), sin(th3_in + pi),0];
XM_in(7,:) = X_in(1,:) + p31*[cos(th1_in), sin(th1_in),0];
XM_in(8,:) = X_in(3,:) + p32*[cos(th2_in + pi), sin(th2_in + pi),0];
XM_in(9,:) = X_in(4,:) + p33*[cos(th2_in + pi), sin(th2_in + pi),0];
XM_in(10,:) = X_in(7,:) + p_me3*[cos(th2_in + pi), sin(th2_in + pi),0];

```

```

for i = 1:length(del)

    %disturb angle

    theta1 = th1_in + del(i);

    %solve inv kin for new angles

    P1 = [a21*cos(theta1+pi);
          a21*sin(theta1+pi)];

    d2 = sum((P2-P1).^2);
    P0 = (P1+P2)/2+(r1^2-r2^2)/d2/2*(P2-P1);
    t = ((r1+r2)^2-d2)*(d2-(r2-r1)^2);
    if t <= 0
        fprintf('The circles don''t intersect.\n')
        Pa = NaN;
        Pb = NaN;
        pout = [NaN; NaN];

    else
        T = sqrt(t)/d2/2*[0 -1;1 0]*(P2-P1);
        Pa = (P0 + T); % Pa and Pb are circles' intersection points
        Pb = (P0 - T);
        if norm(Pa) > norm(Pb)
            pout = Pa;
        else
            pout = Pb;
        end
    end

end

theta2 = mod(atan2((pout(2) - P1(2)), (pout(1) - P1(1))),2*pi);

alpha = mod(atan2((P2(2) - pout(2)), (P2(1) - pout(1))),2*pi);

theta3 = alpha + pi;

%theta derivatives
dth1 = (theta1 - th1_in)/dt;
dth2 = (theta2 - th2_in)/dt;
dth3 = (theta3 - th3_in)/dt;

% distance from CoM final
X_f(1,:) = [0,0,0];
X_f(2,:) = X_f(1,:) + 131*[cos(theta1), sin(theta1),0];
X_f(3,:) = X_f(2,:) + 132*[cos(theta2), sin(theta2),0];
X_f(4,:) = X_f(1,:) + 133*[cos(theta2), sin(theta2),0];
X_f(5,:) = X_f(4,:) + a21*[cos(theta1 + pi), sin(theta1 + pi),0];
X_f(6,:) = X_f(5,:) + a1*[cos(theta3), sin(theta3),0];
X_f(7,:) = X_f(6,:) + 12*[cos(theta1), sin(theta1),0];
X_f(8,:) = X_f(7,:) + a3*[cos(theta2 - pi), sin(theta2 - pi),0];
X_f(9,:) = X_f(7,:) + 13*[cos(theta2 - pi), sin(theta2 - pi),0];
X_f(10,:) = X_f(6,:) + 11*[cos(theta3 + pi), sin(theta3 + pi),0];

```

```

XM_f(1,:) = X_f(5,:) + p1*[cos(theta3 + pi), sin(theta3 + pi),0];
XM_f(2,:) = X_f(6,:) + p2*[cos(theta1), sin(theta1),0];
XM_f(3,:) = X_f(8,:) + p3*[cos(theta2 + pi), sin(theta2 + pi),0];
XM_f(4,:) = X_f(4,:) + p11*[cos(theta1 + pi), sin(theta1 + pi),0];
XM_f(5,:) = X_f(7,:) + p12*[cos(theta3 + pi), sin(theta3 + pi),0];
XM_f(6,:) = X_f(8,:) + p13*[cos(theta3 + pi), sin(theta3 + pi),0];
XM_f(7,:) = X_f(1,:) + p31*[cos(theta1), sin(theta1),0];
XM_f(8,:) = X_f(3,:) + p32*[cos(theta2 + pi), sin(theta2 + pi),0];
XM_f(9,:) = X_f(4,:) + p33*[cos(theta2 + pi), sin(theta2 + pi),0];
XM_f(10,:) = X_f(7,:) + p_me3*[cos(theta2 + pi), sin(theta2 + pi),0];

dr = (XM_f - XM_in)/dt;

dr_end = (X_f(10,:) - X_in(10,:))/dt;

%check angular momentum

Hs = (I31 + I11 + I2)*dth1 + (I33 + I32 + I3)*dth2 + (I13 + I12 + I1)*dth3 + m1*cross(XM_f(1,:)',dr(1,:))...
    + m2*cross(XM_f(2,:)',dr(2,:)) + m3*cross(XM_f(3,:)',dr(3,:)) + m11*cross(XM_f(4,:)',dr(4,:)) + ....
    m12*cross(XM_f(5,:)',dr(5,:)) + m13*cross(XM_f(6,:)',dr(6,:)) + m31*cross(XM_f(7,:)',dr(7,:)) + ....
    m32*cross(XM_f(8,:)',dr(8,:)) + m33*cross(XM_f(9,:)',dr(9,:)) + m_e3*cross(XM_f(10,:)',dr(10,:)) ...
    + m_e1*cross(X_f(10,:)',dr_end');

H_hist(i) = Hs(3);
theta_hist(:,i) = [thetal; theta2; theta3];

if abs(thetal-th1_in) < tol && abs(theta2-th2_in) < tol && abs(theta3-th3_in) < tol %&& (thetal-th1_i
    H_bnd(i) = Hs(3);
else
    H_bnd(i) = NaN;
end

end

[H_min, ind] = min(abs(H_bnd), [], 'omitnan');
theta_input = theta_hist(:,ind);

del_ang = [theta_input(1) - th1_in;
           theta_input(2) - th2_in;
           theta_input(3) - th3_in];

hing_in = [del_ang(1);
           del_ang(2);
           del_ang(3) - del_ang(2)];

djmax(1) = abs(hing_in(1))/(8*(dt/8)^4);
djmax(2) = abs(hing_in(2))/(8*(dt/8)^4);
djmax(3) = abs(hing_in(3))/(8*(dt/8)^4);

return

```

```

%% parameters

global m1 m11 p11 q11 m2 m3 m31 p31 q31 l2 e2 f2 m12 m13 m32 m_e1 m_e3 l33 a21 l1 a1 l31 l32 a3 l3 p12 p13 p32 p33 .
    m33 p_me3 p1 p2 p3 a23 l11 l12 l13 I1 I2 I3 I11 I12 I13 I31 I32 I33
l1=0.8;          l2=2.3;          l3=0.4;          l4=3.2; % main four-bar linkage
m1=0.141;       m2=0.406;       m3=0.119;       m4=0;
e1=0.209;       e2=1.044;       e3=0.016;       e4=0.5*14;

f1=0;   f2=0; f3=0;   f4=0;
s1 = sqrt(e1^2+f1^2);      s21 = sqrt(e2^2+f2^2);
s23 = sqrt((l2-e2)^2+f2^2); s3 = sqrt(e3^2+f3^2);

m11=0.415; m12=0.119; m13=0.119; m31=0.142; m32=0.059; m33=0.059; % principal vector linkage
p11=0.439; p12=0.070; p13=0.070; p31=0.403; p32=0.037; p33=0.037;
q11=0; q12=0; q13=0; q31=0; q32=0; q33=0;

m_e1 = 0.3; %gimbal + payload
m_e3 = 0.6;

p_me3 = 0.250; %distance of motor 3

mtot=m1+m2+m3+m11+m12+m13+m31+m32+m33 + m_e1 + m_e3; % total mass

th1 = deg2rad(0+180);
th2 = deg2rad(110+180);
th3 = deg2rad(45+180);

I1 = 8650652e-9;   I2 = 222907011e-9;   I3 = 1761313e-9;
I11 = 224638047e-9; I12 = 197139e-9;   I13 = 197139e-9;
I31 = 9938821e-9;  I32 = 33698e-9;    I33 = 33698e-9;

acc1 = 0.2;
acc2 = 0.2;
acc3 = 0.2;

%% solve balance

a1=(m1*s1 + m_e1*l1 +m12*p12+m13*p13)/(mtot-m11-m33-m32-m31);
a3=(m3*s3 + m_e3*p_me3 +m32*p32+m33*p33)/(mtot-m31-m13);

%%% To complete: solving ELMS to find P2
a21 = (m31*p31 - m11*p11 + l2*(m32 + m12 + m13 + m3 + m_e3) + e2*m2)/ (m32 + m12 + m13 + m3 + m_e3 + m1 + m_e1 + m2);
x2 = a21;

%% convert

a23 = l2 - x2;
p1 = e1 - a1;
p2 = e2;
p3 = e3 - a3;

```

```

l11 = a21 + a23;
l12 = a1;
l13 = a1;
l31 = a23;
l32 = a3;
l33 = a3;

%% Kinematic positions

%links
X(1,:) = [0,0];
X(2,:) = X(1,:) + l31*[cos(th1), sin(th1)];
X(3,:) = X(2,:) + l32*[cos(th2), sin(th2)];
X(4,:) = X(1,:) + l33*[cos(th2), sin(th2)];
X(5,:) = X(4,:) + a21*[cos(th1 + pi), sin(th1 + pi)];
X(6,:) = X(5,:) + a1*[cos(th3), sin(th3)];
X(7,:) = X(6,:) + l2*[cos(th1), sin(th1)];
X(8,:) = X(7,:) + a3*[cos(th2 - pi), sin(th2 - pi)];
X(9,:) = X(7,:) + l3*[cos(th2 - pi), sin(th2 - pi)];
X(10,:) = X(6,:) + l1*[cos(th3 + pi), sin(th3 + pi)];

%masses
XM(1,:) = X(5,:) + p1*[cos(th3 + pi), sin(th3 + pi)];
XM(2,:) = X(6,:) + p2*[cos(th1), sin(th1)];
XM(3,:) = X(8,:) + p3*[cos(th2 + pi), sin(th2 + pi)];
XM(4,:) = X(4,:) + p11*[cos(th1 + pi), sin(th1 + pi)];
XM(5,:) = X(7,:) + p12*[cos(th3 + pi), sin(th3 + pi)];
XM(6,:) = X(8,:) + p13*[cos(th3 + pi), sin(th3 + pi)];
XM(7,:) = X(1,:) + p31*[cos(th1), sin(th1)];
XM(8,:) = X(3,:) + p32*[cos(th2 + pi), sin(th2 + pi)];
XM(9,:) = X(4,:) + p33*[cos(th2 + pi), sin(th2 + pi)];

XM(10,:) = X(7,:) + p_me3*[cos(th2 + pi), sin(th2 + pi)];

%% build model

init_build('2D');

% create linkages through beams 1-12
bm1 = add_plbeam(X(1,:),X(2,:),1); %beam 1
bm2 = add_plbeam(X(2,:),X(3,:),1,{'trans_p',bm1,'q'}); %beam 2
bm3 = add_plbeam(X(3,:),X(4,:),1,{'trans_p',bm2,'q'}); %beam 3
bm4 = add_plbeam(X(4,:),X(5,:),1,{'trans_p',bm3,'q'},{'rot_p',bm3,'q'});
bm5 = add_plbeam(X(4,:),X(1,:),1,{'trans_p',bm3,'q'}, {'trans_q',bm1,'p'});
bm6 = add_plbeam(X(6,:),X(5,:),1,{'trans_q',bm4,'q'});
bm7 = add_plbeam(X(5,:),X(10,:),1,{'rot_p',bm6,'q'}, {'trans_p',bm6,'q'});
bm8 = add_plbeam(X(6,:),X(7,:),1,{'trans_p',bm6,'p'});
bm9 = add_plbeam(X(7,:),X(3,:),1,{'trans_p',bm8,'q'}, {'trans_q',bm3,'p'});
bm10 = add_plbeam(X(8,:),X(2,:),1,{'trans_q',bm1,'q'});
bm11 = add_plbeam(X(7,:),X(8,:),1,{'trans_p',bm8,'q'}, {'trans_q',bm10,'p'});
bm12 = add_plbeam(X(8,:),X(9,:),1,{'rot_p',bm11,'q'}, {'trans_p',bm11,'q'});

```

```

%position point mass beams
bm13 = add_plbeam(X(5,:),XM(1,:),1,{{'trans_p',bm7,'p'},{'rot_p',bm7,'p'}}); %m1
bm14 = add_plbeam(X(6,:),XM(2,:),1,{{'trans_p',bm8,'p'},{'rot_p',bm8,'p'}}); %m2
bm15 = add_plbeam(X(8,:),XM(3,:),1,{{'trans_p',bm12,'p'},{'rot_p',bm12,'p'}}); %m3
bm16 = add_plbeam(X(4,:),XM(4,:),1,{{'trans_p',bm4,'p'},{'rot_p',bm4,'p'}}); %m11
bm17 = add_plbeam(X(7,:),XM(5,:),1,{{'trans_p',bm9,'p'},{'rot_p',bm9,'p'}}); %m12
bm18 = add_plbeam(X(8,:),XM(6,:),1,{{'trans_p',bm10,'p'},{'rot_p',bm10,'p'}}); %m13
bm19 = add_plbeam(X(1,:),XM(7,:),1,{{'trans_p',bm1,'p'},{'rot_p',bm1,'p'}}); %m31
bm20 = add_plbeam(X(3,:),XM(8,:),1,{{'trans_p',bm2,'q'},{'rot_p',bm2,'q'}}); %m32
bm21 = add_plbeam(X(4,:),XM(9,:),1,{{'trans_p',bm5,'p'},{'rot_p',bm5,'p'}}); %m33

bm22 = add_plbeam(X(8,:),XM(10,:),1,{{'trans_p',bm12,'p'},{'rot_p',bm12,'p'}}); %m_e3

%add masses
add_nodalloads('xm', XM(1,:), {'trans',bm13,'q'}, m1); %m1
add_nodalloads('xm', XM(2,:), {'trans',bm14,'q'}, m2); %m2..
add_nodalloads('xm', XM(3,:), {'trans',bm15,'q'}, m3);
add_nodalloads('xm', XM(4,:), {'trans',bm16,'q'}, m11);
add_nodalloads('xm', XM(5,:), {'trans',bm17,'q'}, m12);
add_nodalloads('xm', XM(6,:), {'trans',bm18,'q'}, m13);
add_nodalloads('xm', XM(7,:), {'trans',bm19,'q'}, m31);
add_nodalloads('xm', XM(8,:), {'trans',bm20,'q'}, m32);
add_nodalloads('xm', XM(9,:), {'trans',bm21,'q'}, m33);

add_nodalloads('xm', [], {'trans',bm7,'q'}, m_e1);
add_nodalloads('xm', [], {'trans',bm22,'q'}, m_e3);

%add inertias
add_nodalloads('xm', [], {'rot',bm13,'q'}, I1);
add_nodalloads('xm', XM(2,:), {'rot',bm14,'q'}, I2);
add_nodalloads('xm', XM(3,:), {'rot',bm15,'q'}, I3);
add_nodalloads('xm', XM(4,:), {'rot',bm16,'q'}, I11);
add_nodalloads('xm', XM(5,:), {'rot',bm17,'q'}, I12);
add_nodalloads('xm', XM(6,:), {'rot',bm18,'q'}, I13);
add_nodalloads('xm', XM(7,:), {'rot',bm19,'q'}, I31);
add_nodalloads('xm', XM(8,:), {'rot',bm20,'q'}, I32);
add_nodalloads('xm', XM(9,:), {'rot',bm21,'q'}, I33);

% fix origin
add_constrdofs('fix',X(1,:),{'trans',bm1,'p'},[1,2]);

%hinges
hinge1 = add_pltor([], {'rot_q' bm1 'p'}); %driving motor from base
hinge2 = add_pltor([], {'rot_q' bm5 'q'}); %driving motor from base

hinge3 = add_pltor([], {'rot_p' bm1 'q'} {'rot_q' bm10 'q'});
hinge4 = add_pltor([], {'rot_p' bm1 'q'} {'rot_q' bm2 'p'});
hinge5 = add_pltor([], {'rot_p' bm2 'q'} {'rot_q' bm3 'p'});
hinge6 = add_pltor([], {'rot_p' bm2 'q'} {'rot_q' bm9 'q'});
hinge7 = add_pltor([], {'rot_p' bm3 'q'} {'rot_q' bm5 'p'});
hinge8 = add_pltor([], {'rot_p' bm7 'p'} {'rot_q' bm4 'q'});
hinge9 = add_pltor([], {'rot_p' bm6 'p'} {'rot_q' bm8 'p'});
hinge10 = add_pltor([], {'rot_p' bm8 'q'} {'rot_q' bm9 'p'});
hinge11 = add_pltor([], {'rot_p' bm9 'p'} {'rot_q' bm11 'p'});

```

```

hinge12 = add_pltor([], {'rot_p' bm11 'q'} {'rot_q' bm10 'p'});

%hinge13 = add_pltor([], {'rot_q' bm10 'q'});

%hinge constraints
add_constrdofs('fix',[],{'rot', hinge1, 'p'});
add_constrdofs('fix',[],{'rot', hinge2, 'p'});
%add_constrdofs('fix',[],{'rot', hinge13, 'p'});

add_constrdofs('dyne',hinge1,1);
add_constrdofs('dyne',hinge2,1);
add_constrdofs('dyne',hinge12,1);

add_constrdofs('rlse',hinge3,1);
add_constrdofs('rlse',hinge4,1);
add_constrdofs('rlse',hinge5,1);
add_constrdofs('rlse',hinge6,1);
add_constrdofs('rlse',hinge7,1);
add_constrdofs('rlse',hinge8,1);
add_constrdofs('rlse',hinge9,1);
add_constrdofs('rlse',hinge10,1);
add_constrdofs('rlse',hinge11,1);
%add_constrdofs('rlse',hinge12,1);

extra_dynamics_options = { '';
    'gravity 0 0 0 ';
    'timestep 2 100';
    '';
    'END';
    'HALT';
    '';
    ['INPUTS 1 ' num2str(hinge1) ' 1']; %input torque 1
    ['INPUTS 2 ' num2str(hinge2) ' 1']; %input torque 2
    ['INPUTS 3 ' num2str(hinge12) ' 1']; %input torque 3
    ['OUTE 1 ' num2str(hinge1) ' 1'];
    ['OUTE 2 ' num2str(hinge2) ' 1'];
    ['OUTE 3 ' num2str(hinge12) ' 1'];
    ['OUTEP 4 ' num2str(hinge1) ' 1'];
    ['OUTEP 5 ' num2str(hinge2) ' 1'];
    ['OUTEP 6 ' num2str(hinge12) ' 1'];
    ['OUTX 7 ' num2str(elem_coordnumb(bm13,3)) ' 1'];
    ['OUTX 8 ' num2str(elem_coordnumb(bm13,3)) ' 2'];
    ['OUTX 9 ' num2str(elem_coordnumb(bm14,3)) ' 1'];
    ['OUTX 10 ' num2str(elem_coordnumb(bm14,3)) ' 2'];
    ['OUTX 11 ' num2str(elem_coordnumb(bm15,3)) ' 1'];
    ['OUTX 12 ' num2str(elem_coordnumb(bm15,3)) ' 2'];
    ['OUTX 13 ' num2str(elem_coordnumb(bm16,3)) ' 1'];
    ['OUTX 14 ' num2str(elem_coordnumb(bm16,3)) ' 2'];
    ['OUTX 15 ' num2str(elem_coordnumb(bm17,3)) ' 1'];
    ['OUTX 16 ' num2str(elem_coordnumb(bm17,3)) ' 2'];
    ['OUTX 17 ' num2str(elem_coordnumb(bm18,3)) ' 1'];
    ['OUTX 18 ' num2str(elem_coordnumb(bm18,3)) ' 2'];
};

```

```

[ 'OUTX 17 ' num2str(elem_coordnumb (bm18,3)) ' 1'];
[ 'OUTX 18 ' num2str(elem_coordnumb (bm18,3)) ' 2'];
[ 'OUTX 19 ' num2str(elem_coordnumb (bm19,3)) ' 1'];
[ 'OUTX 20 ' num2str(elem_coordnumb (bm19,3)) ' 2'];
[ 'OUTX 21 ' num2str(elem_coordnumb (bm20,3)) ' 1'];
[ 'OUTX 22 ' num2str(elem_coordnumb (bm20,3)) ' 2'];
[ 'OUTX 23 ' num2str(elem_coordnumb (bm21,3)) ' 1'];
[ 'OUTX 24 ' num2str(elem_coordnumb (bm21,3)) ' 2'];
[ 'OUTX 25 ' num2str(elem_coordnumb (bm7,3)) ' 1'];
[ 'OUTX 26 ' num2str(elem_coordnumb (bm7,3)) ' 2'];
[ 'OUTX 27 ' num2str(elem_coordnumb (bm22,3)) ' 1'];
[ 'OUTX 28 ' num2str(elem_coordnumb (bm22,3)) ' 2'];
[ 'OUTXP 29 ' num2str(elem_coordnumb (bm13,3)) ' 1'];
[ 'OUTXP 30 ' num2str(elem_coordnumb (bm13,3)) ' 2'];
[ 'OUTXP 31 ' num2str(elem_coordnumb (bm14,3)) ' 1'];
[ 'OUTXP 32 ' num2str(elem_coordnumb (bm14,3)) ' 2'];
[ 'OUTXP 33 ' num2str(elem_coordnumb (bm15,3)) ' 1'];
[ 'OUTXP 34 ' num2str(elem_coordnumb (bm15,3)) ' 2'];
[ 'OUTXP 35 ' num2str(elem_coordnumb (bm16,3)) ' 1'];
[ 'OUTXP 36 ' num2str(elem_coordnumb (bm16,3)) ' 2'];
[ 'OUTXP 37 ' num2str(elem_coordnumb (bm17,3)) ' 1'];
[ 'OUTXP 38 ' num2str(elem_coordnumb (bm17,3)) ' 2'];
[ 'OUTXP 39 ' num2str(elem_coordnumb (bm18,3)) ' 1'];
[ 'OUTXP 40 ' num2str(elem_coordnumb (bm18,3)) ' 2'];
[ 'OUTXP 41 ' num2str(elem_coordnumb (bm19,3)) ' 1'];
[ 'OUTXP 42 ' num2str(elem_coordnumb (bm19,3)) ' 2'];
[ 'OUTXP 43 ' num2str(elem_coordnumb (bm20,3)) ' 1'];
[ 'OUTXP 44 ' num2str(elem_coordnumb (bm20,3)) ' 2'];
[ 'OUTXP 45 ' num2str(elem_coordnumb (bm21,3)) ' 1'];
[ 'OUTXP 46 ' num2str(elem_coordnumb (bm21,3)) ' 2'];
[ 'OUTXP 47 ' num2str(elem_coordnumb (bm7,3)) ' 1'];
[ 'OUTXP 48 ' num2str(elem_coordnumb (bm7,3)) ' 2'];
[ 'OUTXP 49 ' num2str(elem_coordnumb (bm22,3)) ' 1'];
[ 'OUTXP 50 ' num2str(elem_coordnumb (bm22,3)) ' 2'];
};

```

```

build_model('alt1',extra_dynamics_options);

```

```

%% run model

```

```

spacar(4,'alt1');

```

```

loadsbm('alt1');

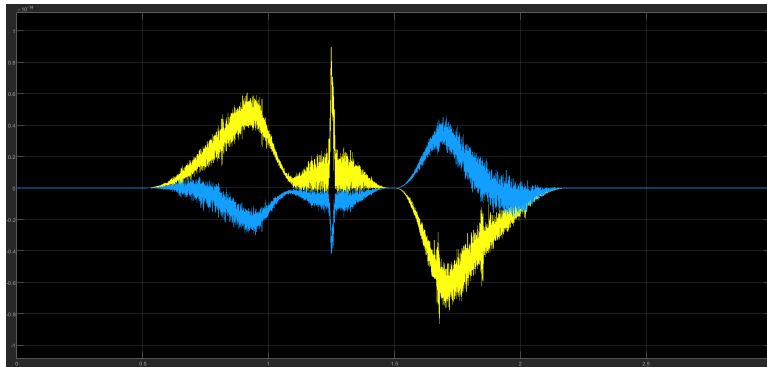
```

# G | Appendix: Additional Simulation Results

This appendix lists some of the additional results from the active balancing simulation. First the linear momentum is plotted for one result to verify the manipulator was force balanced. This was the same for the rest of the results. Next additional factors are plotted such as only averaging the feedforward torques with feedback. Another was implementing an H2 controller instead of 3 PDs.

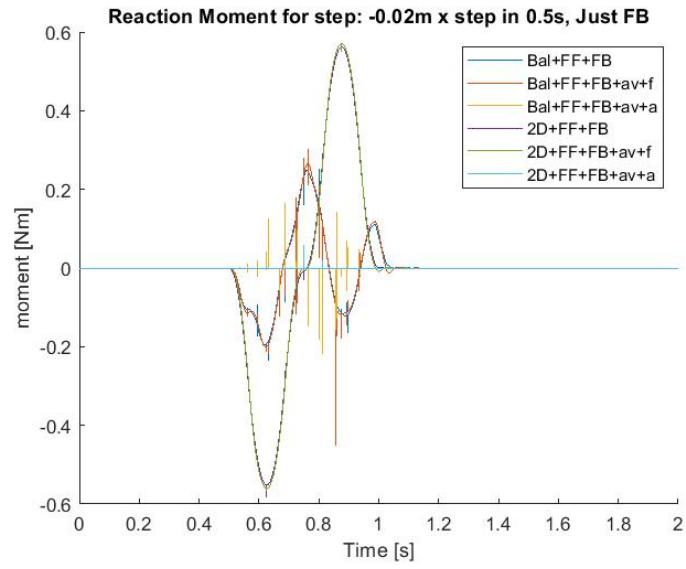
## G.1 Linear Momentum

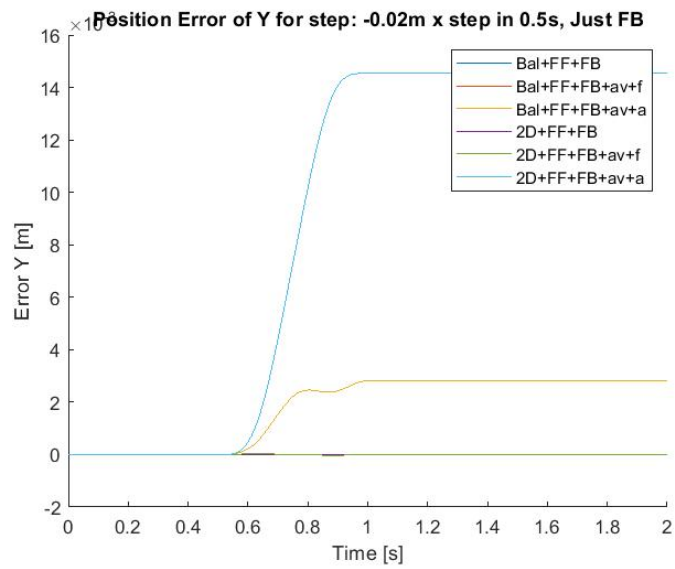
This is the linear momentum result for a c-path. All the rest were also zero. Note the scale is  $10e-14$ . Linear momentum is on the y axis and time is on the x axis. Yellow is the x linear momentum, blue is the y linear momentum.



## G.2 Feedforward Averaging with Feedback Results

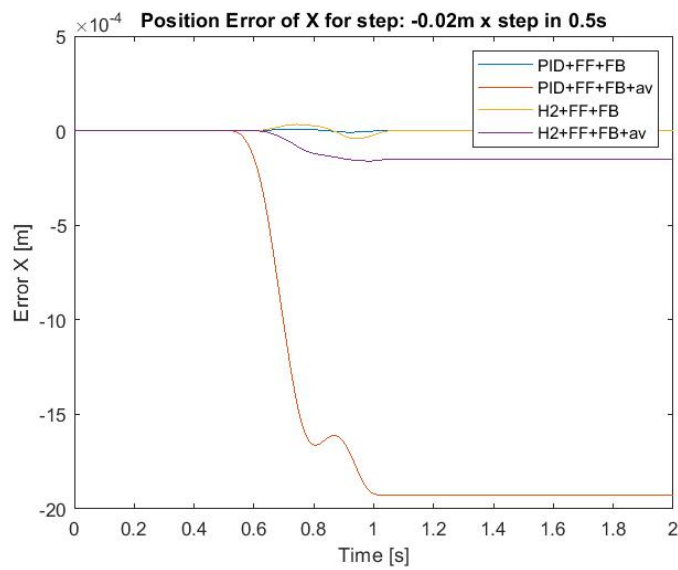
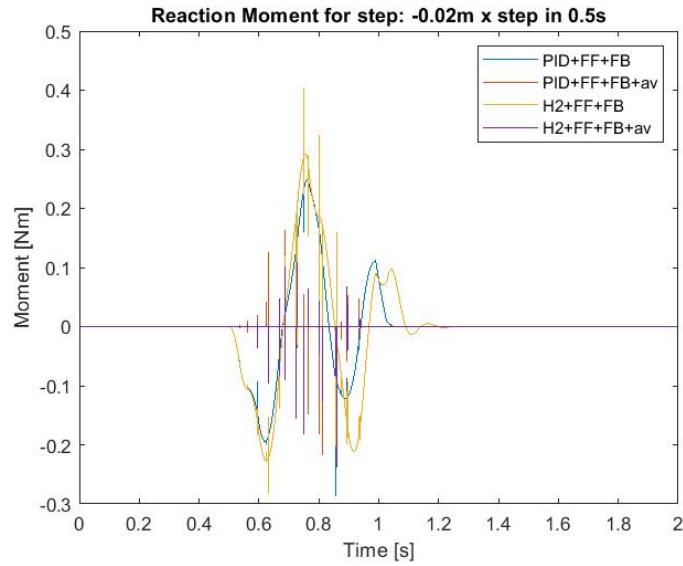
The results are shown with the others for a step of  $-0.02\text{m}$  in X. "av+f" is for when just the feedforward torque is averaged and "av+a" is when all the input torques are averaged. The averaging of just the feedforward with feedback is very similar to just having feedforward and feedback.

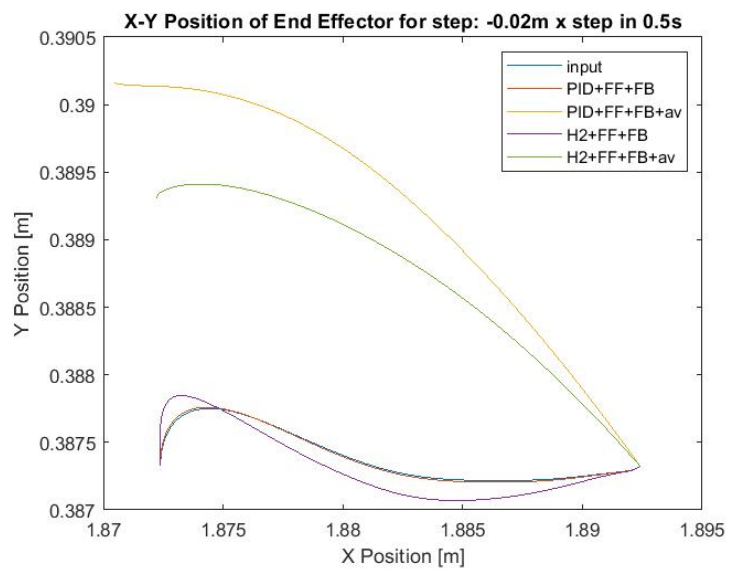
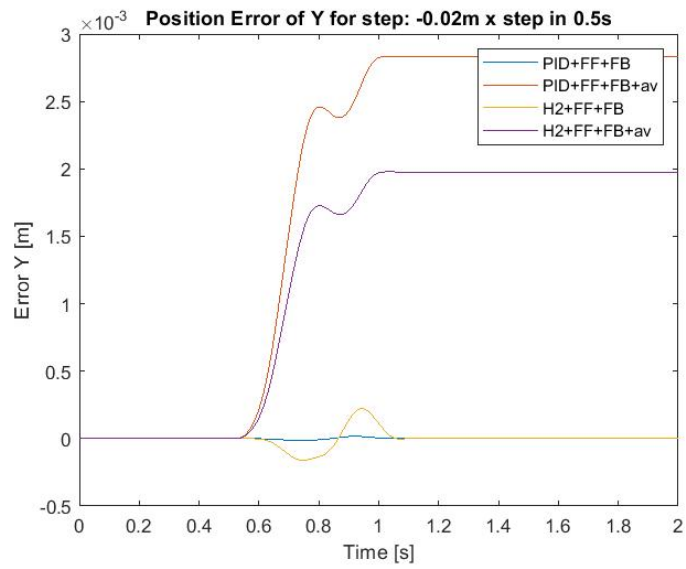




### G.3 H2 Controller Results

An H2 controller was implemented instead of 3 PIDs. The simulink model is shown. The plots are also shown comparing h2 and pid for feedforward and feedback with and without averaging. The reaction moment is slightly higher for H2 without averaging. For positioning error x the H2 is better in x and y.





# Bibliography

- [1] Pal Johan From, Jan T Gravdahl, and Kristin Y Pettersen. *Vehicle-manipulator systems*. Springer, 2016.
- [2] Konstantin Kondak, Felix Huber, Marc Schwarzbach, Maximilian Laiacker, Dominik Sommer, Manuel Bejar, and Aníbal Ollero. Aerial manipulation robot composed of an autonomous helicopter and a 7 degrees of freedom industrial manipulator. In *2014 IEEE international conference on robotics and automation (ICRA)*, pages 2107–2112. IEEE, 2014.
- [3] Matko Orsag, Christopher Korpela, Paul Oh, Stjepan Bogdan, and Anibal Ollero. *Aerial Manipulation*. Springer, 2018.
- [4] Hossein Bonyan Khamseh, Farrokh Janabi-Sharifi, and Abdelkader Abdessameud. Aerial manipulation—a literature survey. *Robotics and Autonomous Systems*, 107:221–235, 2018.
- [5] Somasundar Kannan, Miguel A Olivares-Mendez, and Holger Voos. Modeling and control of aerial manipulation vehicle with visual sensor. *IFAC Proceedings Volumes*, 46(30):303–309, 2013.
- [6] Roberto Rossi, Angel Santamaria-Navarro, Juan Andrade-Cetto, and Paolo Rocco. Trajectory generation for unmanned aerial manipulators through quadratic programming. *IEEE Robotics and Automation Letters*, 2(2):389–396, 2016.
- [7] Todd W Danko and Paul Y Oh. A hyper-redundant manipulator for mobile manipulating unmanned aerial vehicles. In *2013 International Conference on Unmanned Aircraft Systems (ICUAS)*, pages 974–981. IEEE, 2013.
- [8] Christopher Korpela, Matko Orsag, and Paul Oh. Towards valve turning using a dual-arm aerial manipulator. In *2014 IEEE/RSJ International Conference on Intelligent Robots and Systems*, pages 3411–3416. IEEE, 2014.
- [9] Fabio Ruggiero, Miguel Angel Trujillo, R Cano, H Ascorbe, Antidio Viguria, C Pérez, Vincenzo Lippiello, Aníbal Ollero, and Bruno Siciliano. A multilayer control for multicopter uavs equipped with a servo robot arm. In *2015 IEEE international conference on robotics and automation (ICRA)*, pages 4014–4020. IEEE, 2015.
- [10] Yoshinori Ohnishi, Takeshi Takaki, Tadayoshi Aoyama, and Idaku Ishii. Development of a 4-joint 3-dof robotic arm with anti-reaction force mechanism for a multicopter. In *2017 IEEE/RSJ International Conference on Intelligent Robots and Systems (IROS)*, pages 985–991. IEEE, 2017.
- [11] Osama M Abdul Hafez, Mohammad A Jaradat, and Khaled S Hatamleh. Stable under-actuated manipulator design for mobile manipulating unmanned aerial vehicle (mm-uav). In *2017 7th International Conference on Modeling, Simulation, and Applied Optimization (ICMSAO)*, pages 1–6. IEEE, 2017.
- [12] Anibal Ollero, Guillermo Heredia, Antonio Franchi, Gianluca Antonelli, Konstantin Kondak, Alberto Sanfeliu, Antidio Viguria, J Ramiro Martinez-de Dios, Francesco Pierri, Juan Cortés, et al. The aeroarms project: Aerial robots with advanced manipulation capabilities for inspection and maintenance. *IEEE Robotics & Automation Magazine*, 25(4):12–23, 2018.
- [13] Stelios Andreou and Evangelos G Papadopoulos. Design of a reactionless pointing mechanism for satellite antennas. In *11th ESA Workshop on Advanced Space Technologies for Robotics and Automation (ASTRA 2011)*, pages 12–14, 2011.
- [14] DJI. Dji matrice 600 specs, 2020.

- [15] Yangnian Wu and Clément M Gosselin. Synthesis of reactionless spatial 3-dof and 6-dof mechanisms without separate counter-rotations. *The International Journal of Robotics Research*, 23(6):625–642, 2004.
- [16] Paulo Debenest, Eduardo F Fukushima, Yuki Tojo, and Shigeo Hirose. A new approach to humanitarian demining. *Autonomous Robots*, 18(3):323–336, 2005.
- [17] Van der Wijk V. Longval J. Laliberté T. Foucault S. and Gosselin C. Shaking force and shaking moment balanced high-speed manipulator on a floating platform: The dela-1.
- [18] Satja Sivčev, Joseph Coleman, Edin Omerdić, Gerard Dooly, and Daniel Toal. Underwater manipulators: A review. *Ocean Engineering*, 163:431–450, 2018.
- [19] Lei Yan, Wenfu Xu, Zhonghua Hu, and Bin Liang. Virtual-base modeling and coordinated control of a dual-arm space robot for target capturing and manipulation. *Multibody System Dynamics*, 45(4):431–455, 2019.
- [20] Shabbir Kurbanhusen Mustafa, Wen Bin Lim, Guilin Yang, Song Huat Yeo, Wei Lin, and Sunil Kumar Agrawal. Cable-driven robots. *Handbook of manufacturing engineering and technology*, pages 1–52, 2013.
- [21] Ole Alexer N Eidsvik, Bent Oddvar Arnesen, and Ingrid Schjøllberg. Seaarm-a subsea multi-degree of freedom manipulator for small observation class remotely operated vehicles. In *2018 European Control Conference (ECC)*, pages 983–990. IEEE, 2018.
- [22] Tam Nhat Le, Hiroki Dobashi, and Kiyoshi Nagai. Kinematical and static force analysis on redundant drive wire mechanism with velocity constraint modules to reduce the number of actuators. *ROBOMECH Journal*, 3(1):22, 2016.
- [23] Jesús Morales, Jorge L Martinez, Anthony Mandow, Javier Serón, Alfonso Garcia-Cerezo, and Alejandro Pequeno-Boter. Center of gravity estimation and control for a field mobile robot with a heavy manipulator. In *2009 IEEE International Conference on Mechatronics*, pages 1–6. IEEE, 2009.
- [24] Prodrone. Pd6b aw arm, 2019.
- [25] Todd W Danko, Kenneth P Chaney, and Paul Y Oh. A parallel manipulator for mobile manipulating uavs. In *2015 IEEE international conference on technologies for practical robot applications (TePRA)*, pages 1–6. IEEE, 2015.
- [26] Carmine Dario Bellicoso, Luca Rosario Buonocore, Vincenzo Lippiello, and Bruno Siciliano. Design, modeling and control of a 5-dof light-weight robot arm for aerial manipulation. In *2015 23rd Mediterranean Conference on Control and Automation (MED)*, pages 853–858. IEEE, 2015.
- [27] Hannibal Paul, Koji Ono, Robert Ladig, and Kazuhiro Shimonomura. A multicopter platform employing a three-axis vertical articulated robotic arm for aerial manipulation tasks. In *2018 IEEE/ASME International Conference on Advanced Intelligent Mechatronics (AIM)*, pages 478–485. IEEE, 2018.
- [28] Sunil K Agrawal and Abbas Fattah. Reactionless space and ground robots: novel designs and concept studies. *Mechanism and Machine theory*, 39(1):25–40, 2004.
- [29] Michele D Carpenter and Mason A Peck. Reducing base reactions with gyroscopic actuation of space-robotic systems. *IEEE Transactions on Robotics*, 25(6):1262–1270, 2009.
- [30] Patrick J Bennett, Garret Cook, Matthew R Jones, Kaveh Ashenayi, Michael F Henry, and Alexander MacDonald. Aerial camera system, May 8 2018. US Patent 9,964,836.
- [31] Serdar Soyly, Bradley J Buckham, and Ron P Podhorodeski. Redundancy resolution for underwater mobile manipulators. *Ocean Engineering*, 37(2-3):325–343, 2010.

- [32] Hisashi Osumi, Yasushi Utsugi, and Masahiro Koshikawa. Development of a manipulator suspended by parallel wire structure. In *Proceedings. 2000 IEEE/RSJ International Conference on Intelligent Robots and Systems (IROS 2000)(Cat. No. 00CH37113)*, volume 1, pages 498–503. IEEE, 2000.
- [33] Hisashi Osumi and Masayuki Saitoh. Control of a redundant manipulator mounted on a base plate suspended by six wires. In *2006 IEEE/RSJ International Conference on Intelligent Robots and Systems*, pages 73–78. IEEE, 2006.
- [34] Tobias Bruckmann and Andreas Pott. *Cable-driven parallel robots*, volume 12. Springer, 2012.
- [35] Guangying Jiang and Richard Voyles. Hexrotor uav platform enabling dextrous interaction with structures-flight test. In *2013 IEEE international symposium on safety, security, and rescue robotics (SSRR)*, pages 1–6. IEEE, 2013.
- [36] Christopher Reichert, Katharina Müller, and Tobias Bruckmann. Robust internal force-based impedance control for cable-driven parallel robots. In *Cable-Driven Parallel Robots*, pages 131–143. Springer, 2015.
- [37] DexterWide. Cable robot cogiro and yaskawa sia20f: Path following – anr project dexterwide, 2019.
- [38] Lei Yan, Zonggao Mu, and Wenfu Xu. Base centroid virtual manipulator modeling and applications for multi-arm space robots. In *2014 13th International Conference on Control Automation Robotics & Vision (ICARCV)*, pages 1542–1547. IEEE, 2014.
- [39] Matko Orsag, Christopher Korpela, and Paul Oh. Modeling and control of mm-uav: Mobile manipulating unmanned aerial vehicle. *Journal of Intelligent & Robotic Systems*, 69(1-4):227–240, 2013.
- [40] Roberto Lampariello, Johann Heindl, Ralf Koeppe, and Gerd Hirzinger. Reactionless control for two manipulators mounted on a cable-suspended platform. In *2006 IEEE/RSJ International Conference on Intelligent Robots and Systems*, pages 91–97. IEEE, 2006.
- [41] Y. Adachi and K. Yoshida. Motion control of unconstrained underwater robot considering gravity and buoyancy. *Transactions of the Japan Society of Mechanical Engineers Series C*, 61(583):1050–1057, 1995.
- [42] H. Osum, T. Matsumoto, and M. Nakamura. Reaction force control of counter weights for a manipulator suspended by 6 wires. *Seimitsu Kogaku Kaishi/Journal of the Japan Society for Precision Engineering*, 83(9):863–869, 2017.
- [43] Ryo Miyazaki, Rui Jiang, Hannibal Paul, Yanzhao Huang, and Kazuhiro Shimonomura. Long-reach aerial manipulation employing wire-suspended hand with swing-suppression device. *IEEE Robotics and Automation Letters*, 4(3):3045–3052, 2019.
- [44] Emray Goossen and Katherine Goossen. Autonomous payload parsing management system and structure for an unmanned aerial vehicle, April 14 2011. US Patent App. 12/576,583.
- [45] DJI. Dji spreading wings s1000 specs, 2020.
- [46] V. van der Wijk. *Methodology for analysis and synthesis of inherently force and moment-balanced mechanisms*. PhD thesis, University of Twente, Netherlands, 4 2014.
- [47] Volkert van der Wijk. The grand 4r four-bar based inherently balanced linkage architecture for synthesis of shaking force balanced and gravity force balanced mechanisms. *Mechanism and Machine Theory*, 150:103815, 2020.
- [48] Volkert van der Wijk. On the grand 5r five-bar based inherently balanced linkage architecture. 2020.
- [49] Volkert van der Wijk, Just L Herder, and Bram Demeulenaere. Comparison of various dynamic balancing principles regarding additional mass and additional inertia. *Journal of mechanisms and robotics*, 1(4), 2009.

- [50] Kazuya Yoshida. A general formulation for under-actuated manipulators. In *Proceedings of the 1997 IEEE/RSJ International Conference on Intelligent Robot and Systems. Innovative Robotics for Real-World Applications. IROS'97*, volume 3, pages 1651–1657. IEEE, 1997.
- [51] P Piersigilli, I Sharf, and AK Misra. Reactionless capture of a satellite by a two degree-of-freedom manipulator. *Acta Astronautica*, 66(1-2):183–192, 2010.
- [52] Lam Technologies. M1233031 stepper motor.